THE DEVELOPMENT OF NANOPOROUS METAL MEMBRANES FOR ANALYTICAL SEPARATIONS

Michael Anthony Bromley

BSc (Hons) Forensic Science

April 2013

Submitted in accordance with the requirements of Lancaster University for the degree of Doctor of Philosophy

ABSTRACT

This thesis reports the novel use of semiconductor photocatalysis for the deposition of metal onto insulating surfaces through Photocatalytically Initiated Electroless Deposition (PIED). In PIED, a controllable and spatially selective process has been developed for the photogeneration of robust, conducting metal layers on semiconductor-sensitised insulator surfaces with several advantages over traditional, non-photocatalytic techniques including enhanced controllability and deposit purity, reduced operational costs and environmental impact. Layers of various metals including Ag, Pd and Ni have been generated by PIED onto TiO_2 sensitised quartz glass slides and organic membrane-based substrates.

With the addition of a microparticle template material, nanoporous metal films with both single and multi-layer, highly ordered arrays of sub-μm (hemi) spherical pores have also been depsited directly onto the surface of insulating substrates. This has been achieved by the self-assembly, assisted by the photogenerated hydrophilicity of the TiO_2 sensitiser, of a hexagonally close packed polystyrene microsphere template onto the target substrate prior to metallisation. Metal is then deposited through PIED into the interstitial spaces of the, subsequently removed, microsphere template and directly onto the TiO_2 sensitised substrate surface. The dimensions of the resultant pores in the deposited metal are determined by the size of the microspheres used to for the template while metal film thickness may be controlled by the deposition period.

The fabrication of nanoporous metal by this novel method adds a conductive and permeable metallic structure of high surface area to an otherwise electrically insulating polymer membrane surface. Such metallised insulating substrates have potentially wide applications in membrane and separation technology, energy storage and sensors – especially surface enhanced resonance Raman spectroscopy (SERRS), desalination and electrode / solid electrolyte composites for fuel cells.

STATEMENT OF AUTHORSHIP

I, Michael Anthony Bromley, confirm that the work presented in this thesis has been performed and interpreted by myself except where otherwise stated. I have been the primary author of each included publication with PhD Supervisor Prof. Colin Boxall as co-author.

The Quartz Crystal Microbalance data presented in Chapter 2 was acquired by co-author Sarah Galea at the University of Central Lancashire with additional supervision and financial support provided by co-authors Philip S. Goodall and Simon Woodbury at the National Nuclear Laboratory, Cumbria.

DECLARATION

The work described in this thesis was conducted at the Centre for Materials Science, University of Central Lancashire and the Engineering Department, Lancaster University between October 2007 and April 2013. Unless otherwise stated, it is the work of the author and has not been previously submitted in support of a higher degree.

Signature: _____

Michael Bromley

April 2013

ACKNOWLEDGEMENTS

I gratefully acknowledge and thank Lancaster University for the studentship that has enabled me to complete this degree as well as the Royal Society of Chemistry, the Engineering and Physical Sciences Research Council and the Lloyd's Register Educational Trust for their financial support.

I also thank my PhD supervisor Colin Boxall for his scientific and academic guidance, perennial enthusiasm and complex approaches to relatively simple matters which have perpetuated my research; the members of the Engineering Department for their technical and administrative support and the staff and students within the research group who have made this an enjoyable place of work.

Finally, I would like to thank my family for their unconditional support, especially my love Samantha and our darling daughter Lydia Rose.

CONTENTS

GLOSSARY OF TERMS

MAJOR SYMBOLS

A	–	area
e^-	–	electron
E^0	–	standard electrode potential
E_{cb}	–	conduction band edge
e^-_{cb}	–	conduction band electron
E_{fb}	–	flat band potential
E_g	–	band gap
E_{mp}	–	mixed potential
E_{vb}	–	valence band edge
h^+	–	hole
h^+_{vb}	–	valence band hole
K	–	Kelvin
k	–	quartz crystal mass sensitivity
l	–	chord length
Ø	–	diameter
r	–	radius
R_a	–	average roughness
R_{rms}	–	root mean square roughness

R_s	–	surface resistivity
s	–	sagitta
t	–	time
Δf	–	frequency change
Δm	–	mass change
λ	–	wavelength
ρ	–	bulk density
τ	–	deposited layer thickness

ABBREVIATIONS

AFM	–	atomic force microscopy
BS	–	British Standards
DDW	–	doubly deionised water
EDTA	–	ethylenediaminetetraacetic acid
EN	–	European Normal
EQCM	–	electrochemical quartz crystal microbalance
HCP	–	hexagonally close packed
ISM	–	ion-selective membrane
ISO	–	International Organisation for Standards
LED	–	light emitting diode
m-TiO_2	–	mesoporous titanium dioxide

Ox	–	oxidant
PIED	–	photocatalytically initiated electroless deposition
PS	–	polystyrene
PTFE	–	polytetrafluoroethylene
PVDF	–	polyvinylidene fluoride
QCM	–	quartz crystal microbalance
Red	–	reductant
RPM	–	revolutions per minute
SCE	–	saturated calomel electrode
SEM	–	scanning electron microscopy
SERRS	–	surface enhanced resonant Raman scattering
sq	–	square
THF	–	tetrahydrofuran
UV	–	ultra violet
UVA	–	ultra violet - A
XRD	–	X-ray diffraction

CHAPTER 1

INTRODUCTION

1.1 Overview

The work presented in this thesis reports the novel use of semiconductor photocatalysis for the deposition of metal films onto insulating surfaces through Photocatalytically Initiated Electroless Deposition (PIED). Furthermore, through the addition of a microparticle template material, the deposited films are induced with regular nanoporosity consisting of both single and multi-layer arrays of highly ordered sub-μm (hemi) spherical pores. This novel fabrication of nanoporous metal films directly onto the surface of insulating substrates adds a conductive and permeable metallic structure of high surface area to an otherwise electrically insulating surface.

As a primary objective, this process has been applied to the development of novel, nanoporous, surface-metallised ion-selective membranes for use in separation and preparation of pure isolates of a range of metal ions. Such metallised ion-selective membranes may be of importance to a wide range of activities in which fast, controllable and selective separation of metal ions from complex solutions is key, such as pre-analytical separation, environmental monitoring, environmental remediation, metal recycling, water purification, desalination and process control. These processes are important in a wide range of industries including the pharmaceutical, environmental monitoring, wastewater processing, foodstuffs, mining, power generation and nuclear industries. The aim of this work is therefore to provide a significant contribution to the advancement of analytical and separation science through the development of highly selective membrane technologies while the component techniques and background science, described below, provide various advantages to give an overall manufacturing and separation process with great flexibility.

To achieve this, ion-selective membranes will be metallised using Photocatalytically Initiated Electroless Deposition (PIED). This involves sensitising a substrate surface with a TiO_2 photocatalyst which is then irradiated to provide catalysis of the metal deposition process. An electrical field applied across the metallised membrane will then allow electrochemical control of the separation process, providing a more rapid and selective separation technique than currently achieved with existing ion-selective or supported ligand membranes. In order to be analytically useful the deposited metal must be porous, hence, the feasibility of imposing an ordered nanoporosity into electrolessly deposited metal films will be investigated. The successful deposition of nanoporous metal films onto electrically insulating surfaces will represent and innovative and novel development in the field of materials fabrication with products having potential applications in Surface Enhanced Resonant Raman Scattering, manufacture of batteries and capacitors and photocatalytically enhanced, Ag biocide surfaces in addition to the primary application of separation membranes.

1.2 Background

1.2.1 Ion-selective Membranes

Semi-permeable membranes such as ion selective and ion exchange membranes act as barriers to convectional mass transport between two solutions while permitting the diffusion and migration driven transport of specific ions. These membranes are typically polymers such as polyvinylidene fluoride (PVDF) and have a supported ligand to facilitate ion transport. The ligand consists of chelating groups distributed throughout the polymer and is chosen to have selectivity for specific target ions and particular valence states of that ion. This project aims to further improve selectivity and separation efficiency by enabling electrochemical control of the solution environment adjacent to the membrane surface. To achieve this, porous and conductive layers of an electrochemically appropriate metal are to be deposited onto commercially available PVDF membrane surfaces through the innovative advancement and combination of several existing materials fabrication techniques

including electroless metal deposition and the introduction of regular porosity into this deposited metal.

1.2.2 Metallised Membranes

The deposition of conducting, porous metal layers onto existing porous polymer ion-selective membranes enables the application of an electrical potential across the metallised membrane, whilst maintaining permeability, and allows for the electrochemical control of target ions at the membrane surface. Through rapid separation and both high specificity and electrochemically tunable selectivity, the resultant novel membranes will offer improved performance over conventional supported ligand, ion selective and ion exchange membranes. The only requirements for a successful separation are that the target species is electrochemically active (in the case of metal ions, this includes a wide choice of d-block and f-block metal ions) and that the separating membrane can be appropriately loaded with a ligand showing selectivity towards one of the oxidation states of the target species. Such advantages are desirable in analytical techniques requiring pre-measurement separation or pre-concentration and hence the anticipated results, membranes and techniques developed will find application in, *inter alia*, environmental / effluent monitoring, the geological sciences (e.g. soil waters), oceanography, the recovery of heavy metal ions and the isolation of d-block metals, lanthanides and actinides in the nuclear industry.

Specifically in the aforementioned example of the nuclear industry, most radio-analytical procedures revolve around the requirement to separate the analytes of interest from the sample matrix and prepare a suitably pure source for counting. These demanding separations often remain rooted in the traditions of classical inorganic chemistry and ion-exchange chromatography [1-5], hence a more efficient separation method would be of significant interest to the industry. With a novel, metallised ion-selective membrane, electrochemical control at the membrane surface may allow access to unusual oxidation states that are too reactive for use in conventional separations, e.g. Am (VI). The fact that actinides can be oxidised to higher oxidation states (IV & above) than lanthanides and

d-block metals [6] can therefore be exploited to achieve their bulk separation from d-block and lanthanide fission / activation products. An additional benefit of such electrochemical generation of specific redox states is to avoid reagent addition and produce an environmentally “cleaner” process with reducing chemical reagent handling, risk of contamination and waste management.

Prior to the manufacture and deployment of these enhanced separation membranes, the required production techniques must be developed. Primarily these are electroless deposition, photocatalysis and templated metal deposition, each of which will be discussed in the following sections.

1.2.3 Metal Deposition

The deposition of metals onto other surfaces has long been utilised to modify and enhance various materials. Most frequently this is done with the use of an electric current to reduce metal ions in solution and deposit them onto an electrode surface in a process known as electroplating or electrodeposition. As electrodeposition requires the flow of electricity, it is wholly limited to use on conducting surfaces. However, as is the case for the metallisation of polymer based membranes, it may be desirable to deposit metal onto non-conducting materials, something which may be achieved by electroless deposition.

Electroless deposition is an auto-catalytic reaction in which metal ions are deposited from solution onto a substrate through their reduction by a chemical reducing agent [7]. This long established technique [8] is independent of electrical current it can therefore be used to deposit metals onto an insulating surface. The reaction is, however, dependent on catalysis of metal ion reduction by the substrate surface and therefore usually involves several sensitisation steps before the deposition process can take place [9,10]. Typically this is achieved by seeding the substrate surface with a catalytic metal such as Pd, usually in a two step process involving the adsorption of Sn-Pd particles and the removal of the Sn with concentrated HCl to expose the Pd catalyst [11]. Such sensitisation processes must be repeated several times to achieve a sufficiently catalytic surface, which can be costly and

time consuming while the resulting metal deposit will contain Pd and traces of Sn, the latter being a particularly troublesome impurity for electrochemically based applications.

Hence, there is a need for electroless methods of deposition of metal layers onto insulating substrates which obviate the complex substrate treatment regimes. As an alternative to electrochemical sensitisation, metallic nuclei may be generated photochemically through photon absorption by a semiconductor. The use of such a technology would enable the Pd-based sensitisation methods traditionally used in electroless deposition to be replaced with a much simpler sensitisation process in which a thin semiconductor film is deposited onto the substrate in a single step prior to electroless deposition. The principles of this are discussed in the following section.

1.2.4 Photocatalytic Deposition

Semiconductor particles are utilised as efficient photocatalysts for a range or processes such as pollution abatement [12], corrosion inhibition [13], precious metal recovery [14,15] and heavy element removal from effluent streams [16]. In each case, absorption of ultra-band gap energy photons by the particles generates electron-hole pairs within the semiconductor. These charge carriers can react with species in solution, effecting oxidation and reduction reactions and performing useful electrochemistry. Such reactions may include the electroless deposition of metal ions to form metal nucleates at the semiconductor surface through the action of the photogenerated electrons.

Metallisation of semiconductors, in particular TiO_2, by photocatalytic reduction of metal precursors is an mature technology, established as early as 1969 [17,18]. However, the use of photocatalysis in metal deposition remains surprisingly limited and, even throughout the last decade, has remained an infrequently studied area. As a result, photocatalysis is often merely used as a subsidiary process within other, wider areas of application or for the formation of isolated nanoparticles rather than a coherent metallic layer.

The field of pollution abatement has naturally expanded to include the photocatalytic reduction of metal ions for their removal from solution: Tanaka *et al* describe the photoreduction of Pd^{2+}, Mn^{2+}, Tl^{+} and Co^{2+} [19]; Herrmann *et al* report similar photoreduction of Ag^{+} [20]; and more recently, Kanki *et al* describe the photoreduction of Cu^{+} [21]. Each of these methods uses TiO_2 powder added to a solution for the purpose of photocatalytically removing metal ions - hence the focus remains on metal extraction rather than the metallisation of the semiconductor or the formation of a coherent metal layer thereon. Without an interest in surface metallisation, the possibility for merging the deposited particles into complete films has not been investigated. Despite this, such works clearly demonstrate and enhance the understanding of the principles behind photocatalytic metal deposition.

Perhaps the most frequent combination of metals and semiconductors may be found in doping, *i.e.* the incorporation of select metal ions into the semiconductor lattice in order to introduce energy levels within the band gap. While this may be used to optimise a semiconductor photocatalytically by shifting band edge absorption [22], inhibiting charge carrier recombination [23] or encouraging charge transfer [24], it does not typically involve the photocatalytic reduction or deposition of metals onto the semiconductor. Rather, metal ions such as Pt, Pd, Ag and Au are incorporated into the semiconductor lattice via an impregnation method, such as the addition of the desired metal to a TiO_2 slurry which is then calcined to form a doped TiO_2 powder of solid film [25], or the addition of metal to a surfactant based TiO_2 sol-gel for the production of mesoporous doped TiO_2 films [26].

However, doping techniques carry potential applications towards photocatalytic metal reduction, such as in the process reported by Noh *et al* [27,28]. Through the inclusion of Pd in a TiO_2 coating solution, Pd^{2+} ions are incorporated within a TiO_2 film which is subsequently irradiated through a photomask to reduce the Pd^{2+} to Pd metal. This clearly demonstrates the use of photocatalysis for metal reduction but the principles are not applied to direct metal deposition onto an extant semiconductor or substrate. Rather, the technique is described as a photo-patterned sensitisation technique for surface modification.

More recent work within the same group by Byk *et al* provides a focus on metallisation of the TiO_2 film by applying electroless Ni deposition to Pd patterned substrates [29]. As with traditional sensitisation methods used in electroless plating, the metallic Pd formed through photocatalysis acts as a catalytic basis for Ni deposition. Here photocatalysis is employed, by virtue of photomasking, to produce spatially selective sensitisation of a substrate surface but subsequent Ni deposition remains a separate process which is independent of photocatalysis. Despite this application to metal deposition, the use of photocatalysis here remains in producing isolated particles rather than coherent metal films and cannot be considered a metal deposition process itself.

The direct photocatalytic deposition of Ag nanoparticles onto TiO_2 films is demonstrated by Stathatos *et al* [30], further confirming the viability of semiconductor photocatalysis in metal deposition and specifically demonstrating the electroless deposition of Ag from solution. However, photocatalysis is again only ustilised in the production of small scale metal particles and the deposition is not expanded towards the formation of complete, coherent metal layers.

In conjunction with interest in H_2 separation, the formation of such coherent metal layers is an area which has drawn more recent attention. It is well known that Pd shows a high affinity for H_2 and consequently it has become commonly used in H_2 separation membranes. As a result it has become desirable to produce Pd films on insulating surfaces and semiconductor photocatalysis offers one potential method to achieve this. In a claimed novel method, Wu *et al* described the production of Pd membranes through photocatalytic deposition with a particular focus on controlling the thickness of the deposited metal layer [31,32]. This provides a true application of photocatalysis for metal deposition with Pd metallisation taking place onto commercial TiO_2 ceramic membranes directly from solution under ultra-band gap irradiation. The work also describes the dependency of the photocatalytic process on factors such as irradiation time, temperature, pH and bath constituent concentrations and hence offers considerable contribution towards the understanding of photocatalytic metal deposition.

The aforementioned work of Wu was continued by Li *et al* with the aim of improving the inherently unstable photocatalytic reaction baths, a problem commonly encountered with the electroless deposition of Pd, and the quality / density of the photocatalytically deposited Pd film [33]. By replacing methanol with EDTA as the hole scavenger, Li enhance the stability of the photocatalytic Pd bath and provided an important contribution to the development of photocatalytic Pd deposition. Through complexation of the metal precursor, EDTA slows the high rate of auto-catalytic deposition, which is typical of unstable Pd baths, in favour of the photocatalytically driven deposition process. The result of this is a more controlled electroless deposition and the formation of a denser Pd film with finer granularity.

Despite this advancement, further work from Li *et al* moved towards an alternate photocatalytic deposition method in which the substrate is irradiated only after being removed from the electroless plating bath. Upon removal from the bath, a thin liquid film is retained on the substrate surface and subsequent irradiation allows for photocatalytic reduction of the adsorbed metal ions to occur. While this method avoids homogeneous bath decomposition, the quantity of metal deposited from the liquid film is very small and the process must be repeated 20x in order to achieve a complete Pd layer of 400 nm thickness [34,35].

Of the most recent reports of the use of photocatalytic deposition, Zhao *et al* described the deposition of Pd onto TiO_2 nanotubes, the photocatalyst being used to reduce Pd for direct metallisation [36]. However, this is performed slowly over 12 hours and only used to produce Pd nucleation sites prior to a continued, non-photocatalytic, electroless deposition conducted as a separate process. Ultimately this process utilises photocatalysis merely as a separate, non-solution phase sensitisation step; the potential of semiconductor photocatalysis for metal deposition again being under exploited.

Thus, in spite of the demonstrated viability of photocatalytic deposition and the advantages provided in process simplicity, versatility and cost over complimentary techniques such as chemical vapour deposition [37], electroless [38] and even electro-plating [39], there

remains an absence of an exhaustive body of research. Even in the most recent publications describing photocatalytic metal deposition, the photocatalyst is not exploited to full process advantage and the primary directive has not spread beyond the production of Pd films for H_2 separation.

Therefore, this work has sought to understand and apply the technique for the metallisation of various insulating substrate surfaces. Particularly, the deposition of both Ag and Pd has been explored, so allowing for the study of PIED in both 1 and 2 electron reduction processes.

1.2.5 Photocatalytically Initiated Electroless Deposition (PIED)

As discussed above, semiconductor materials such as TiO_2, SnO_2, WO_3 can act as photocatalysts, generating electron-hole pairs upon the absorption of ultra-band gap light energy. These charge carriers may be used to drive useful redox reactions with species, such as metal ions, on or at the semiconductor surface [12]. This has been appropriated for metal ion reduction within the PIED process, photocatalytically initiating metal nucleation directly onto the semiconductor surface and providing an alternative to the interfacial chemical metal nucleation methods employed in conventional electroless deposition. Once metal nucleation sites have been formed by photocatalytic means then, in the presence of an appropriate reductant, further deposition may occur onto those nucleate sites by auto-catalytic electroless deposition. These are the principle processes of PIED and enable the formation of coherent and conductive metal layers on otherwise electrically insulating substrate materials. The only pre-sensitisation process required for this metallisation is for the substrate to be coated with an appropriate semiconductor, such as the chemically robust TiO_2. PIED therefore obviates the need for Sn-Pd catalysts so eliminating the associated contamination and cost penalties.

1.2.6 Induced Porosity

The formation of porous metal films on electrically conducting surfaces through electrodeposition is frequently reported [40-44]. However, metal materials with an ordered, sub-μm scale pore structure interfaced directly with an insulating substrate are attractive for use in clean energy production (fuel cells [45]), energy storage [46,47], sensors (especially surface enhanced resonance Raman techniques [48,49]) and separation science [50]. It is therefore desirable, and in the case of metallised separation membrane technologies, essential, that controllable porosity can be introduced into PIED generated metal films on insulating substrates. A number of possible methods exist in the prior art in which porosity is introduced into electrodeposited metal films through the formation of a template around which metal deposition can take place, such techniques have been investigated for their compatibility and use with PIED.

The use of liquid crystalline phases formed by lyotropic surfactants at high concentrations has been demonstrated by Attard & Bartlett *et al* [51-53]. Normal hexagonal (H_1) liquid crystalline phase surfactants are used as a template for the synthesis of nanostructured Pt films on metal substrates whereby electrodeposition occurs in the interstitial spaces of the rod-like micelles. The dimensions and separation of the micelles, and so the pore structure of the resultant metal layer, can be controlled by varying the surfactant : solvent ratio and surfactant chain length.

This use of surfactant micelles in the plating bath allows for extremely small theoretical pore sizes (<10 nm) although this requires highly specific conditions to maintain the correct phase type and orientation. Such conditions may be incompatible with those required for stable and efficient electroless plating baths, hence, alternate methods of template formation are likely to be more suitable for use with PIED.

Bartlett *et al* [54] described the use of a monolayer of hexagonally close packed polystyrene (PS) microspheres, self-assembled on metal electrode surfaces for the formation of metal films with ordered arrays of sub-μm spherical voids prepared by electrodeposition into the

interstitial spaces within the microsphere array. Microsphere templates offer a fixed and stable structure on the substrate surface and do not interfere with the conditions of the electroless plating solution, thus overcoming the compatibility issues presented by the use of surfactant-based templates. As microsphere templates can also be deposited and visually characterised prior to metallisation, something not possible with liquid crystalline surfactants while the template is *in situ*, the expected arrangement and dimensions of the subsequently induced porosity is highly predictable. Furthermore, PS spheres are commercially available in sizes ranging from 50 nm to 3 μm, allowing for the production of metal films with a wide range of pore sizes using the same deposition technique.

Microspheres can be self-assembled in a single layer, hexagonally close packed array by controlled evaporation [55,56] or by a Langmuir-Blodgett technique [57,58]. The former produces hexagonally close packed microsphere arrays through the evaporation of water from a meniscus of microsphere suspension maintained on the substrate surface. As the liquid depth at the meniscus centre becomes approximately equal to one microsphere diameter, spheres are deposited onto the substrate surface and are drawn together into a close packed arrangement through lateral capillary forces between individual spheres.

Defects within the ordered microsphere arrays are common and may be caused by irregularities on the substrate surface, poorly controlled evaporation or the formation of gas bubbles in the sphere suspension. Microsphere organisation in this way is also efficient only on a hydrophilic surface, allowing the sphere suspension to spread evenly and self-assembly to occur unencumbered. Here, an inherent process advantage is anticipated as the TiO_2 sensitisation layers required for PIED are able to display super-hydrophilicity when irradiated with ultra-band gap light energy [59]. Therefore a period of irradiation prior to microsphere assembly will assist in the formation of a suitable microsphere template.

The disadvantages of evaporation based methods such as the occurrence of array defects and a restriction on the substrate area which can be conveniently templated may be overcome by the use of Langmuir-Blodgett-like techniques. These involve the assembly of

the microspheres into a hexagonally close packed monolayer on a liquid surface before transferring the whole array to a substrate. However, further difficulties are introduced in applying the Langmuir-Blodgett technique to PS spheres and ensuring that they are effectively arranged on the liquid surface. Several approaches to this problem have been published including the use of surfactants to control surface tension [57] and thermo-treatment of the spheres to render them hydrophobic [58] although each case represents a complication to the overall production process and as such, controlled evaporation will be primarily utilised.

1.3 Perceived Novelty

Although many of the underpinning processes involved in the formation of nanoporous and conducting metal films through PIED exist in current literature, the method presented here provides several areas of novelty.

As described in section 1.2.4, photocatalytic metal reduction is an established technology [17,18] and has been utilised for the removal of metal ions from solution [19-21], as a subsidiary step within a broader metal deposition process [29] and for the direct deposition of metal nanoparticles onto a semiconductor surface [30]. However, the photocatalyst is rarely fully exploited for the deposition of coherent and conducting metal films such as those generated using PIED.

The first report of such a technique, the novel photocatalytic deposition of Pd, was made by Wu *et al* [31,32] in which ultra-thin metallic Pd films are generated directly onto TiO_2 membrane surfaces. While broadly similar to PIED, this method relies entirely on photocatalysis to drive the metal deposition and hence, once the TiO_2 surface is wholly covered by the deposited metal, the activity of the photocatalyst is lost and metallisation ceases. In contrast, PIED uses photocatalytic deposition to drive initial metal nucleation and combines it with the continued auto-catalytic metal growth typical of more traditional, non-photocatalytic, electroless deposition processes. This enables PIED to be not only photo-controlled in its onset but also independent of photocatalysis once initiated, facilitating

the deposition of metal films with much greater thickness than those possible through previously reported photocatalytic deposition techniques.

Further novelty is found in the deposition of nanoporous metal films through a PS microsphere template. Firstly, although the self-assembly of microspheres into HCP arrays is well documented [55-58], the use of a TiO_2 sensitisation layer to facilitate that assembly through photo-induced super-hydrophilicity upon ultra-band gap irradiation has not been previously reported. More significantly though, while the deposition of porous metal has been previously demonstrated with various template materials [51-54], each report involves the electrodeposition of metal onto electrically conducting substrate surfaces. Given that PIED employs photocatalytic and chemically auto-catalytic electroless deposition processes, there is no such dependency on electrical current, enabling the metallisation of a much broader range of substrate materials, conducting or otherwise. The application of PIED through a PS microsphere template onto electrically insulating materials represents the first reported electroless deposition of conducting metal films with highly ordered nanometre scale porosity onto any form of non-conducting substrate. This is a point of significant novelty, as evidenced by the application for patent protection of the technology in Chapter 4, and potentially offers an important contribution to the research field.

1.4 Overview of Chapters

Each chapter within this thesis represents a stand-alone publication though the running theme throughout can be summarised as follows.

Chapter 2 presents the first report of PIED including details of the main principles and demonstrating the deposition of non-porous Ag and Pd onto glass and PVDF membrane substrates. Also included is the study of the kinetics of PIED through simultaneous chronopotentiometric and gravimetric analysis using a quartz crystal microbalance (QCM).

Chapter 3 expands in detail the background science of semiconductor photocatalysis, photocatalytic metal deposition and the current understanding of related prior art. PIED of

non-porous Ag and Pd on glass is also reported in greater detail with studies of the nucleation and continued deposition processes, the effect of varied irradiation and deposition times and methods with which to control metal deposition. The applicability of PIED to the deposition of other metals such as Ni is also investigated.

Chapter 4 is comprised of a published application for a patent to protect the developed innovation of a method of forming porous metal films on insulating surfaces while the first report of such Ag and Pd films on glass and the observed effect that the inclusion of a microsphere template has on the rate of PIED is made in Chapter 5. Chapter 6 expands on this to include the deposition of metal films of increased thickness and the first report of the deposition of porous Ag films on PVDF membrane.

Chapter 7 provides a more detailed report of PIED of Ag and Pd with induced nanoporosity on glass, revealing the specific nucleation and growth patterns which occur when depositing around a microsphere template, the effects of temperature and the specific difficulties encountered and overcome in the case of PIED of nanoporous Pd. Also presented here is the formation of metal films of monolayer porosity and multi-layer porosity as well as the control of pore size through variation of template microsphere diameter.

Finally, Chapter 8 presents the application of all previously developed techniques to the nanoporous metallisation of PVDF membranes and details the challenges and adaptations involved. Specifically, these include the method of TiO_2 sensitisation, microsphere array formation and the effectiveness of the photocatalytic nucleation stage. Despite these, the novel production of nanoporous metallised PVDF membranes is demonstrated.

CHAPTER 2

PHOTOCATALYTIC INITIATION OF ELECTROLESS DEPOSITION

Journal of Photochemistry and Photobiology A: Chemistry, 216, 2-3, (2010), 228-237

DOI: 10.1016/j.jphotochem.2010.07.029

Michael A. Bromley[a], Colin Boxall[a,*], Sarah Galea[b], Philip S. Goodall[c], Simon Woodbury[c]

[a] Engineering Department, Lancaster University, Lancaster LA1 4YR, UK

[b] Centre for Materials Science, University of Central Lancashire, Preston PR1 2HE, UK

[c] Central Lab., National Nuclear Laboratory, Sellafield, Seascale, Cumbria CA20 1PG, UK

"Harness your stupidity, sir! Employ your witlessness! Use your empty-headed, simplistic moron mind and find a solution!"

Kryten 2X4B-523P

2.1 Publication Summary

- Research article accepted into the Journal of Photochemistry and Photobiology A: Chemistry
- 5-year Impact factor: 2.691
- First report of the one-step photocatalytically initiated electroless deposition (PIED)
- Simultaneous photocatalytic metal nucleation and auto-catalytic growth demonstrated
- Electrically conducting (non-porous) Ag & Pd layers formed on semiconductor sensitised insulator surfaces with spatial selectivity
- Study of PIED kinetics through simultaneous chronopotentiometric and gravimetric analysis

2.2 Author Contributions

- M.A.B.: designed and performed PIED experiments; analysed data from QCM experiments; primary author of the manuscript from first draft to final proof
- C.B.: conceived and supervised the study of M.A.B and S.G.; co-author of manuscript through review of drafts
- S.G.: performed QCM experiments and preceding study of PIED
- P.S.G. & S.W.: provided industrial backing for S.G.'s study

2.3 Abstract

We report a one-step Photocatalytically Initiated Electroless Deposition (PIED) process that allows for the photogeneration of robust, coherent, conducting metal layers on semiconductor-sensitised insulator surfaces. The PIED process involves two steps, performed simultaneously in the same metal precursor solution:

(i) Metal nanoparticles are formed at the surface of the semiconductor by photocatalytic reduction of an appropriate metal precursor;

(ii) The nanoparticles then serve as nucleation centres for an autocatalytic electroless deposition process, growing and coalescing to form a continuous metal layer.

Layers of various metals including Ag and Pd have been generated by PIED on mesoporous TiO_2 (m-TiO_2) coated quartz glass slides and PVDF membranes. Deposition occurs only onto areas of the substrate both sensitised with TiO_2 and irradiated with ultra-band gap energy light. The morphology of the resultant layer is dependent upon the nucleation density occurring during the primary photocatalytic stage of PIED. PIED provides a cheaper, environmentally cleaner and more controllable option than traditional techniques of plating onto dielectric surfaces.

Keywords: photocatalysis, electroless deposition, titanium dioxide, quartz crystal microbalance.

2.4 Introduction

Electroless deposition is a plating process in which metal ions are deposited from solution onto a substrate through their reduction by a chemical reducing agent [7]. As the process is independent of electrical current it can be used to deposit metals onto an insulating surface, something which is not possible through electroplating techniques. The reaction is dependent on catalysis of metal ion reduction by the substrate surface while deposition elsewhere is minimised. The deposited metal must also catalyse the reduction if further deposition is to occur when the substrate surface is completely covered [9]. Electroless plating is most commonly performed with Cu, Ni, Co and precious metals with plating solutions being usually comprised of the metal salt, a reducing agent, a buffer and complexing agents to stabilise.

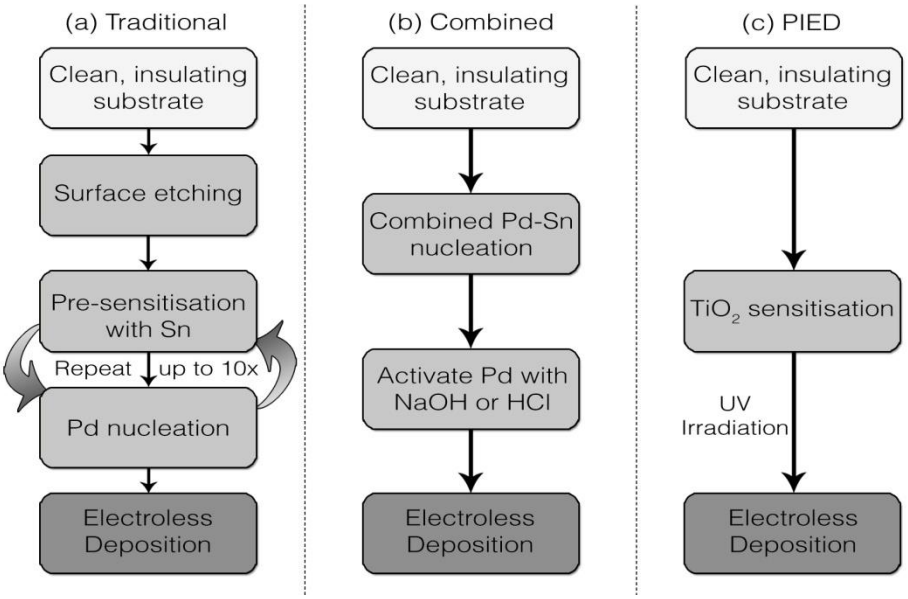

Fig. 1 Flow diagrams for electroless deposition routes involving: (a) sequential Sn-Pd sensitisation; (b) combined Sn-Pd sensitisation; (c) photocatalytic initiation (PIED)

The use of electroless plating on insulating surfaces usually involves sensitisation of the substrate in order for it to catalyse the deposition process, Fig. 1 (a) and (b) [9,10]. Typically a catalytic metal such as Pd would be seeded onto the substrate, most usually in a two step process, Fig. 1 (a); first, pre-sensitisation of the substrate with a $SnCl_2$ solution in hydrochloric acid resulting in the adsorption of Sn^{2+} ions to the surface; second, treatment with a $PdCl_2$

solution in hydrochloric acid during which Sn^{2+} ions on the surface reduce solution Pd (II) ions to form nucleation deposits on the substrate surface [9]. A recent improvement, Fig. 1 (b), combines sensitising and nucleating ions in a single solution. This results in adsorption of Sn-Pd particles with the Sn then removed with concentrated HCl to expose the Pd catalyst [11]. Each method has disadvantages; the sensitisation processes must be repeated several times to achieve a sufficiently catalytic surface, which can be costly and time consuming; lengthy surface preparation involving cleaning, etching and neutralising is required to promote bond formation; and the resulting metal deposit will contain Pd and Sn, the latter being a particularly troublesome impurity for electrochemically based applications.

As an alternative to electrochemical activation, metallic nuclei may be generated photochemically. We report on a one-step photocatalytic method, Photocatalytically Initiated Electroless Deposition (PIED), by which metal nucleation centres may be photochemically generated directly onto semiconductor particles / surfaces. This method, presented in outline in Fig. 1 (c) and Fig. 2, utilises the photocatalytic properties of TiO_2 to initiate electroless deposition for surface metallization.

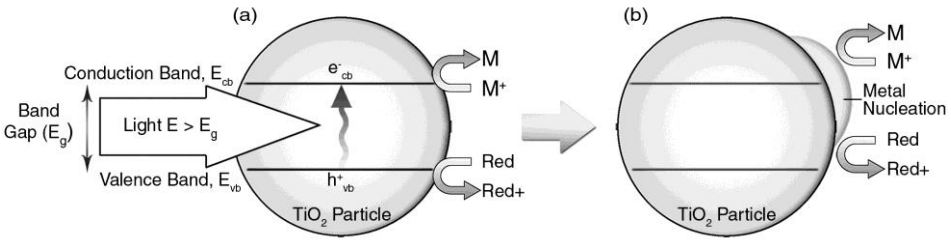

Fig. 2 Two stages of PIED: (q) the photocatalytic process derived from interfacial electron transfer at a photoexcited semiconductor particle; and (b) the autocatalytic electroless deposition process

Semiconductor particles, such as TiO_2, SnO_2, WO_3, can act as efficient photocatalysts for a range or processes such as pollution abatement [12], corrosion inhibition [13], precious metal recovery [14,15] and heavy element removal from effluent streams [16]. In these reactions, absorption of ultra-band gap energy photons generate electron-hole pairs within the semiconductor particles, Fig. 2 (a). These charge carriers can react with species in solution, effecting oxidation and reduction reactions and performing useful electrochemistry.

Such reactions may include the electrodeposition of metal ions to form metal nucleates at the semiconductor surface through the action of the photogenerated electrons.

Metallisation of semiconductors by photocatalytic reduction of metal precursors is an established technology [16], primarily developed to improve the efficiency of TiO_2 for O_2 reduction [15] or H_2O oxidation [60]. For example, Stathatos *et al*, 2000 [30] described the photocatalytic deposition of Ag nanoparticles onto m-TiO_2 films through a single electron transfer photo-reduction. However, the result of such a process is typically is a nanoparticle coating rather than a coherent metallic layer.

The photocatalytic generation of such metal nanoparticles at semiconductor surfaces offers an alternative to the electrochemical metal nucleation methods employed in conventional electroless deposition shown in Fig. 1 (a) & (b). Once metal nucleation sites have been formed by photocatalytic means then, in the presence of an appropriate reductant, further deposition can occur onto those nucleate sites by conventional electroless deposition reactions, Fig. 2 (b). These are the principal steps of PIED. As such, PIED may obviate the need for Sn-Pd catalysts so eliminating contamination from prior nucleation whilst the fewer steps and materials required may provide a cheaper, environmentally cleaner and (through control of incident light intensity) more controllable option than the usually employed methods for dielectric plating.

Two generic embodiments of PIED may be envisaged. In the first embodiment, the reductant or hole scavenger employed during the photocatalytic initiation step (Fig. 2 (a)) is a different reagent to the reductant employed during the autocatalytic electroless deposition / metal nucleate growth step (Fig. 2 (b)). In this context, the photo-initiated nuclei formation and growth steps can be performed in two ways: first, by immersion of the surface to be coated in a hole scavenger / precursor metal ion solution followed by a second immersion in a reductant / metal ion solution, so-called “two-step” PIED; and second, by immersion of the substrate in a solution containing the precursor metal ion and both the hole scavenger and reductant, so-called “one-step” PIED. In the second generic embodiment, the hole

scavenger and the reductant for the metal growth step are the same and so this may be classified as a “one-step” PIED process. It is this latter embodiment that is the subject of this communication.

Coupled photocatalytic and electroless deposition of Pd using TiO_2 as a catalyst has been reported previously by Wu *et al* [31,32]. Pd deposition was achieved in a two step process using methanol as a hole scavenger and hydrazine as a reductant. The same team have also reported the deposition of Pd onto alumina discs by a similar method [33,34]. Yang *et al* [61] report a one-step process for photo-initiated deposition of Cu onto ZnO sensitised substrates under UV irradiation. However, ZnO readily photo-corrodes [62] suggesting this process could be driven by galvanic displacement rather than metal ion reduction by photogenerated electrons. A galvanic displacement mechanism would lead to the incorporation of metallic Zn into the electrolessly deposited metal, an undesirable effect for reasons of deposit purity (*vide supra*).

In light of the above, we describe the generation of Ag and Pd layers on TiO_2-sensitised insulator substrates in true one-step PIED for the first time. Use of TiO_2 obviates semiconductor photo-corrosion whilst deposition of Ag and Pd allows for the study of 1 and 2 electron reduction PIED processes. Of relevance to process development is that well studied, conventional electroless deposition recipes are available for both metals wherein the reductants have also been used as hole scavengers in TiO_2 photocatalysis. These reductants are of differing reducing power, allowing inferences to be made regarding the effect of this parameter on deposit morphology.

2.5 Experimental

2.5.1 Materials and Reagents

All reagents used are AnalaR grade or higher, and purchased from Sigma Aldrich (Gillingham, Dorset, UK) or Alfa Aesar (Heysham, Lancashire, UK). Doubly distilled water, further purified by a deionisation system (E-pure model 04642, Barnstead / Thermodyne,

Dubuque, Iowa, USA.) to a resistivity of 18.2 MΩ / cm. Nitrogen Whitespot grade is provided by BOC Ltd., Guildford, Surrey, UK.

2.5.2 TiO_2 Sensitisation of Substrates Using Reverse Micelle Sol-Gels

Quartz substrates were coated with a mesoporous TiO_2 (m-TiO_2) layer via sol-gel spin coating. A reverse micellar sol-gel, as described by Yu *et al* [59], was prepared by vigorously mixing Triton X-100 (26.0 g) and cyclohexane (150 ml) to form a reverse micellar solution. After 30 min water (1.08 g) is added and the solution appears turbid. This turbidity clears upon addition of titanium (IV) isopropoxide (99.999%) (23.0 g). The solution was then stirred for 60 min at 293 K, so forming a colloidal suspension of TiO_2 nanoparticles. Acetylacetone (10 ml) is added to stabilise the solution. The resultant sol-gel is applied to substrates by spin coating for 5 seconds at 2900 rpm using an inverted model 636 rotating disk electrode system (Princeton Applied Research, Tennessee, USA). Coated substrates are then fired in a furnace at 773 K for 1 hour to anneal the TiO_2 and produce a resilient coating. Annealing at this temperature produces TiO_2 with predominantly anatase structure and coatings are composed of interconnected, mono-dispersed, spherical primary particles approximately 10 nm in diameter within a mesoporous structure (*vide infra*). Phase identification was achieved through Raman spectroscopy using a Renishaw Ramascope 1000 (Renishaw, Gloucestershire, UK) with back-scattering geometry and a 17 mW He-Ne (632.8 nm) laser. UV-Vis spectra of films were obtained using UV-Vis spectrophotometry (Hewlett-Packard 8452A, Bristol, United Kingdom). Surface topography, roughness etc, were assessed using Atomic Force Microscopy (AFM; Q-Scope 250, Quesant, California, USA). Sensitised substrates were stored in darkness at room temperature prior to use.

2.5.3 TiO_2 Sensitisation of Substrates Using Nanoparticulate Sols

Polyvinylidene fluoride (PVDF) membranes (0.2 μm pore size, Millipore) are unable to withstand 773 K annealing and so were sensitised by coating with a nanoparticulate TiO_2 sol (TiPE® O502, TitanPE Technologies Inc., Shanghai, China) deposited via spin coating (see

above) for single side sensitisation and by manual dip-coating for two sided sensitisation. The sol contains nanoparticulate anatase TiO_2 with average primary particle size of < 8 nm in water based solution. Coated PVDF membranes were oven dried at 373 K to remove solvent and so produce a coating of anatase nanoparticles. Membranes were stored in darkness at room temperature prior to use.

2.5.4 Preparation of Ag Electroless Plating Solution

Electroless Ag plating solutions were prepared to the composition given in Table 1. All components are added to a small quantity of distilled water in the order listed, ensuring full dissolution with each addition. The completed solution was made up to volume with distilled water and purged with N_2 for 20 min to deoxygenate. The pH of the solution was 11.5 and PIED was carried out at 298 K. Electroless plating solutions are freshly made immediately before use for optimum performance. As $AgNO_3$ is light sensitive Ag solutions are prepared and stored in amber flasks in darkness.

Role	Component	Concentration
Metal precursor	Silver Nitrate	1.496 g / dm^3 (8.8 mmol / dm^3)
Complexant	Ethylenediamine	3.245 g / dm^3 (54 mmol / dm^3)
Stabiliser	3,5-diiodotyrosine	0.017 g / dm^3 (39.2 µmol / dm^3)
Reducing agent / scavenger	Potassium Sodium Tartrate	0.7356 g / dm^3 (26 mmol / dm^3)
pH	-	11-12
Temp	-	298 K

Table 1 Composition of Ag electroless plating solution

2.5.5 Preparation of Pd Electroless Plating Solution

Electroless Pd solutions, developed in these laboratories, were prepared to the composition given in Table 2. $PdCl_2$, di-sodium EDTA and ammonium hydroxide (28% w/v NH_3 in water) were added and, to ensure formation of the Pd-amine complex, stirred with gentle heating until the solution cleared. The solution was cooled and hydrazine reducing agent added. The solution was then made up to volume with distilled water and purged with N_2 for 20 min.

As above, electroless plating solutions were made immediately before use for optimum performance.

Role	Component	Concentration
Metal precursor	Palladium Chloride	3.60 g / dm^3 (20.3 mmol / dm^3)
Complexant	Ammonium Hydroxide (28%)	350.0 ml / dm^3 (5.2 mol / dm^3 NH_3)
Stabiliser	Di-sodium EDTA	62.4 g / dm^3 (167.7 mmol / dm^3)
Reducing agent / scavenger	Hydrazine (65%)	11.0 ml / dm^3 (216.7 mmol / dm^3)
pH	-	11-12
Temp	-	298 K

Table 2 Composition of Pd electroless plating solution

2.5.6 One-Step Photocatalytically Initiated Electroless Deposition

TiO_2 sensitised substrates were placed directly into freshly prepared electroless plating solutions in a quartz reaction vessel for improved UV transmittance. A N_2 stream was bubbled through the plating solutions during deposition in order to purge the solution of oxygen which can compete with metal ions for reduction at the photocatalytic surface. The N_2 stream also provides a source of agitation to prevent local depletion of metal ions at the substrate surface. The reaction vessel was then placed inside a circular photoreactor (Lidam Scientific, Dartford, UK) comprised of two hemi-cylinders, each containing 6 x 8W UVA lamps. A thermostated water supply may be passed through the incorporated jacket of the quartz vessel allowing for control of the plating solution temperature. Water flow is maintained by peristaltic pump and temperature controlled by a thermostatic water bath. Post deposition the substrate is removed from the plating solution, rinsed with distilled water and dried in air. Microstructure of the resultant layers was imaged using SEM (FEI Quanta 200).

2.5.7 Measurement of Kinetics of PIED onto TiO_2

Rates of metal deposition were measured *in situ* using a quartz crystal microbalance (QCM, Type 5510, Institute of Physical Chemistry, Warsaw, Poland) with an Autolab PGSTAT10 system (Windsor Scientific Ltd., Slough, UK), driven by GPES 4.5 software

(EcoChemie, Utrecht, The Netherlands) allowing simultaneous QCM and chronopotentiometric measurements to be taken – electrochemical QCM (EQCM). The mass sensitive oscillators (PAN, Warsaw, Poland) were 14 mm diameter, AT cut, 10 MHz resonant frequency quartz crystals. 6 mm diameter Au films were vacuum deposited onto each side of the piezoelectric crystals as electrical contacts and solution interfaces. The frequency was measured with a Programmable Frequency Timer / Counter (Philips PM6680 JFluke Mfg. Co., Inc., Everett, WA). Mass change (**Δ**m) was calculated from the frequency change (**Δ**f) by the Sauerbrey equation [63]

$$\Delta m = -k \times \Delta f \tag{1}$$

Where, in this simplified form of Sauerbrey, k is the mass sensitivity of the 10 MHz crystal. The value of k was determined experimentally by combined microgravimetry and cyclic voltammetry during electrochemical deposition and dissolution of Ag [64]. This was found to be 1.242 ng / Hz, comparable to the theoretical value of 1.249 ng / Hz obtained using the full form of Sauerbrey equation [63].

Quantification of metal deposition rate is useful for mechanistic analysis. This can be expressed as the rate of change of resonant frequency shift d**Δ**f/dt (Hz / s) or as the rate of change in the deposited layer thickness d**τ**/dt (nm / min). If it is assumed that the metal is depositing over the m-TiO_2 layer as a coherent deposit with the density of the bulk metal, these two rates are related as follows:

$$\frac{d\tau}{dt}\left(nm / \min\right) = \frac{0.6k}{A\rho}\frac{d\Delta f}{dt}\left(Hz / s\right) \tag{2}$$

where k is in ng / Hz, A is the piezoelectrically active crystal area in cm^2 and **ρ** is the bulk density of the deposited metal in g / cm^3 (10.5 g / cm^3 for Ag, 11.4 g / cm^3 for Pd).

Chronopotentiometry was conducted using a saturated calomel electrode (SCE) as a reference (EIL, Chertsey, Surrey, UK) and Pt wire of 2.5 x 10^{-4}m Ø, 99.99+% purity (Advent Research Materials Ltd., Halesworth, Suffolk, UK) as a counter electrode.

Quartz crystals were coated with m-TiO_2 via the reverse micellar sol-gel spin-coating method of section 2.5.2. A bespoke stage was fitted to the rotating disk electrode system to hold the crystal. The stage allowed coating of the Au crystal face while masking the contacts at the outer edge. Coated crystals were annealed at 623 K for 1 hour.

EQCM experiments were performed in a ground floor laboratory sited directly on building foundations and isolated from heavy machinery and vibration sources. For experiments conducted under irradiation, monochromated 315 nm light from a 900 W Xe lamp was used to irradiate the crystal face through a quartz beaker. Both Δf and chronopotentiometric measurements were made during (photocatalytically initiated) electroless deposition onto (i) bare, Au-coated quartz piezoelectrodes, (ii) m-TiO_2 coated piezoelectrodes in the dark and (iii) m-TiO_2 coated piezoelectrodes irradiated with 315 nm light. The experimental set-up is in shown in Fig. 3.

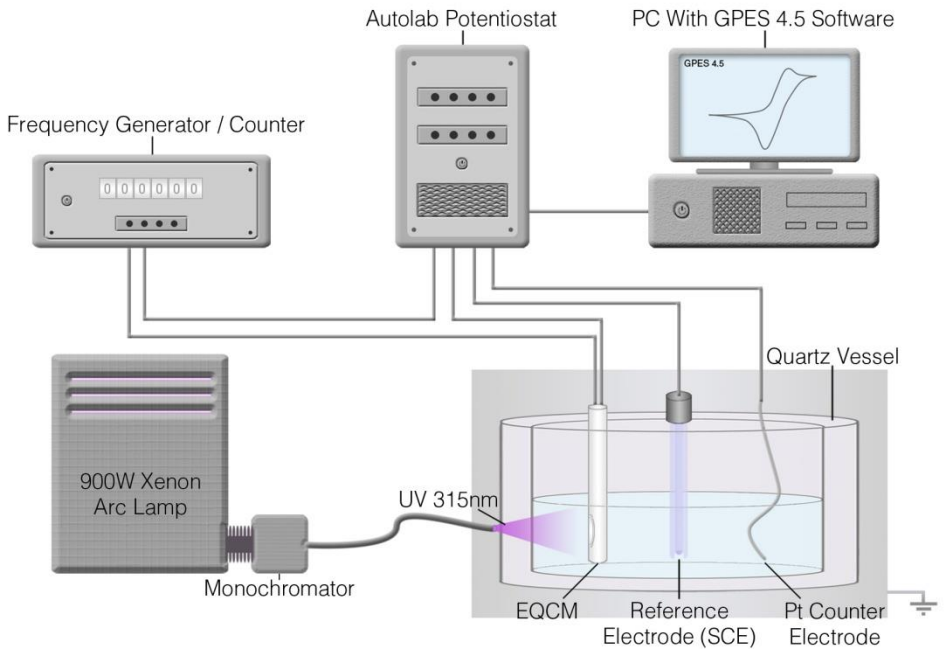

Fig. 3 Schematic of apparatus used for photoelectrochemical studies of PIED using the electrochemical quartz crystal microbalance (EQCM)

2.6 Results and Discussion

2.6.1 Characterisation of m-TiO_2 Layers on Quartz Glass Substrates

Raman spectroscopy (see section 2.S1) and XRD measurements (not shown) show that the films formed on quartz glass substrates and Au piezoelectrodes are predominantly anatase. UV-Vis spectra (section 2.S2) indicate a band gap of 3.54 eV, blue shifted from the bulk value of 3.2 eV as the films are comprised of particles small enough to exhibit the quantum size effect. Atomic Force Microscopy (section 2.S3) indicated a constituent particle diameter of ~10 nm and maximum topographical height of 6 nm. Yu *et al* [59] attribute a maximum thickness of 170 nm to the spin-coated layers.

2.6.2 One-step PIED of Ag and Pd on Quartz Glass and PVDF

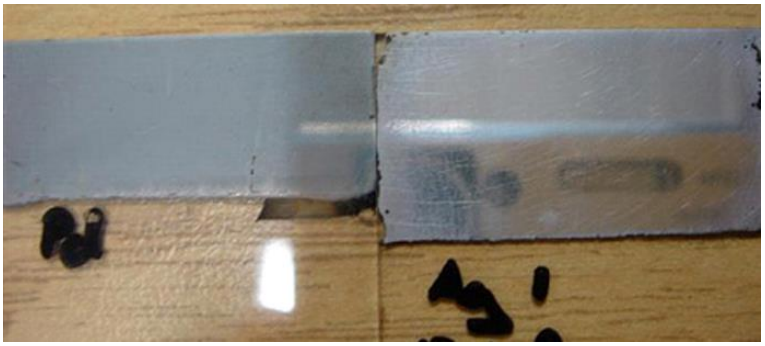

Fig. 4 Pd (left) and Ag (right) deposited by PIED onto the m-TiO_2 sensitised area of quartz slides. Samples irradiated with 315 nm light for 60 min

Using the method of section 2.5.6 and the solution compositions of Table 1 & Table 2, Ag and Pd PIED has been performed successfully on TiO_2 sensitised quartz glass slides. The resultant layers, Fig. 4, are coherent, conductive and display a shiny, mirrored metallic finish. Deposits do not delaminate with adhesion demonstrated via British Standard metal adhesion test BS EN ISO 2819:1995; this involves an adhesive tape being made to stick to the metal layer surface and then pulled away with applied force. The metal layer is said to be adherent to the underlying substrate if it does not fail / delaminate under the said operation. Deposition only occurs on areas both sensitised with TiO_2 and irradiated with ultra-band gap light. Visual

inspection and SEM analysis shows that, even after 2 hours immersion in Ag and Pd electroless plating solutions, no deposition occurs on m-TiO_2–sensitised surfaces in the dark.

Longer deposition times result in thicker deposits, suggesting that extent of metal deposition can be controlled by deposition time. Interestingly, Ag samples prepared using an initial irradiation time of 30 min followed by 30 min deposition in the dark have a similar visual finish to Ag samples prepared by 60 min deposition with irradiation throughout. This is consistent with the suggested mechanism of Fig. 2, wherein PIED occurs in two stages with photo-initiated nucleation being followed by autocatalytic metal deposition. In this context, the plating solution reductant (tartrate for Ag, hydrazine for Pd) participates in both stages, acting as a hole scavenger and then reductant during the first (Fig. 2 (a)) and second (Fig. 2 (b)) stages respectively.

To further investigate the role of irradiation / nucleation time in PIED, m-TiO_2 coated quartz slides were irradiated in Ag electroless plating solution for periods of 0.5, 1, 2, 3, 4 and 5 min, after which they remained immersed in solution in the dark for periods of 5, 10 and 15 min. As above, no deposition occurred on samples that had not undergone irradiation. In contrast however, any period of irradiation >30 s initiated a PIED process that produced coherent layers after a sufficient period of dark growth. Table 3 summarizes simple conductivity measurements of the resultant Ag layers where conductivity is indicated when zero resistance is measured between two conductance probes placed 25 mm apart on the sample surface. Conducting layers were produced when the combined light and dark plating time exceeded ~10 min.

Irradiation time	0.5 min	1 min	2 min	3 min	4 min	5 min
Dark 0 min	x	x	x	x	x	x
Dark 5 min	x	x	x	x	✓	✓
Dark 10 min	x	x	✓	✓	✓	✓
Dark 15 min	✓	✓	✓	✓	✓	✓

Table 3 Summary of conductivity of PIED Ag layers on m-TiO_2 coated quartz.

x = non-conducting ✓= conducting

As discussed above, the irradiation period promotes the formation of Ag nuclei on the TiO_2 surface. SEM images indicate that longer irradiation times and, by implication larger surface concentrations of metal nuclei, lead to metal deposits with a finer grain size and more reflective appearance, Fig. 5 (a), whilst shorter irradiation times and so fewer nuclei sites result in a coarser, more granular deposit structure, Fig. 5 (b). Thus, longer irradiation / nucleation times are needed for higher reflectivity deposits.

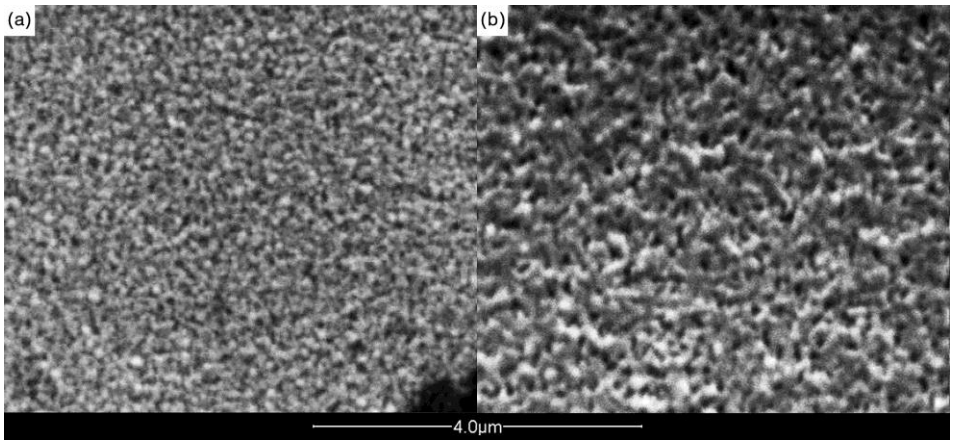

Fig. 5 SEM images of PIED-generated Ag deposit on m-TiO_2 coated quartz slides: (a) after 10 min continuous irradiation; and (b) after 5 min irradiation followed by 5 min growth in the dark

PIED has also been used to deposit Ag, Fig. 6, and Pd onto nanoparticulate TiO_2 sensitised PVDF membranes. In both instances, deposited layers are conducting and metallic in appearance. Deposition can be applied to a single side of the membrane by floating it on the electroless plating solution surface, or on both sides by full immersion. No through membrane deposition or conductivity is observed.

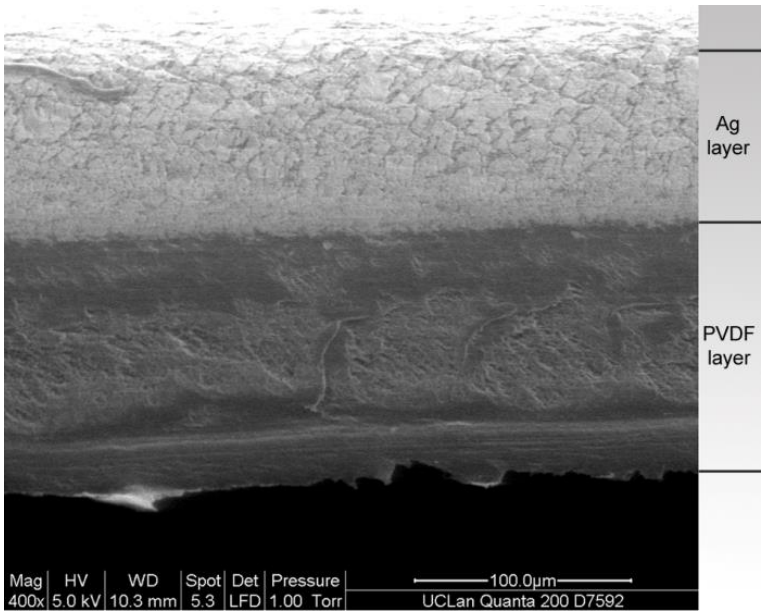

Fig. 6 Cross-sectional SEM image of PIED generated Ag layer on PVDF membrane. Sample prepared by irradiating nanoparticulate TiO_2-sensitised PVDF membrane with 315 nm light for 30 min

2.6.3 EQCM Studies of PIED – Silver

Cyclic voltammetry studies of ferricyannide (not shown) indicate that, once coated with m-TiO_2, approximately 64% of the Au piezoelectrode surface remains accessible to solution through the titania layer. Within the context of EQCM-based studies of PIED, this Au surface accessibility may allow for Ag / Pd metal to be deposited by conventional electroless means onto the underlying Au piezoelectrode during a PIED experiment. Whilst the two effects would then need deconvoluting, the use of such piezoelectrode / TiO_2 composites allows for comparison of the electro-chemical properties of uncoated crystals with those of irradiated and non-irradiated m-TiO_2 coated crystals and thus the elucidation of key mechanistic information.

Using the set-up of Fig. 3, measurements at pH 11.5 show that the mixed potential (E_{mp}) of the Ag / tartrate system is +0.12 V whilst the flat band potential (E_{fb}, measured in-house from the photocurrent onset potential) of m-TiO_2 is -0.65 V. Due to this difference between E_{fb} and E_{mp}, significant band bending and space charge / depletion layer formation would be expected at the semiconductor-electrolyte interface at equilibrium in the dark [65]. At the resultant +0.77 V from flat band, the space charge layer thickness in the TiO_2 will be in the

range 8–20 nm [66], compared to a primary constituent particle diameter of 15 nm [59], suggesting that majority carrier depletion occurs throughout the m-TiO_2 structure.

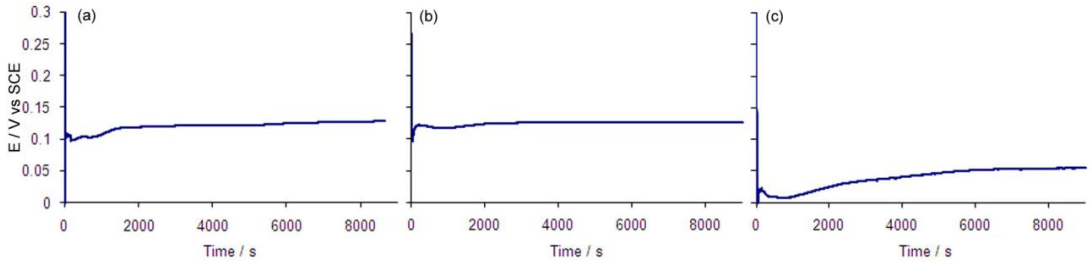

Fig. 7 Chronopotentiometric measurements for Ag PIED on (a) bare Au in the dark (b) m-TiO_2 coated Au in the dark (c) m-TiO_2 coated Au under ultra-band gap irradiation

With these observations in mind, Fig. 7 shows the results of chronopotentiometry conducted during Ag PIED onto (a) a bare Au piezoelectrode in the dark, (b) an m-TiO_2 coated Au piezoelectrode in dark and (c) an m-TiO_2 coated Au piezoelectrode irradiated with 315 nm light. Both dark experiments, where t = 0 corresponds to the immersion of the piezoelectrode into the electroless plating solution, show similar results with a stable potential of +0.12 V as a function of immersion time, indicating that the presence of m-TiO_2 does not significantly affect E_{mp} in the dark. On irradiation, a negative potential shift of 75-100 mV from +0.12 V is observed, Fig. 7 (c) where t=0 corresponds to the onset of irradiation. This may be understood through the action of the reducing agent, tartrate, as an effective TiO_2 hole scavenger, leading to an accumulation of photogenerated electrons within the semiconductor. This causes a negative shift in (E_{mp} - E_{fb}) and an unbending of the bands. We would expect that this, in turn, will facilitate the transfer of photogenerated electrons to Ag (I) in solution and hence enhance the rate of metal nuclei formation (Fig. 2 (a)). We shall return to this point below.

Fig. 8 & Fig. 9 show simultaneously recorded gravimetric results for the samples of Fig. 7. Specifically, they show the recorded frequency change (Δf) and the rate of change of Δf (dΔf/dt) as functions of time, the latter being directly proportional to the metal deposition rate (see section 2.5.7). All three traces in Fig. 8 display a frequency drop corresponding to a mass increase as metal deposition occurs.

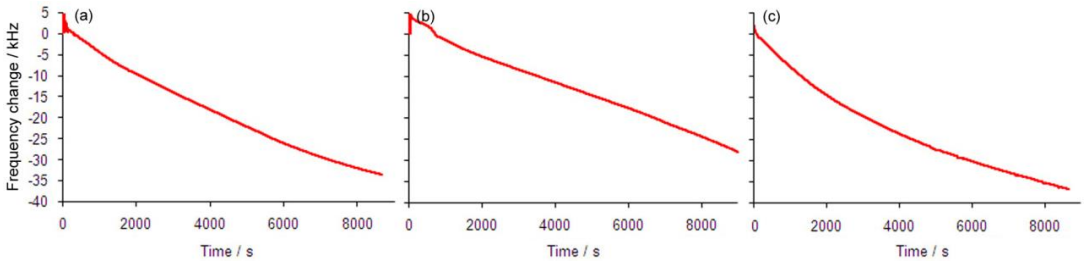

Fig. 8 QCM measurements showing change of frequency (mass) as a function of time for PIED of Ag / tartrate on (a) bare Au in the dark, (b) m-TiO_2 coated Au in dark and (c) m-TiO_2 coated Au in light

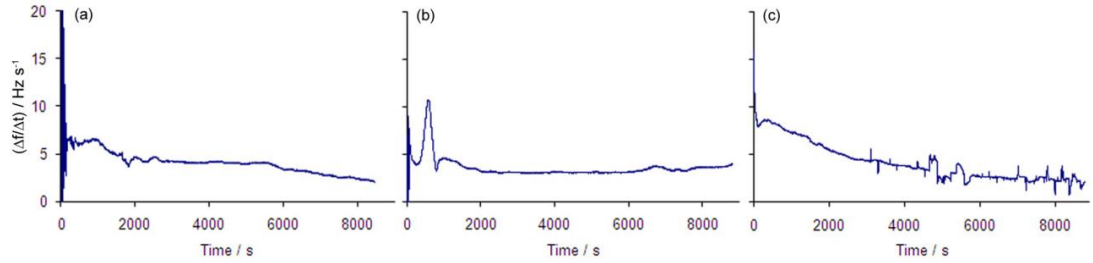

Fig. 9 QCM measurements showing the rate of change of frequency (rate of change of crystal mass) as a function of time for PIED of Ag / tartrate on (a) bare Au in the dark, (b) m-TiO_2 coated Au in dark and (c) m-TiO_2 coated Au in light

As discussed above, no Ag growth occurs at the TiO_2 / solution interface in the dark. Again as discussed above, Fig. 8 (b) indicates that, for m-TiO_2 coated piezoelectrodes in the dark, conventional electroless deposition does indeed occur on the Au that remains accessible to the external solution through the TiO_2 layer. However, from Fig. 9 (a) & (b), the rate of deposition at $t < 500$ s at the bare Au surface is ~50% greater than that seen at m-TiO_2 coated piezoelectrodes in the dark, suggesting that the TiO_2 is partially suppressing the rate of electroless deposition of Ag at the Au surface of the coated electrode by restricting access of the Ag (I) ion to that surface.

Fig. 9 (a) & (c) show that deposition onto the irradiated m-TiO_2 surface and bare Au have similar growth modes. The dark m-TiO_2 trace, Fig. 9 (b), has a feature at around 580 - 800 s indicating a sharp increase in the rate of deposition followed by a sharp decrease and eventually by a steady rate of deposition at $t > 1000$ s. The sharp increase in rate of deposition at $t = 580$ s correlates with the point where growth *through* the TiO_2 layer is complete and Ag growth channels coalesce over the electrode surface. The decrease in rate

at t = 780 s corresponds to the end of this period of lateral growth after which the layer grows perpendicular to the electrode surface and out into solution.

The feature observed at 580 s in Fig. 9 (b) is predictably absent on the bare Au trace, Fig. 9 (a), but is also missing from the trace recorded from an m-TiO_2 coated piezoelectrode under ultra-band gap irradiation, Fig. 9 (c). We attribute this to the fact that, as mentioned, two simultaneous processes are occurring on the latter sample: (i) growth of a deposit by conventional electroless means from the Au electrode / m-TiO_2 interface through the m-TiO_2 layer, as per Fig. 9 (b); and (ii) Ag deposition at the outermost surface of the m-TiO_2 layer through PIED, as indicated by Fig. 7 (c). Comparison of Fig. 9 (c) with (a) leads us to conclude that the latter process dominates in Fig. 9 (c) as a result of (i) a photoinduced increase in electron concentration within the TiO_2 matrix and (ii) the unbending of the bands upon irradiation (*vide supra*), both of which result in an increase in electron access to the semiconductor–electrolyte interface, so increasing the electrochemical activity of the m-TiO_2 / piezoelectrode composite.

Eventually, at t > 2000 s, all three systems grow in the same manner – specifically the metal layer grows into free solution by autocatalytic deposition in a direction perpendicular to the substrate surfaces. This similarity of behaviour is confirmed by the similarity of measured growth rates at t = 6000 s. At these long deposition times, the metal is depositing as a coherent layer over the m-TiO_2 surface – consequently, equation (2) holds and deposition rate can be expressed in terms rate of change of layer thickness with time. Accordingly, on bare Au the growth rate is 1.01 nm / min, on m-TiO_2 in the dark the rate is 0.9 nm / min and on irradiated m-TiO_2 the rate is 0.6 nm / min. This rate is lower than that seen in the dark, possibly due to local depletion of the tartrate concentration at the metal growth front through photocatalytically driven oxidation processes. This growth rate equates to 0.88×10^{-6} g / cm^2 / min which, given the differences in solution composition involved, compares well with that of 1.3×10^{-6} g / cm^2 / min recorded by Kubota and Koura during the electroless deposition of Ag on a Pt electrode pre-sensitised with $SnCl_2$ [67].

2.6.4 EQCM Studies of PIED – Palladium

Chronopotentiometry and gravimetry were also used to monitor PIED of Pd, Fig. 10 and Fig. 11. The chronopotentiometric traces of Fig. 10 show that, at the initiation of deposition, E_{mp} values of −0.699 and −0.703 V are obtained for the bare and m-TiO_2 coated Au piezoelectrodes respectively in the dark. These are significantly negative of the analogous values recorded for the Ag / tartrate system of +0.12 V and are close to the measured E_{fb} of m-TiO_2 of −0.65 V. A measure of the thermodynamic driving force for metal deposition can be obtained by subtraction of the metal E^0 value from E_{mp}. This gives a driving force / overpotential of −1.3 V for Pd and −0.45 V for Ag, a difference reflected in the rates of deposition determined from Fig. 9 and Fig. 11.

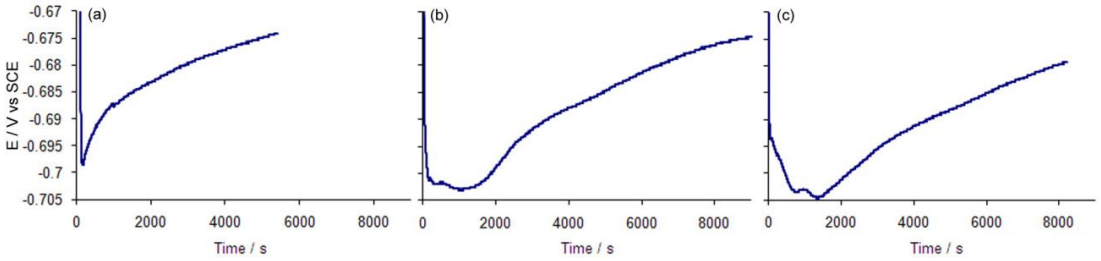

Fig. 10 Chronopotentiometric measurements for Pd PIED on (a) bare Au in the dark, (b) m-TiO_2 coated Au in the dark and (c) m-TiO_2 coated Au under ultra-band gap irradiation

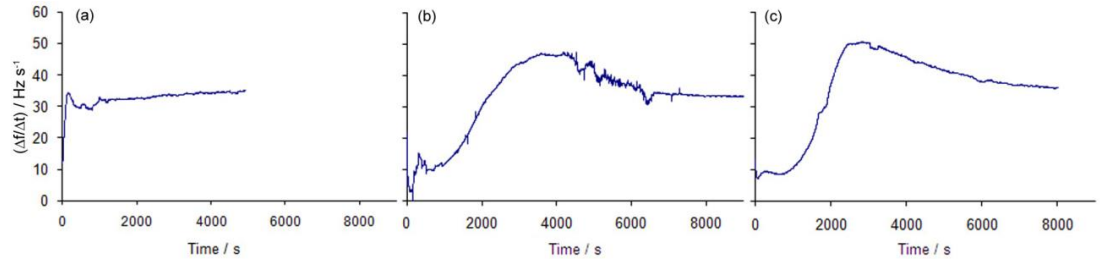

Fig. 11 QCM measurements showing the rate of change of frequency (mass) as a function of time for PIED of Pd on (a) bare Au in the dark, (b) m-TiO_2 coated Au in dark and (c) m-TiO_2 coated Au in light

From Table 1 & Table 2, it can be seen that the concentration of Pd is twice that of Ag in their respective plating solutions. However, comparison of Fig. 9 and Fig. 11 indicates that peak deposition rates obtained from the Pd/hydrazine system at m-TiO_2 coated piezoelectrodes are at least 4.5× and up to 16× greater than those for the Ag / tartrate system. Specifically, peak rates for the Ag system are 9.9 Hz / s (from Fig. 9 (b)) and 6.7 Hz / s (Fig. 9 (c)) in the

dark and light respectively, whilst peak rates for the Pd system are 49 Hz / s (Fig. 11 (b)) and 56.8 Hz / s (Fig. 11 (c)) in the dark and light respectively. Steady state rates at t > 6000 s (where Eq. (2) holds, *vide supra*) show similar trends where, from above, rates for Ag deposition are 3.56 Hz / s or 0.9 nm / min on m-TiO_2 in the dark and 2.4 Hz / s or 0.6 nm / min and under irradiation. Analogous rates for the Pd system are 37.4 Hz / s or 8.7 nm / min in the dark and 40.9 Hz / s or 9.5 nm / min under irradiation. The enhancement in Pd deposition rate with respect to Ag is at least in part derived from the difference in E_{mp} values observed, these in turn being determined by the reducing power of the reductant employed. That a difference in the steady state deposition rate can be seen on variation of thermodynamic driving force for metal ion reduction indicates that, at the very least, Ag deposition in the Ag / tartrate system is under electrochemical control.

Irradiation of the m-TiO_2 coated piezoelectrode with 315 nm light generates a small, 5 mV potential shift to −0.704 V, Fig. 10 (c), from which the system then gradually recovers. Again, this is in contrast to the Ag / tartrate system, where a significantly larger change in E_{mp} of 75 – 100 mV occurs upon irradiation (Fig. 7 (a)). Given the proximity of E_{mp} for the Pd / hydrazine system to the flat band potential of −0.65 V of our m-TiO_2, we would expect little to no band bending in the dark, that which does exist leading to the formation of a very shallow accumulation layer. Further, given the small change in E_{mp} upon irradiation, we expect little difference in the light with virtually no photogenerated band bending superimposed on the putative shallow accumulation layer formed in the dark. This accumulation layer might be expected to lead, in the dark or light, to greater ease of access of majority charge carriers to the semiconductor–electrolyte interface in the TiO_2 / Pd / hydrazine system compared to the TiO_2 / Ag / tartrate system, so enhancing the rate of nucleation (Fig. 2 (a)) and, ultimately, deposition (Fig. 2 (b)). However, this will be offset by the shallowness of the band bending providing little driving force for photogenerated charge separation in the TiO_2 / Pd / hydrazine system, resultant recombination suppressing the free electron concentration and the so the nucleation rate of Fig. 2 (a). This lower nucleation rate notwithstanding, the more negative value of E_{mp} in the

Pd / hydrazine system compared with the Ag / tartrate system will, in the case of the former, produce higher rates of autocatalytic deposition (Fig. 2 (b)) at those nucleation centres that do form. This accelerated rate of deposition at fewer nucleation centres in the Pd system would be expected to give rise to a more granular, less reflective deposit than in the Ag system with its faster rate of (charge separation assisted) nucleation and slower (tartrate driven) autocatalytic growth. Comparison of the photographs of PIED derived Ag and Pd layers of Fig. 4 shows that this is indeed what is seen, an observation that is further supported by comparison of the SEM images of Fig. 12.

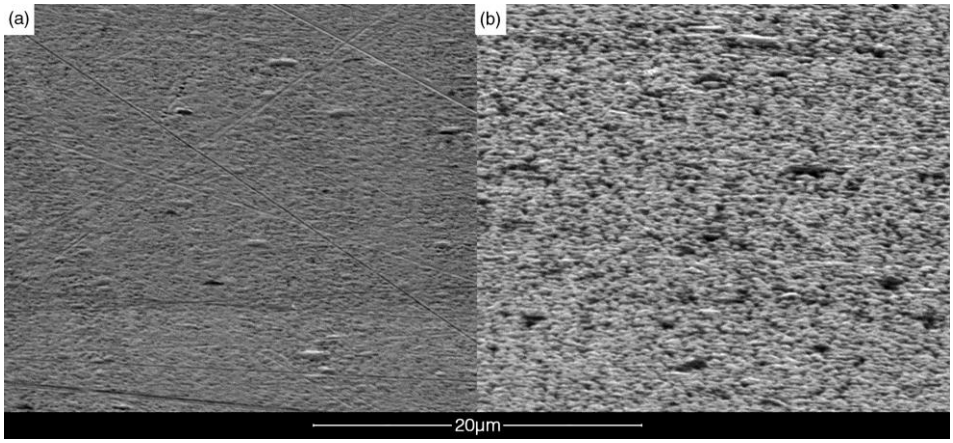

Fig. 12 SEM images of (a) an Ag deposit and (b) a more granular Pd deposit, generated by PIED on m-TiO_2 coated quartz slides. Samples irradiated with 315 nm light for 3600 s

In light of the preceding relating to the Pd system and the earlier discussion of the Ag system, the form of the QCM traces of Fig. 11 may be understood as follows. For the uncoated piezoelectrode in the dark, Fig. 11 (a), there is first an induction period of ~40 s during which conventional Pd-on-Au nucleation is initiated, a phenomenon typical of most electroless deposition processes. This is then followed by a period of deposition rate acceleration, reaching a peak at ~200 s, as nucleation sites are formed and nucleate growth begins. Finally, at t > 200 s, the rate decreases as nuclei coalesce through lateral growth and precursor metal ion depletion occurs into solution. Once the surface is covered, deposition reaches a stable rate determined by the balance between E_{mp} controlled electrochemical kinetics and mass transfer.

Analogous processes occur at the m-TiO_2 coated piezoelectrodes. A period of Pd-on-Au nucleation at the TiO_2 / Au interface at t < 400 s (most clearly seen in Fig. 11 (c)) is followed by a period of steady Pd layer growth / deposition through the m-TiO_2 layer. At t < 1000 s, the dΔf/dt vs. time plots of Fig. 11 (b) and (c) clearly show suppression in rate of deposition at m-TiO_2 coated compared to bare piezoelectrodes, Fig. 11 (a). As in the Ag results of Fig. 9, this is due to the inhibition of solution phase mass transport of Pd (II) to the Au surface in the presence of the m-TiO_2 layer.

At t > 1000 s, in both light and dark, the m-TiO_2 coated samples show an acceleration in deposition rate as the deposition fronts emerge from the mesoporous structure of the TiO_2 and growth channels spread laterally across the semiconductor, coalescing to form a coherent metal surface. Once coalescence is complete, characterised by a peak in the deposition rate, the deposition rate relaxes to a stable rate as per the uncoated piezoelectrodes. As discussed above with relation these steady state rates for the Pd system can be as much as 8–16× greater than the equivalent rates for the Ag system, due in no small part to the greater reductive power of hydrazine compared to tartrate.

As per the Ag system, two simultaneous processes are occurring in the Pd deposition experiments of Fig. 11: (i) deposit growth by conventional electroless means from the Au electrode/m-TiO_2 interface and (ii) metal deposition at the m-TiO_2 / solution interface through PIED. Comparison of Fig. 11 (c) and (b) indicates that, in contrast to the Ag/tartrate system, the former process is dominating in Fig. 11 (c).

This is not to discount a contribution by PIED to the result of Fig. 11 (c). In the dark, the peak deposition rate of 49 Hz / s on coated electrodes is reached at ~4000 s whilst under irradiation the peak rate of 56.8 Hz / s is reached after ~2800 s. This is consistent with a PIED enhancement in the nucleation / deposition rate running in parallel with conventional electroless deposition occurring at the Au / TiO_2 interface. As indicated by Fig. 4 and Fig. 12, PIED is fully effective in the generation of Pd layers on wholly insulating substrates where it will be the only initiating process.

2.7 Conclusions

We report a novel one-step photocatalytically initiated electroless deposition (PIED) process that allows for the photogeneration of coherent and conducting metal layers on semiconductor sensitised insulator surfaces. Deposition occurs only onto those areas of the substrate both sensitised with TiO_2 and irradiated with ultra-band gap light, so suggesting the future development of PIED driven photo-microlithography. PIED obviates the need for Sn–Pd activation catalysts so eliminating contamination from prior nucleation whilst the fewer steps and materials required provide a cheaper, environmentally cleaner and (through variation of incident light intensity) more controllable option than the traditional techniques of dielectric plating. Using PIED, Ag and Pd layers have been generated on m-TiO_2 coated quartz and PVDF substrates.

Through judicious choice of a hole scavenger that can also act as a reductant in an electroless deposition process, the PIED process allows for the metal nucleation and growth stages to be conducted simultaneously. The former process is driven by photocatalytically promoted metal ion reduction, whilst the latter proceeds auto-catalytically on the resultant metal nuclei. SEM and EQCM studies indicate that the morphology and appearance of the resultant metal layer is strongly dependent upon the nucleation density arising during the primary photocatalytic stage of PIED. High nucleation density and a slow nuclei growth rate, such as obtained on m-TiO_2 sensitised surfaces in the Ag / tartrate electroless plating system, result in a smooth, reflective layer. A lower nucleation density combined with fast nuclei growth, as in the Pd / hydrazine system, results in a less reflective and often dull grey metal surface.

In the case of Ag deposition using a tartrate reductant, mixed potential (E_{mp}) measurements at m-TiO_2 coated Au piezoelectrodes indicate that E_{mp} shifts by up to −100 mV upon irradiation during PIED. This would be expected to lead to an unbending of bands within the semiconductor matrix, enhancing the availability of photogenerated electrons at the semiconductor surface with a consequent increase in metal nucleation rate.

QCM measurements confirm that this is indeed the case with photo-initiated nucleation rates being larger than those seen on bare metal substrates. In the case of Pd deposition using a hydrazine reductant, E_{mp} measurements at m-TiO_2 coated Au piezoelectrodes indicate that the TiO_2 layer is at near flat band in both the dark and when irradiated with ultra-band gap light. The resultant lack of driving force for charge carrier separation leads to a higher recombination rate for this system compared to that of Ag with a consequent lower rate of photo-initiated nucleation, as determined by microgravimetry. This lower nucleation density, combined with the rapidity of growth afforded by hydrazine reductant (indicated by QCM experiments), results in the Pd deposit having a coarser morphology than that of the Ag deposit. In light of the above, we can conclude that high reflectivity deposits with small grain sizes are favoured by (i) high nucleation rates and consequent high nuclei densities (achieved through use of good hole scavengers and long irradiation times) and (ii) slow nuclei growth rates (achieved through use of hole scavengers that are poor reductants in conventional electroless deposition processes). The thickness of the final deposit can be controlled through the deposition (as opposed to irradiation) time.

2.8 Acknowledgements

The authors wish to thank the organizers of SP-3 for the invitation to submit this paper. The authors also wish to thank the Royal Society of Chemistry UK for studentships for MAB and SG, and Sellafield Ltd, the Nuclear Decommissioning Authority (NDA) and The Lloyds Register Educational Trust for financial support. The Lloyds Register Educational Trust is an independent charity working to achieve advances in transportation, science, engineering and technology education, training and research worldwide for the benefit of all.

APPENDIX

SUPPLEMENTARY INFORMATION

2.S1 Raman Spectroscopic Characterisation of m-TiO_2 Films

Raman spectroscopy allows the study of the vibrational modes within a sample. The pattern of these modes and related Raman scattering can then be interpreted to identify specific molecular arrangements. In this case Raman was used to determine the crystalline phase of the m-TiO_2, *i.e.* anatase or rutile. Factor group analysis shows that anatase has the following six Raman active vibration modes; A_{1g} + 2 B_{1g} + 3 E_g [68]; while Ohsaka has reported the Raman spectrum of a single anatase crystal, showing that the six modes appear at 144 / cm (E_g), 197 / cm (E_g), 399 / cm (B_{1g}), 513 / cm (A_{1g}), 519 / cm (B_{1g}) and 639 / cm (E_g) [69]. In contrast, rutile has four raman active modes; A_{1g} + B_{1g} + B_{2g} + E_g, appearing at 143 / cm (B_{1g}), 447 / cm (E_g), 612 / cm (A_{1g}) and 826 / cm (B_{2g}) [70]. This information is summarized below in Table 4.

Raman active bands of anatase TiO_2		Raman active bands of rutile TiO_2	
Mode	Wavenumber / cm	Mode	Wavenumber / cm
E_g	144	B_{1g}	143
E_g	197	-	-
B_{1g}	399	-	-
-	-	E_g	447
A_{1g}	513	-	-
B_{1g}	519	-	-
-	-	A_{1g}	612
E_g	639	-	-
-		B_{2g}	826

Table 4 Active bands in the Raman spectra of anatase and rutile TiO_2

As the Raman laser interacts with the sample, a small amount of light is scattered through excitation. As excited molecules relax they return to a slightly different vibrational or rotational state and hence the wavelength of the emitted photon is altered in what is termed a Stokes

shift. Raman spectra of our m-TiO_2 films, Fig. 13, exhibited no Stokes lines at Raman shifts of 447, 612 and 826 / cm, indicating that the sample contains no rutile. Stokes lines were observed at Raman shifts of 143, 398, 515 and 640 / cm, each corresponding to those expected for anatase TiO_2. Further, close inspection of the spectra indicates that the asymmetry of the line at 143 / cm may be obscuring a 6th line at ~200 / cm while the feature at 515 / cm may be comprised of two lines at 513 and 519 / cm. We therefore assign the crystalline phase to being that of anatase. This is in good agreement with XRD measurements conducted by Yu *et al* on similarly prepared samples [59] from which they conclude that these films are polycrystalline anatase, exhibiting preferential orientation in the (101) direction.

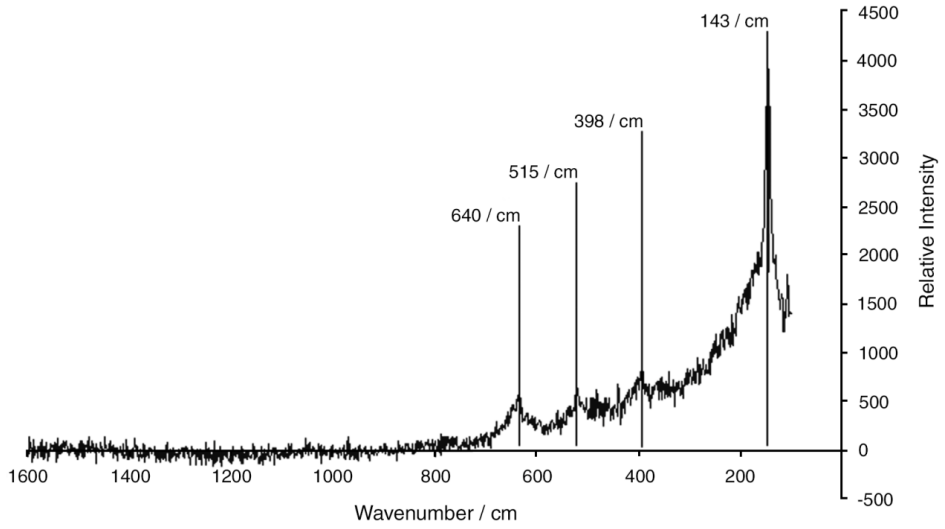

Fig. 13 Raman spectrum of m-TiO_2 film on a planar quartz substrate

2.S2 UV-Visible Spectroscopic Characterisation of m-TiO_2 Films

UV-Visible spectroscopic analysis was performed to assess the absorption of light energy by the m-TiO_2 as electrons are elevated from the valance to conduction band and hence provide an indication of the semiconductor band gap. The UV-Vis spectra of our m-TiO_2 films, Fig. 14, demonstrate additional agreement with the results of Yu *et al* [59] in that the films exhibit no absorbance in the visible with a rapidly increasing absorbance with decreasing wavelength below 350 nm. This corresponds to a band gap of 3.54 eV.

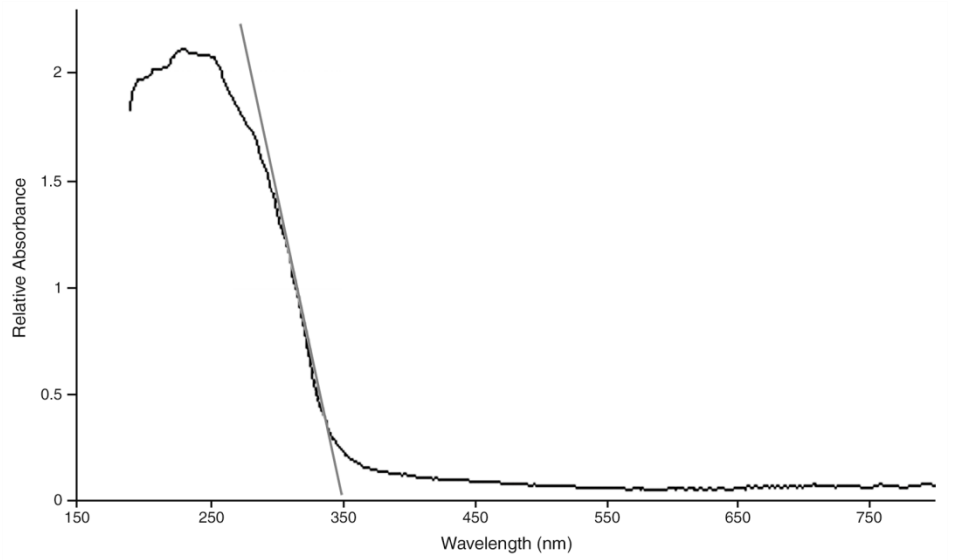

Fig. 14 UV-visible absorption spectrum of m-TiO_2 film on a planar quartz substrate

2.S3 AFM Characterisation of m-TiO_2 Films

AFM analysis of m-TiO_2 layers, Fig. 15 reveals a rough surface topography with a maximum height range of 14.35 nm. Surface roughness analysis provides average roughness, R_a, and root mean square roughness, R_{rms}, values of 1.34 nm and 1.68 nm respectively. For a projected area of 1.00 μm^2, the 3-dimesional area is measured to be 1.10 μm^2, an increase of 10%, demonstrating that the mesoporous structure of the TiO_2 layer offers an increased surface area over a theoretically smooth substrate.

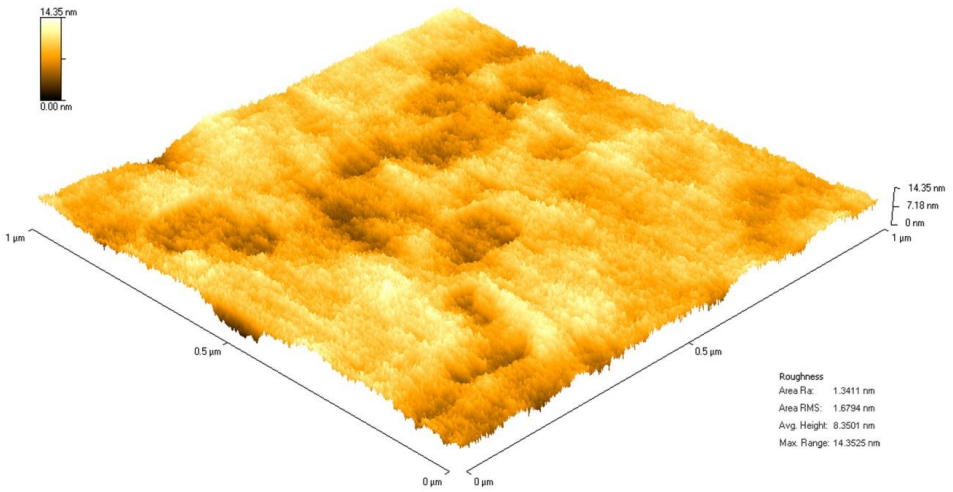

Fig. 15 3-dimensional contact mode AFM image of m-TiO_2 annealed at 773 K

2.S4 AFM Characterisation of TiPE TiO_2 Films

AFM analysis of TiPE G500 layers shows a clear difference between layers formed from the TiPE nanoparticulate suspension, Fig. 16, and those formed from m-TiO_2 sol-gel, Fig. 15. The surface topography, while broadly undulating, appears considerably smoother and has a reduced maximum height range of 11.25 nm. Surface roughness analysis provides smaller R_a and R_{rms} values of 1.24 nm and 1.57 nm confirming a reduced roughness in comparison to the m-TiO_2 film. This is further demonstrated by the 3-dimesional surface area of 1.01 μm^2 for a projected area of 1.00 μm^2; a significantly lower surface area than that of m-TiO_2 over the same space. This lesser surface area and reduced roughness of TiPE films may be of consequence to the adhesion of subsequently deposited metal layers as the smoother TiPE layers may be expected to provide less adhesion for the metal film than the rougher m-TiO_2.

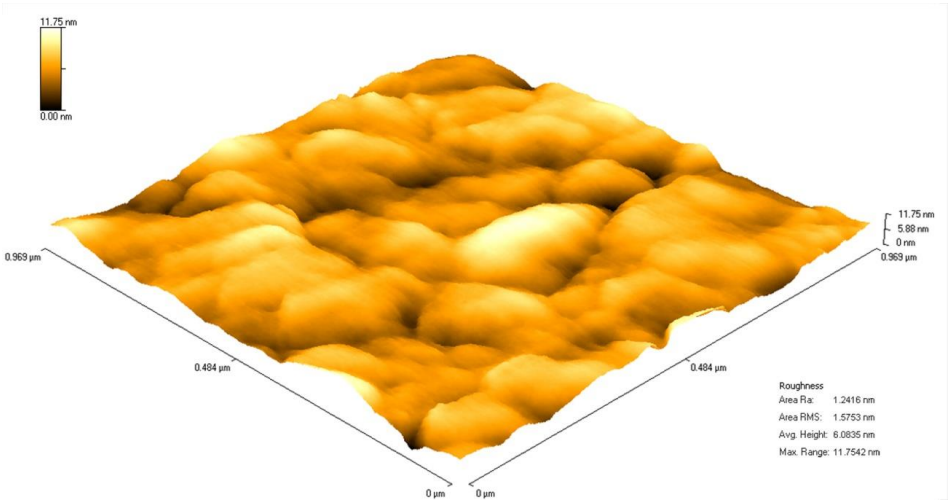

Fig. 16 3-dimensional contact mode AFM images of TiPE G500 annealed at 773 K

CHAPTER 3

SEMICONDUCTOR PHOTOCATALYSIS AND METAL DEPOSITION

J.C.Taylor (Ed.), *Advances in Chemistry Research*. Volume 13, Nova Science Publishers Inc., Hauppauge, New York, 2012, Chapter 2

ISBN: 978-1-62100-562-9 (ebook) 978-1-62100-519-3 (hardcover)

Michael A. Bromley, Colin Boxall*

Engineering Department, Lancaster University, Lancaster LA1 4YR, UK

"Don't do anything that affects anything, unless it turns out you were supposed to do it, in which case for the love of God, don't not do it!"

Prof. Hubert J. Farnsworth

3.1 Publication Summary

- Invited chapter contribution to Advances in Chemistry Research, Vol. 13
- Review of related prior art in photocatalytic metal deposition
- Detailed report of the photocatalytic nucleation and auto-catalytic deposition processes
- Investigation of the effect of varying the periods of irradiated and non-irradiated immersion
- Investigation of metal deposition control factors
- The applicability of PIED to the deposition of other metals such as Ni is explored

3.2 Author Contributions

- M.A.B.: designed and performed all experiments, analysis and characterisation; primary author of the manuscript from first draft to final proof
- C.B.: conceived and supervised the study; co-author of manuscript through review of draft

3.3 Abstract

Semiconductor photocatalysis has many, varied applications with frequent research in environmental areas such as pollution abatement, heavy metal recovery, water and air purification and the destruction of microorganisms as well as hydrogen production from water, corrosion inhibition and self-cleaning surfaces. However, another field with considerable scope lies in the use of photocatalysis for metal deposition.

Photocatalytic metallisation of semiconductor surfaces is an established technology that has been employed predominantly to improve and enhance the photocatalytic properties of the semiconductor, a process known as doping. This review examines the use of semiconductor photocatalysis in driving conventional metal deposition techniques, in photocatalytic sensitisation of substrates prior to a further electroless deposition step and its potential utility in the initiation of electroless metal deposition for the formation of complete metal layers. The latter will focus particularly on the recently developed Photocatalytically Initiated Electroless Deposition (PIED) process, a one-step metal deposition process which utilises photocatalysis to directly metallise insulating substrate surfaces. The process is spatially selective and offers several advantages over traditional, non-photocatalytic techniques such as enhanced controllability and purity of the deposit as well as being operationally cheaper and environmentally cleaner with reduced material requirements and fewer preparation steps.

PIED has been successfully utilised to produce layers of various metals including Ag and Pd on mesoporous TiO_2 (m-TiO_2) coated quartz glass slides and polymer substrates. Such metallised insulating materials have potentially wide applications in membrane and separation technology, electrode / solid electrolyte composites for energy storage and fuel cells.

3.4 Introduction

3.4.1 Metal Deposition

The deposition of metals onto other surfaces has long been utilised to modify and enhance various materials. Most frequently this is done with the use of an electric current to reduce metal ions in solution and deposit them onto an electrode surface in a process known as electroplating or electrodeposition. The most common example of this is galvanisation, a process widely used for corrosion protection. As electrodeposition requires the flow of electricity, it is wholly limited to use on conducting surfaces. However, it may regularly be desirable to deposit metal onto non-conducting materials, something which may be achieved by electroless deposition.

Electroless deposition is a plating process in which metal ions are deposited from solution onto a substrate through their reduction by a chemical reducing agent [7]. It is most commonly performed with metals such as Cu, Ni, Co and precious metals with plating solutions being typically comprised of the metal salt, a reducing agent, a buffer and complexing agents to stabilise the metal ion with respect to unwanted deposition processes. As electroless deposition is independent of electrical current it can be used to deposit metals onto an insulating surface. The reaction is, however, dependent on catalysis of metal ion reduction by the substrate surface while, in order to achieve metallisation of only the desired target areas, deposition elsewhere is minimised. The deposited metal must also catalyse the reduction if further deposition is to occur when the target substrate surface is completely covered [9].

As the substrate surface is required to catalyse metal reduction, electroless plating usually involves several sensitisation steps before the deposition process can take place, Fig. 17 (a,b) [9,10]. Typically a catalytic metal such as Pd is seeded onto the substrate, usually in a two step process, Fig. 17 (a). In this, the substrate is first pre-sensitised by application of a solution of $SnCl_2$ in hydrochloric acid resulting in the adsorption of Sn^{2+} ions to the surface. This is followed by treatment with a $PdCl_2$ solution in hydrochloric acid during

which Sn^{2+} ions on the surface reduce solution Pd (II) ions to form nucleation deposits of Pd metal on the substrate surface [9]. In an improvement to this, Fig. 17 (b), the sensitising and nucleating ions are combined in a single solution. This results in adsorption of Sn-Pd particles with the Sn then removed with concentrated HCl to expose the Pd catalyst [11]. Each method has disadvantages; the sensitisation processes must be repeated several times to achieve a sufficiently catalytic surface, which can be costly and time consuming; lengthy surface preparation involving cleaning, etching and neutralising is required to promote bond formation; and the resulting metal deposit will contain Pd and Sn, the latter being a particularly troublesome impurity for electrochemically based applications.

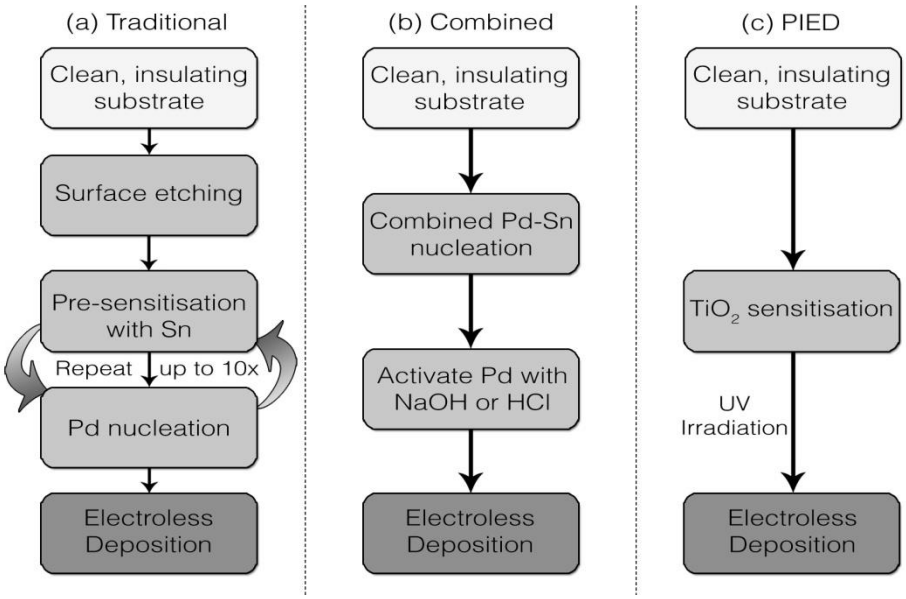

Fig. 17 Flow diagrams for electroless deposition routes involving: (a) sequential Sn-Pd sensitisation; (b) combined Sn-Pd sensitisation; (c) photocatalytic initiation (PIED).

As an alternative to electrochemical sensitisation, metallic nuclei may be generated photochemically, Fig. 17 (c). Photochemical sensitisation involves photon absorption by a semiconductor to generate electron-hole pairs. The photogenerated electrons may then take part in redox reactions with local species, such as metal ions in solution, so generating metal nucleation centres directly onto the semiconductor surface. This may be employed as photo-induced nucleation with final metal deposition performed separately or as a complete, one-step surface metallisation method such as in Photocatalytically Initiated Electroless Deposition (PIED), a process which will be discussed in more detail later.

3.4.2 Semiconductor Photocatalysis

Photocatalysis is a complex process involving the generation of charge carriers within a semiconductor material through the application of energy, usually in the form of light. With no availability of reactants, the photogenerated electron-hole pair may undergo recombination but, given appropriate conditions, the photocatalytic effect can be sufficient to drive redox reactions with species on the semiconductor surface or in local solution if the process is thermodynamically viable [12]. Given the generic nature of this process, semiconductor photocatalysis has found use in many, varied applications.

TiO_2 in particular has been studied throughout the 20^{th} century with a focus on its utilisation for photocatalysis of interfacial redox reactions such as pollutant destruction, chemical synthesis and energy production [71]. The 21^{st} century has seen a movement towards optimisation with the design of TiO_2 nanostructures for high degrees of hydrophilicity [72,73] and modifications for visible light sensitivity [74-79].

However, the photocatalysis of redox reactions for the aforementioned processes is the area which still commands the widest range of scientific research including environmental studies such as pollution abatement in air and water [80-83], purification of drinking water [84-87], treatment of wastewater [86,88-91], air purification [92-97], laboratory scale abatement [82,98,99], the reduction of organic pollutants [100-104], the reduction of inorganic pollutants [105-107], the photocatalytic oxidation of organic pollutants by O_2 [15,81,108], destruction of gaseous organic pollutants and photo-deodourisation [92,109]; energy production areas such as fuel generation using visible light [110,111], photoelectrochemical cells for water splitting [112-116], photoelectrochemical cells for electricity production [115,117,118] and biocidal applications such as the destruction of bacteria [119,120], viruses [121], killing malignant cancer cells [122] and self-sterilising surfaces [92,123]. With an ever increasing range of studies in areas such as these, it remains surprising that the field of photocatalytic metal deposition has not been as widely exploited.

For the context of electroless metal deposition, we are primarily interested in n-type semiconductors as the excess of electrons are important in the reduction of metal ions. Furthermore, certain intrinsic semiconductors, such as TiO_2, ZnO and MoO_3, naturally exhibit n-type properties [124] and as such are particularly appealing as they forgo the need for doping and allow for the deposition of a purer metal layer.

3.4.2.1 Band Edges

In semiconductors, the conduction and valence band edges, E_{cb} and E_{vb} respectively, represent the potential energy of photogenerated electrons, e^-_{cb}, and holes, h^+_{vb}, and determine the thermodynamic viability of photocatalytic reactions in which they may be involved, Fig. 18.

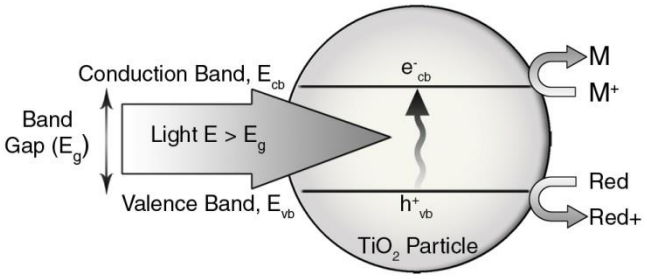

Fig. 18 Charge transfer at excited photocatalyst particle.

Without kinetic complications, the interfacial charge transfer reactions occurring at irradiated semiconductor particles can be summarised as follows:

$$\begin{aligned} e^-_{cb} + Ox &\rightarrow Ox^- \\ h^+_{vb} + Red &\rightarrow Red^+ \end{aligned} \tag{3}$$

As such, the energetic requirements for these reactions to occur spontaneously are:

$$\begin{aligned} E_{cb} &> E\left(Ox/Ox^-\right) \\ E_{vb} &< E\left(Red/Red^+\right) \end{aligned} \tag{4}$$

The energy of photogenerated electrons in the conduction band must be greater, or the electrode potential more negative, than the Nernst level associated with the Ox / Ox^- redox

system. Similarly, the energy of photogenerated holes in the valence band must be less, or the associated potential more positive, than the Nernst level associated with the Red / Red^+ redox system.

As the semiconductor band gap is given by:

$$E_g = E_{cb} - E_{vb} \tag{5}$$

Equations (3) and (4) allow us to derive the following expression of the minimum semiconductor band gap required for spontaneous photoelectrolysis:

$$E_g = E\left(Ox/Ox^-\right) - E\left(Red/Red^+\right) \tag{6}$$

The band edges and band gap energies of a range of semiconductors, determined by measurement of the potentials in aqueous electrolyte solutions at pH 1, are shown in Fig. 19 [110]. TiO_2 displays a potentially useful band gap of 3.2 eV which corresponds to the energy of light in the near UV *i.e.* $\lambda \leq$ ~390 nm. Also, given that the conduction band edge of many metal-oxide semiconductors in aqueous solution is known to shift by -59 mV per pH unit increase [125,126], it should be expected to offer a strong photogenerated driving force for reduction reactions in the basic conditions typical of most electroless plating environments.

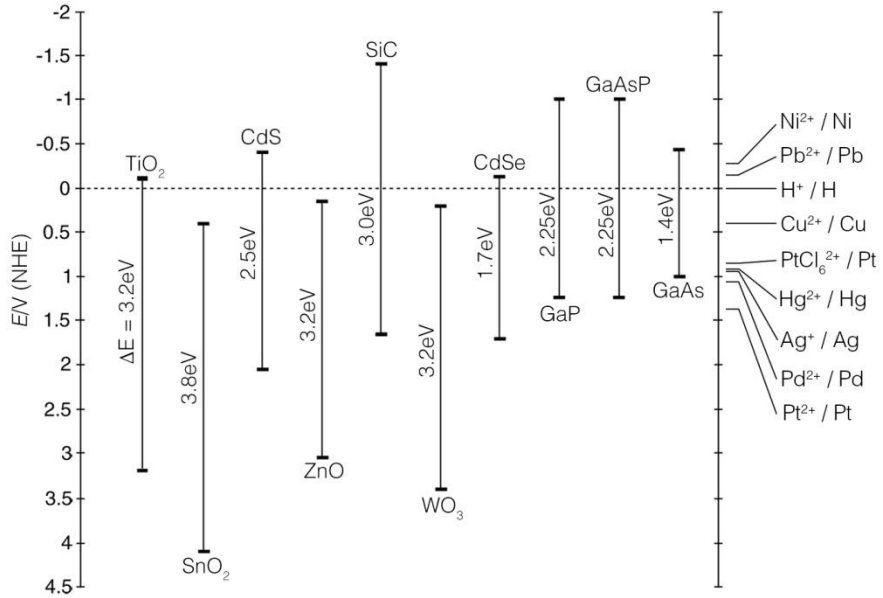

Fig. 19 Band edge position of various semiconductors at pH =1 [110]

3.4.2.2 Space Charge Layers and Band Bending

Whilst the band edges may control the thermodynamics of electron transfer, the kinetics of the charge transfer properties of semiconductors are dependent on whether an accumulation or depletion layer is formed within the material. When a semiconductor is placed in an electrolyte solution, space charge layers, extending 10 – 1,000 nm into the material depending on doping density, may form at the solid / liquid interface as a result of the transfer of electrons into or out of the semiconductor. Space charge influences both physical and chemical properties at the interface including charge carrier recombination, photovoltaic effects and electrode reactions involving interfacial charge transfer between the semiconductor and the electrolyte, the lattermost being critical to the application of photocatalysis to metal deposition.

As mentioned above, the space charge layer can manifest itself as either an accumulation or depletion layer. In n-type semiconductors, the majority charge carrier (electrons in the case of n-type semiconductors) accumulation layer produced at potentials negative of flat band potential, E_{fb}, enables the material to act as a cathode both in darkness and under irradiation. At potentials positive of E_{fb}, the electron depletion layer means that there is a majority charge carrier (electrons) deficit and, without energy input, charge transfer occurs very slowly or may be completely stopped. However, as irradiation promotes electrons to the conduction band, the depletion effect is counteracted and a photo-induced current is observed. Irradiated n-type semiconductors can therefore be considered both as photoanodes and photocathodes, so presenting the opportunity for a controlled initiation of electroless metal deposition.

3.4.2.3 Interfacial Charge Transfer

Interfacial charge transfers can occur in one of two ways; firstly via transfer with a reactant which is adsorbed directly onto the semiconductor surface through a process known as static quenching, or through dynamic quenching in which the charge transfer occurs directly to a reactant which remains free in solution. Each of these transfer processes may occur

during photocatalytic metal deposition although the former is more desirable than the latter. Static quenching will lead to the desired effect of direct metallisation of the semiconductor surface to produce a cohesive and well adhered metal layer. In contrast, dynamic quenching may result in the formation of metal particles, as will be discussed below, in solution which in turn produces electroless bath instability and decomposition.

3.5 Photocatalytic Metal Deposition

As well as the wide range of applications described in section 3.4.2 above, semiconductor photocatalysis has also found use in metal deposition with photocatalytic deposition established as early as 1969 [17,18]. However, the uses of photocatalysis in metal deposition remain surprisingly limited and are often merely used as a subsidiary process within other, wider areas of application. The more common of these areas are described as follows.

3.5.1 Photoreduction of Metal Ions

The use of photocatalysis in pollution abatement has naturally expanded to include the reduction of metal ions for their removal from solution: Tanaka *et al* describe the photoreduction of Pd^{2+}, Mn^{2+}, Tl^{+} and Co^{2+} [19]; Herrmann *et al* report similar photoreduction of Ag^{+} [20]; more recently, Kanki *et al* describe the photoreduction of Cu^{+} [21]. Each of these methods uses TiO_2 powder added to a solution for the purpose of photocatalytically removing metal ions - hence the focus remains on metal extraction rather than the metallisation of the semiconductor or the formation of a coherent metal layer thereon. Despite this, these and related works describe and enhance the understanding of several characteristics of the photocatalytic metal deposition process. The initial metal deposition is understood to be proportional to the radiant flux of photons absorbed by the TiO_2. It is also observed that the initial metal particles formed are approximately 3.8 nm in diameter, increasing in size with further deposition to around 400 nm [20]. Without an interest in surface metallisation, the possibility for merging the deposited particles into complete films was not investigated but the principles of photocatalytic metal deposition have been clearly demonstrated.

3.5.2 Metal Incorporation

Perhaps the most frequent combination of metals and semiconductors is that of doping, *i.e.* the incorporation of select metal particles, such as Pt, Pd, Ag and Au, into the semiconductor lattice in order to introduce energy levels within the band gap. The effect of this is to change the distribution of electrons within the solid and concurrently the behaviour of the semiconductor. Doping is often used to optimise a semiconductor photocatalytically by shifting band edge absorption [22], inhibiting charge carrier recombination [23] or encouraging charge transfer [24]. As doping involves the inclusion of metal particles within the semiconductor structure, the process of formation is typically based around an impregnation method such as the addition of the desired metal to a TiO_2 slurry which is then calcined to form a doped TiO_2 powder of solid film [25] or the addition of metal to a surfactant based TiO_2 sol-gel for the production of mesoporous doped TiO_2 films [26]. Despite potential applications towards photocatalysis, doping does not involve the use of photocatalysis in the process of adding metal ions / particles to the semiconductor.

Noh *et al* reported the inclusion of Pd in a TiO_2 coating solution to produce $TiO_2 – Pd^{2+}$ films in a process more akin to surface modification than doping [27,28]. Pd ions are incorporated within a TiO_2 coating and subsequently irradiated, leading to Pd^{2+} being reduced to Pd metal through photocatalysis. Irradiation is conducted through a photomask in order to control the areas in which photocatalysis and hence the formation of metallic Pd occurs. Although this demonstrates the use of photocatalysis for metal reduction, it is not employed for direct metal deposition onto an extant semiconductor or substrate. Rather, the technique is described as a photo-patterned sensitisation technique for surface modification.

3.5.3 Recent Development

Even throughout the last decade, the use of photocatalysis for the metallisation of surfaces had remained an infrequently studied area. Despite the basic principle having been established for some time, few people have sought to take advantage of the benefits provided by photocatalysis over other, more traditional metal deposition techniques.

In 2000, Stathatos *et al* reported the photocatalytic deposition of Ag nanoparticles [30], again demonstrating the viability of semiconductor photocatalysis in metal deposition but the method was merely used to produce small scale metal particles and not expanded towards the production of complete, coherent metal layers.

The Pd photo-patterning work of Noh *et al* discussed in section 3.5.2 was more recently continued within the same group by Byk *et al* with a focus on applying electroless Ni deposition to Pd patterned substrates [29]. As with traditional sensitisation methods used in electroless plating, the metallic Pd formed through photocatalysis acts as a catalytic basis for Ni deposition. Here photocatalysis is used, by virtue of photomasking, to produce spatially selective sensitisation of a substrate surface with subsequent Ni deposition onto the substrate remaining separate and independent of photocatalysis. Despite this application to metal deposition, the use of photocatalysis here remains in producing isolated particles rather than coherent metal films and cannot be considered a metal deposition process itself.

In conjunction with interest in H_2 separation, the formation of coherent metal layers is an area which has drawn more recent attention. It is well known that Pd shows a high affinity for H_2 and consequently it has become commonly used in H_2 separation membranes. As a result it has become desirable to produce Pd films on insulating surfaces and semiconductor photocatalysis offers one potential method to achieve this. In a claimed novel method, Wu *et al* described the production of Pd membranes through photocatalytic deposition with a particular focus on controlling the thickness of the deposited metal layer [31]. This provides a true application of photocatalysis for metal deposition with Pd metallisation taking place onto commercial TiO_2 ceramic membranes directly from solution under ultra-band gap irradiation with the addition of methanol as a hole scavenger. The work also describes the dependency of photocatalytic deposition on factors such as irradiation time, temperature, pH and bath constituent concentrations and hence offers considerable contribution towards the understanding of photocatalytic metal deposition. Furthermore, the report begins to recognise the advantages offered by the use of photocatalysis over traditional methods with improved adhesion of the Pd layer in comparison to Sn / Pd seeding methods.

Despite this successful utilisation, the method remained largely unexploited compared with complimentary techniques such as chemical vapour deposition [37], electroless [38] and even electro-plating [39]. In 2006, the aforementioned work of Wu was continued by Li *et al* with the aim improving the quality and density of the photocatalytically deposited Pd film for enhanced H_2 permeability [33]. Having previously gained an understanding of how the deposition process was influenced by the factors listed above, the group now investigated the potential for control of this process and the effect that may have on the resulting metal deposit. As a modification of the Pd bath constituents, methanol was replaced with EDTA as the hole scavenger. The photocatalytic reaction baths used throughout the works of Wu *et al* and Li *et al* are inherently unstable, a problem also commonly encountered with the electroless deposition of Pd. Several influencing factors such as increasing pH, bath impurity, temperature hot spots and, in the case of an electroless Pd bath, the powerful reducing agents required to drive Pd reduction, can lead to the formation of catalytic Pd nuclei in solution. In turn these nuclei lead to homogenous auto-catalysis, precipitating Pd metal in solution (so wasting materials) and making the deposition difficult to control. The addition of EDTA proved to be an important contribution to the development of the photocatalytic deposition of metals as, through complexation of the metal precursor, it slows the rate of auto-catalytic deposition typical of unstable baths, in favour of the photocatalytically driven deposition process. Simultaneously, through the scavenging of photogenerated valence band holes, it also enhances the photocatalytic action of TiO_2 through an upward shift in conduction band energy. Li *et al* observed that the addition of EDTA is most effective at an optimised concentration of 0.1 g / L while an excess of over 0.2 g / L results in poisoning of the TiO_2 catalyst and all photocatalytic metal deposition is inhibited [33]. Generally, when the overall rate of metal deposition increases, the growth rate of deposited metal particles increases and the resulting metal layer becomes rougher and more granular. Therefore, the restriction of the metal deposition rate achieved through the use of EDTA as a complexant and hole scavenger resulted in the formation of a denser Pd film with finer granularity.

Further work from Li's group has moved towards an alternate photocatalytic deposition method in which the substrate is irradiated only after being removed from the electroless plating bath rather than while still immersed in it. Substrates are placed in the bath for 30 min, allowing adsorption of metal ions onto the TiO_2 surface. Upon removal from the bath, a thin liquid film is retained on the substrate surface and subsequent irradiation allows for photocatalytic reduction of the adsorbed metal ions to occur. This method offers the advantage of avoiding homogeneous reaction and bath decomposition. However, as the quantity of metal deposited from the liquid film is very small, the process must be repeated 20x in order to achieve a complete Pd layer of 400 nm thickness [34,35].

In one of the most recent reports of the use of photocatalytic deposition, Zhao *et al* deposited Pd onto TiO_2 nanotubes, the photocatalyst being used to reduce Pd for direct metallisation. However, this is performed slowly over 12 hours and only used to produce Pd nucleation sites prior to a continued, non-photocatalytic, electroless deposition conducted as a separate process. Ultimately this process utilises photocatalysis merely as a separate, non-solution phase sensitisation step; the potential of semiconductor photocatalysis for metal deposition again being under exploited.

Thus, in spite of the demonstrated viability of photocatalytic deposition and the various advantages provided over other metal plating methods, there has been little work on the development of the technique. Even in the most recent publications describing photocatalysis for metal deposition, the photocatalyst is not exploited to full process advantage and the primary directive has not spread beyond the production of Pd films for H_2 separation. We have attempted to explore this technology space, the next section describes in detail the development of true photocatalytically initiated electroless deposition (PIED).

3.6 Photocatalytically Initiated Electroless Deposition (PIED)

In the absence of an exhaustive body of research into photocatalytic metal deposition we have sought to understand and apply the technique for the metallisation of various insulating

substrate surfaces. Particularly, we have explored the deposition of both Ag and Pd, so allowing for the study of PIED in both 1 and 2 electron reduction processes.

As discussed above, the photocatalytic generation of metal nanoparticles at semiconductor surfaces by conventional photocatalytic metallisation processes offers an alternative to the interfacial chemical metal nucleation methods employed in conventional electroless deposition shown in Fig. 17 (a) & (b). Once metal nucleation sites have been formed by photocatalytic means then, in the presence of an appropriate reductant, further deposition may occur onto those nucleate sites by conventional electroless deposition reaction. These are the principal processes of PIED. As such, the only pre-sensitisation process required for the metallisation of an insulating substrate is for it to be coated with an appropriate semiconductor, such as the chemically robust TiO_2. PIED therefore obviates the need for Sn-Pd catalysts so eliminating contamination from prior nucleation whilst the fewer steps and materials required may provide a cheaper, environmentally cleaner and, through control of incident light intensity, more controllable processing option than the usually employed methods for dielectric plating.

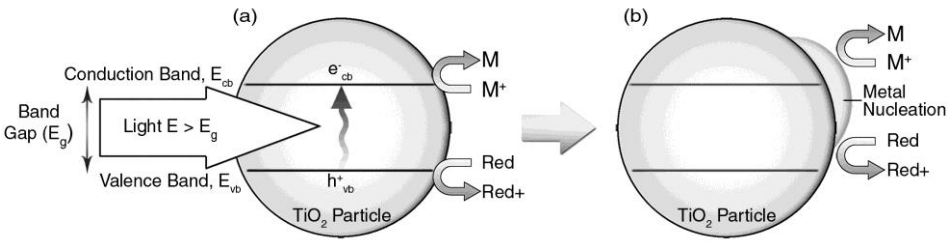

Fig. 20 Two stages of PIED: (a) the photocatalytic process derived from interfacial electron transfer at a photoexcited semiconductor particle; and (b) the autocatalytic electroless deposition process

Two generic embodiments of PIED may be envisaged. In the first embodiment, the reductant or hole scavenger employed during the photocatalytic initiation step (Fig. 20 (a)) is a different reagent to the reductant employed during the autocatalytic electroless deposition / metal nucleate growth step (Fig. 20 (b)). In this context, the photo-initiated nuclei formation and growth steps can be performed in two ways: first, by immersion of the surface to be coated in a hole scavenger / precursor metal ion solution followed by a second immersion in a

reductant / metal ion solution, so-called “two-step” PIED; and second, by immersion of the substrate in a solution containing the precursor metal ion and both the hole scavenger and reductant, so-called “one-step” PIED. In the second generic embodiment, the hole scavenger and the reductant for the metal growth step are the same and so this may be classified as a “one-step” PIED process. It is this latter embodiment that presents the most advantageous method and has become the most developed within work in our laboratories. In either case the TiO_2 sensitisation is performed separately as a pre-sensitisation stage via either (a) sol-gel spin coating and annealing at 773 K to produce a robust mesoporous TiO_2 (m-TiO_2) film; or (b) deposition of pre-formed, commercially available TiO_2 nanoparticles by spin or dip coating techniques.

TiO_2 sensitised substrates are placed directly into freshly prepared electroless plating solutions in a quartz reaction vessel for improved UV transmittance, Fig. 21. A N_2 stream may be bubbled through the plating solution in order to purge the solution of O_2, which can compete with metal ions for reduction at the photocatalytic surface, and provide a source of agitation to prevent local depletion of metal ions. Irradiation is then provided by an enclosed photoreactor (Lidam Scientific, Dartford, UK) comprised of two hemi-cylinders, each containing 6 x 8W UV A lamps.

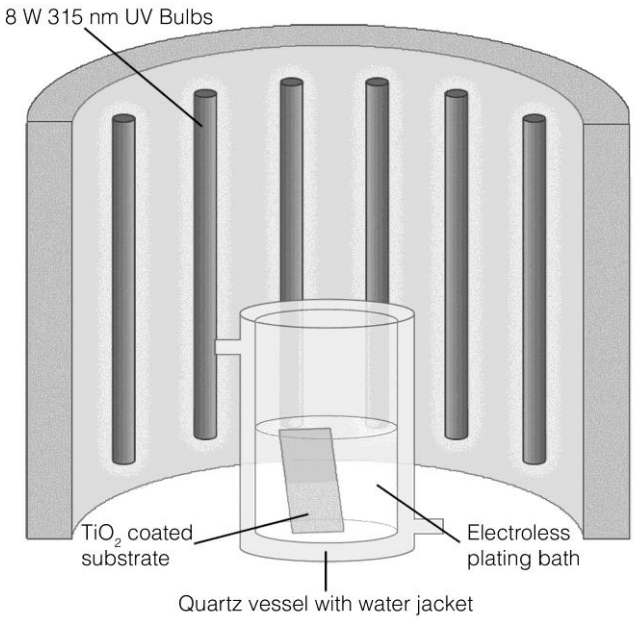

Fig. 21 PIED experimental setup

3.6.1 Energetic Feasibility of PIED

3.6.1.1 Photocatalytically Generated Silver Nucleation

In order for PIED to occur, certain photoelectrochemical energetic requirements must be fulfilled. Consider Ag as the example, the standard electrode potential (E^0) of $Ag^+ + e^- \leftrightarrow Ag$ is +0.5571 V vs SCE [65] while the conduction band edge (E_{cb}) of TiO_2 at pH 11 is -0.78 V vs SCE. As the E_{cb} is more negative that the E^0 of Ag, it should be expected that TiO_2 irradiated with ultra-band gap light energy will be capable of reducing local Ag^+ ions to metallic Ag. Indeed when an m-TiO_2 sensitised glass substrate is immersed in an aqueous $AgNO_3$ solution (8.8 mmol / dm^3) with no other additives or reductant, and is then irradiated with 315 nm UV light, Ag nucleation occurs directly onto the TiO_2 surface. Results from such an experiment are shown in Fig. 22, from which it can be seen that an immersion time of 30 min with full irradiation produces considerable Ag nucleation onto the m-TiO_2 Fig. 22 (b). In contrast, an immersion of the same time in darkness produces virtually no Ag nucleation, Fig. 22 (a). As irradiation time increases a greater amount of Ag is deposited and the coating begins to appear metallic, although it remains non-conductive and not fully continuous. This is confirmed when viewing light transmitted through the sample via LED backlighting, Fig. 23.

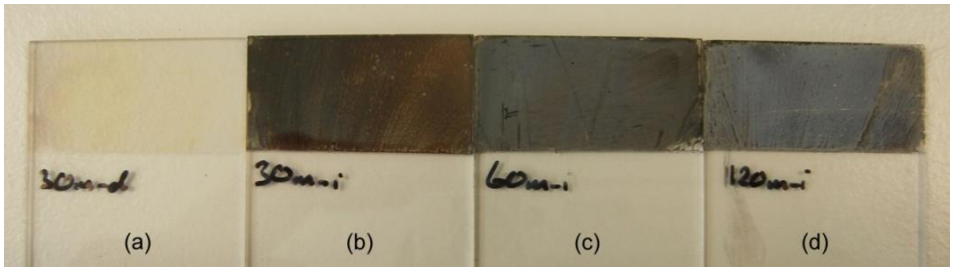

Fig. 22 Ag nucleation onto m-TiO_2 sensitised glass after (a) 30 min darkness, (b) 30 min irradiation, (c) 60 min irradiation, (d) 120 min irradiation

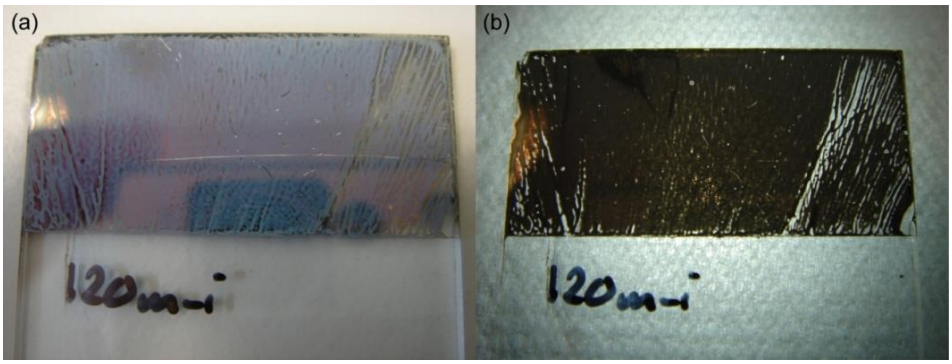

Fig. 23 Ag nucleation after 120 min irradiation; (a) viewed normally, (b) with backlighting

SEM imaging with 3D surface reconstruction shows that the metal deposition occurs with fine granularity and little bias towards continued deposition at existing nucleation sites (*i.e.* deposit growth) is apparent, Fig. 24. This image serves as a benchmark for the metal formation achieved by purely photocatalytic means.

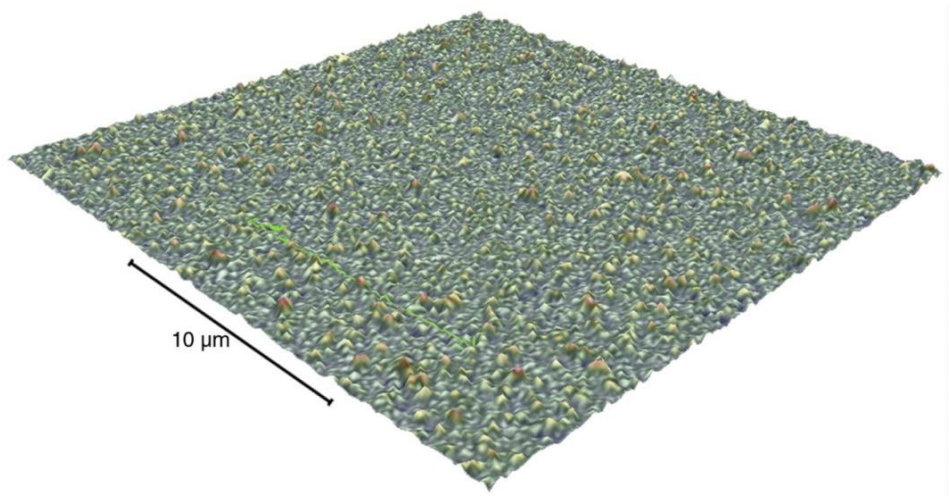

Fig. 24 3D SEM surface reconstruction of Ag deposited onto m-TiO_2 sensitised glass; 60 min irradiation, no chemical reductant

Throughout, the metal deposition occurs exclusively onto the TiO_2 sensitised area demonstrating that the photocatalyst is driving the metal reduction. Continued deposition is slow due to the fact that the available photocatalyst surface decreases as more metal is deposited. From the nature of this system, *i.e.* where a chemical reducing agent is absent, it is observed that, given sufficient time, the entire TiO_2 surface becomes covered with a granular metal deposit, at which point deposition ceases.

3.6.1.2 Photocatalytically Generated Palladium Nucleation

Having successfully demonstrated photocatalytic metal reduction with the single electron transfer of Ag deposition, the process was then applied to Pd, a metal which requires a two electron transfer to be reduced from its metal salt. As a result, deposition of this catalytic, noble metal involves differing energetic requirements. The standard electrode potential, E^0, of $Pd^{2+} + 2e^- \leftrightarrow Pd$ is +0.673 V vs SCE. Again given that the conduction band edge (E_{cb}) of TiO_2 at the typical plating bath pH of 11 is -0.78 V vs SCE, it should be expected that, when irradiated with ultra-band gap light energy, the semiconductor will successfully reduce local Pd^{2+} ions to Pd metal.

In order to assess the feasibility of photocatalytic reduction of Pd without a reducing agent, glass substrates sensitised with m-TiO_2 were immersed in a $PdCl_2$ solution described by Li *et al*, 2006 [33]. The composition of this solution, given in Table 5, consists only of the metal precursor and a complexant (to enhance bath stability) in ultrapure water and, as a result of the lack of the ammoniac constituents normally added, the pH of 4 is considerably lower than typically encountered in existing electroless Pd deposition baths. This pH difference causes a significant shift of the E_{cb} of TiO_2 to -0.38 V although this remains negative of the E^0 of Pd and metal reduction is expected.

Role	Component	Concentration
Metal precursor	Palladium Chloride	0.1 g / dm^3 (0.56 mmol / dm^3)
Complexant	Di-sodium EDTA	0.1 g / dm^3 (0.27 mmol / dm^3)
pH	-	4
Temp.	-	348 K

Table 5 Composition of reductant free Pd bath

Initial samples were immersed and irradiated with 315 nm UV light for 120 min at a temperature of 348 K. No evidence of Pd deposition or nucleation could be seen after this period. Subsequent immersion in darkness for a further 72 hours also revealed no evidence of continued deposition, as should be expected with no reductant present and hence no possibility for auto-catalytic deposition. The experiment was repeated with a 15 hr irradiated

immersion; while considerable evaporation of the Pd bath occurred due to the high operating temperature, Pd deposition was achieved. The resulting Pd deposit had begun to take on a metallic appearance but remained semi-transparent to light and non-conductive due to incoherent coverage. Considering the time frame of the immersion, the amount of Pd deposited was very small, an effect due to the reduced thermodynamic driving force for electron transfer derived from the shift in E_{cb} with pH. However, some Pd metal was deposited, occurring exclusively onto the TiO_2 sensitised area of the substrate. This clearly demonstrates the ability of the photocatalyst to reduce Pd and initiate direct metallisation without the need for a reducing agent. Although the rate of deposition and the required energy input are uneconomical, the potential for TiO_2 to photocatalytically deposit the metal nuclei necessary to initiate electroless Pd deposition has been proven.

3.6.2 Photocatalytic Initiation with Continued Electroless Deposition

3.6.2.1 Photocatalytically Initiated Silver Deposition

In order to achieve continued electroless deposition after successful photocatalytic initiation, it is necessary to provide a source of electrons for further metal reduction. Here the principles of traditional electroless plating are applicable with a typical plating bath containing reducing agent as a source of electrons and complexants to ensure stable dissolution of the metal precursor.

Any electrode immersed in an electrolyte comprised of a mixture of redox couples will, at open circuit, be subject to a so-called mixed potential, E_{mp}. This mixed potential arises because, at open circuit, no net current flows across the electrode-electrolyte interface and so the current associated with any oxidation reactions at the electrode surface must be exactly balanced by the current associated with any reduction processes. As current is a function of potential for all redox couples, the open circuit potential of the electrode adjusts until the rates of the reduction and oxidation reactions are equal and opposite. The potential at which this zero-net current condition is wholly satisfied is the mixed potential.

An m-TiO_2 sensitised substrate is like any other electrode material and, when submerged in a traditional potassium sodium tartrate based Ag electroless plating bath [9], will be subject to the associated mixed potential determined by the balance of the reduction of Ag^+ and the oxidation of tartrate. Simple open circuit potential measurements conducted using a Au working electrode and saturated calomel reference electrode indicate that the E_{mp} of the Ag^+ / tartrate plating system employed here is +0.12 V vs SCE. Separate current-voltage measurements at pH 11, typical of electroless plating baths, indicate that flat band potential, E_{fb}, of m-TiO_2, is -0.65 V vs SCE. TiO_2 exhibits n-type semiconductor properties and, thus, at potentials positive of flat band, such as these associated with the measured E_{mp} of +0.12 V, the bands bend up from the material bulk to the semiconductor-electrolyte interface. This results in the formation of a majority charge carrier / electron depletion layer at the semiconductor surface with an associated energy barrier to electron transfer to the electrolyte. Upon irradiation with ultra-band gap light energy, photo-excited electrons are generated within this depletion layer, the electrical field therein allowing for charge separation to occur. As a result of this separation, the bands unbend and the energy barrier towards electron transfer to the electrolyte is decreased, so allowing for reduction of Ag (I) to Ag at the semiconductor surface. This in turn results in reductively driven Ag nucleation directly onto a TiO_2 surface which can more usually be considered a photoanode.

In accordance with this conceptual model, PIED was successfully achieved onto m-TiO_2 sensitised glass substrates using a traditional Ag electroless plating bath. After a 120 min irradiated deposition period the substrate displayed a smooth Ag coating across the whole m-TiO_2 sensitised area, Fig. 25.

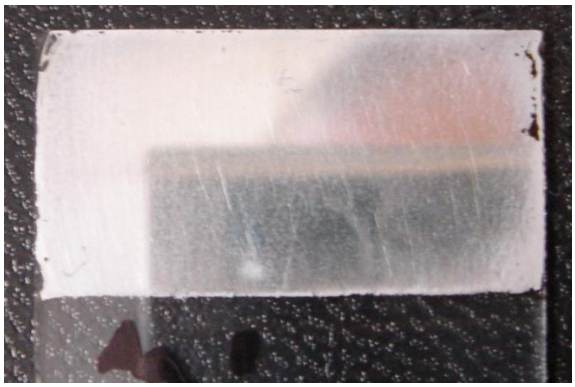

Fig. 25 Ag deposited onto m-TiO_2 sensitised glass via PIED

The resultant metal layer is coherent and conductive whilst displaying a shiny, almost mirrored metallic finish and does not delaminate with adhesion, as demonstrated via British Standard metal adhesion test BS EN ISO 2819:1995. Metal deposition occurs exclusively onto those areas both sensitised with TiO_2 and irradiated with ultra-band gap light making the process selective and controllable.

3.6.2.2 Photocatalytically Initiated Palladium Deposition

As with the Ag system, if continued deposition is to occur after photo initiation / photo-induced metal nucleation, the plating bath must contain a reducing agent such as hydrazine. Using a typical, hydrazine based electroless Pd bath [9,127,128], the overall reaction is as follows:

$$2Pd(NH_3)_4^{2+} + N_2H_4 + 4OH^- \longrightarrow 2Pd + 8NH_3 + N_2 + 4H_2O \qquad (7)$$

With this electroless bath utilised in the PIED setup, Fig. 21, a E_{mp} value of -0.703 V vs SCE is measured using an Au working electrode at open circuit. As described above, E_{fb} of m-TiO_2 at electroless plating bath pH is found to be -0.65 V vs SCE. At measured potentials more negative than the E_{fb} of n-type TiO_2, an electron accumulation layer would be expected. However the E_{mp} here is not significantly lower than the E_{fb} and as such very little charge separation or band bending is observed. With this minimal space charge region, photogenerated electrons are likely to undergo recombination and hence the effect of irradiation on photocatalytically inducing metal nucleation at m-TiO_2 surfaces exposed to the

Pd electroless plating system may be significantly less than that in Ag systems. However, the photocatalytic effect is not expected to be completely eliminated as a small negative potential exists. Significantly though, the photocatalysis will not operate as the principle driving force behind Pd reduction and initial nucleation may be overridden by the auto-catalytic stage.

The above observations notwithstanding, m-TiO_2 sensitised glass substrates were immersed in an electroless Pd bath and irradiated with UV light for 60 min at ambient temperature. After this time the sample displayed complete coverage of the sensitised area with metallic Pd with conductivity present across the entire metal layer. The Pd deposit, Fig. 26, was noticeably less reflective than equivalent Ag deposits, showing a matt appearance as opposed to the reflective Ag surfaces, the latter only tarnishing with time and exposure to air. It is also noted that, while Pd deposition is mainly restricted to the m-TiO_2 sensitised area, there is a greater degree of spread of the deposited metal beyond the edge of the TiO_2 and onto the non-sensitised glass. This spread is only over a small distance, up to 1 mm, but demonstrates that the Pd system is more ready to auto-catalytically deposit metal onto wider areas through dendritic growth suggesting that this, rather than nucleation, is the dominant form of deposition in this system.

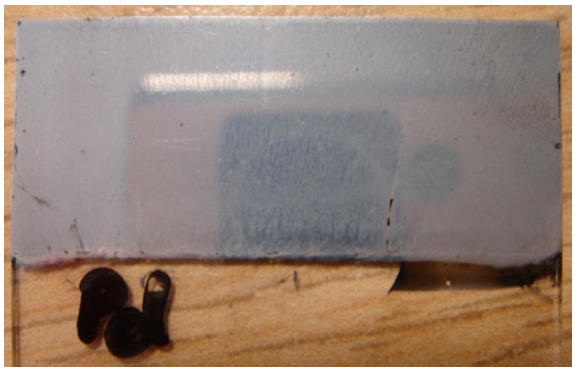

Fig. 26 Pd deposited onto m-TiO_2 sensitised glass via PIED

Typically the electroless Pd bath is much less stable than its Ag counterpart due to the significant hydrazine-derived reductive overpotential in the system (-0.7 V vs SCE for the Pd system against +0.59 V vs SCE for the Pd / Pd^+ redox couple, $E_{mp} - E^0$ = -1.3 V cf. +0.12 V vs

SCE for the Ag system against +0.55 V vs SCE for the Ag / Ag^+ couple, $E_{mp} - E^0$ = -0.43 V) resulting in accelerated auto-catalysis and bath decomposition. This is frequently observed as Pd baths become grey due to Pd precipitation with use. This decomposition effect may also be promoted by the TiO_2 as, while photocatalytic initiation generates nucleation sites on the TiO_2 surface, it can also lead to the formation of free metallic Pd in solution and subsequent decomposition of the plating bath. However, a Pd bath may also decompose without any specific initiation given sufficient time without exposure to any photocatalyst. Such decomposition may be caused by the presence of adventitious bath impurities or elevated bath temperature. In order to minimise these factors, high grade chemicals are used as bath constituents, filtration is applied to the bath prior to substrate immersion and temperature is thermostatically controlled via a water jacketed reaction vessel, Fig. 21.

In addition to this difference in stability between the Pd and Ag baths, there is also a noted difference in the resulting deposits the PIED process produces. As described earlier, Pd deposits typically appear matt and less lustrous than comparable Ag deposits. As this visual appearance is an indication of the structure and smoothness of the metal surface, it can be expected that the Pd deposits have a degree of increased roughness or a structural characteristic which would affect this.

The SEM analysis of Fig. 27 supports this conclusion. From this it can be seen that that while the many nucleation sites and steady deposition rate of the Ag system leads to a fine grained deposit, Fig. 27 (a), the accelerated rate of deposition at fewer nucleation centres in the Pd system gives rise to a more granular, Fig. 27 (b), and hence less reflective deposit.

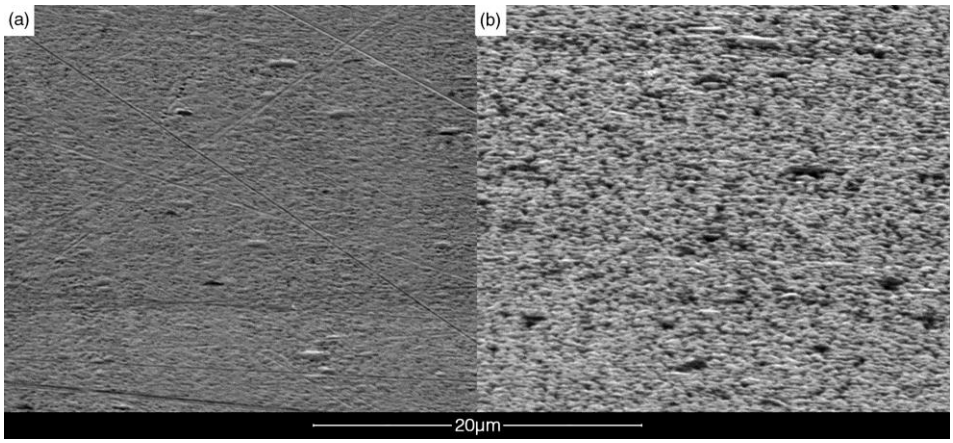

Fig. 27 SEM images of (a) an Ag deposit and (b) a more granular Pd deposit, generated by PIED on m-TiO_2 coated glass

3.6.2.3 Photocatalytically Initiated Electroless Deposition of Other Metals

Having achieved successful deposition of both Ag and Pd using PIED, it is expected that other metals can be deposited via the same process. Depending on pH, the TiO_2 conduction band edge is negative of the redox potential of a wide range of metal couples and hence should be expected to be applicable to the PIED of these metals. Fig. 28 shows the TiO_2 band edges at low pH and demonstrates how the redox potential of photogenerated electrons in the conduction band is more negative than the standard electrode potentials for metals such as Pt, Pd, Ag and Cu.

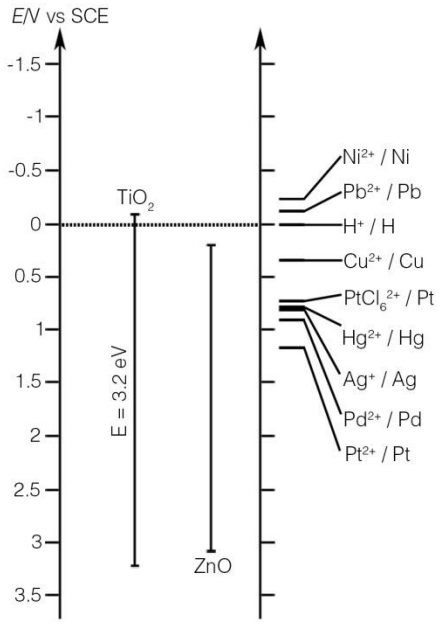

Fig. 28 Band edge position of TiO_2 and ZnO with standard electrode potentials of metals at pH = 1

With a standard electrode potential (E^{0}) of -0.257 V, Ni lies negative of the conduction band edge of TiO_2 at low pH and would therefore be expected to be non-depositable by PIED. However, in house measurements show the flat band potential (E_{fb}) of m-TiO_2 to be -0.65 V vs SCE under the basic conditions (pH 11) normally associated with electroless plating baths. The E^{0} of the Ni couple is invariant with pH. Thus, it should therefore be expected that, under such basic conditions, the photocatalyst would be capable of reducing metals such as Ni as well.

As with previous PIED procedures glass substrates were sensitised with m-TiO_2 before being immersed in an electroless Ni bath, composed of $NiSO_4$, sodium hypophosphite and sodium citrate [9,129], and irradiated through a quartz reaction vessel. A 60 min irradiated immersion in an un-optimised electroless Ni bath at an operating temperature of 363 K resulted in varying success as some substrates displayed areas of reflective, metallic Ni (so confirming the value of the analysis above) while others an inconsistent, matt deposit. Considerable bath decomposition also occurred, largely encouraged by the elevated operating temperature. It is also noteworthy that the plating bath becomes significantly darkened by the Ni precipitation so restricting light transmittance through the solution to the photocatalyst and hence reducing its effectiveness.

To increase bath stability and avoid decomposition the operating temperature was reduced. After a 120 min irradiated immersion at 348 K the Ni bath remained stable and smooth, mirrored Ni deposits were formed on m-TiO_2 sensitised surfaces, Fig. 29.

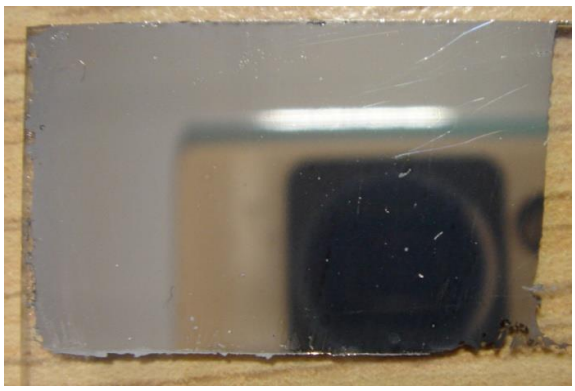

Fig. 29 Ni deposited onto m-TiO_2 sensitised glass via PIED

The Ni layer was conductive and morphologically consistent over the whole sensitised area with no deposition occurring onto non-sensitised surfaces. The reduced operating temperature greatly increased the stability of the Ni bath without inhibiting metal deposition. Indeed the temperature was further reduced to both 333 K and 323 K with successful observation in both cases of reflective Ni deposits over the entire, and exclusive to, the TiO_2 sensitised areas.

Thus, PIED has proven easily adaptable to various metals with minimal optimisation. The Ni bath used above was not optimised for PIED in any way other than reducing the operating temperature. This is beneficial in enhancing stability and improving the quality of the deposited metal and is made possible by the active initiation of deposition by the TiO_2 photocatalyst rather than a sole dependency on auto-catalytic deposition. Having said this, if PIED is to be deployed for technologically useful depositions, some knowledge of the parameters relevant to process control is imperative – most especially, how deposit morphology, thickness and coherence are related to intensity of irradiation, strength of reductant and immersion time. The following sections address some of these issues.

3.6.3 Timed Irradiation Studies

In order to investigate how the properties if PIED generated metal layers depend in immersion / irradiation time, Ag was deposited onto m-TiO_2 for varying periods of full irradiation with ultra-band gap light energy throughout the deposition period. As a control, an m-TiO_2 sensitised slide was immersed in the electroless Ag solution for 30 min with no irradiation. The control sample showed a small amount of Ag nucleation on the m-TiO_2 sensitised region, visible as a light brown, transparent covering, Fig. 30. It should be noted that the amount of nucleation, while relatively small, is significantly greater than that seen after the same period of time in the absence of a reducing agent, Fig. 22 (a).

The nucleation seen here, in Fig. 30, occurs onto the semiconductor even though no irradiation was provided. The effect is therefore not photocatalytic but instead is driven by the reducing power of the tartrate within the plating solution. Nucleation proliferates on the

m-TiO_2 due to the high surface roughness and many low coordination state (high surface energy) sites in comparison to the untreated glass. 3D SEM imaging demonstrates that the Ag nucleation sites form with wide spacing and with much less frequency than observed with irradiation, Fig. 24. Each nucleation site is also comparatively large due to focused auto-catalytic deposition at that point.

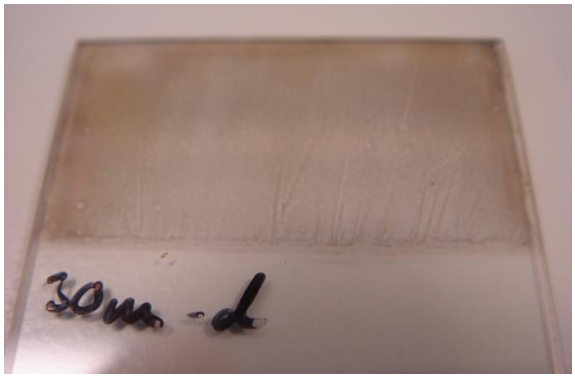

Fig. 30 Ag nucleation onto m-TiO_2 sensitised glass after 30 min in darkness

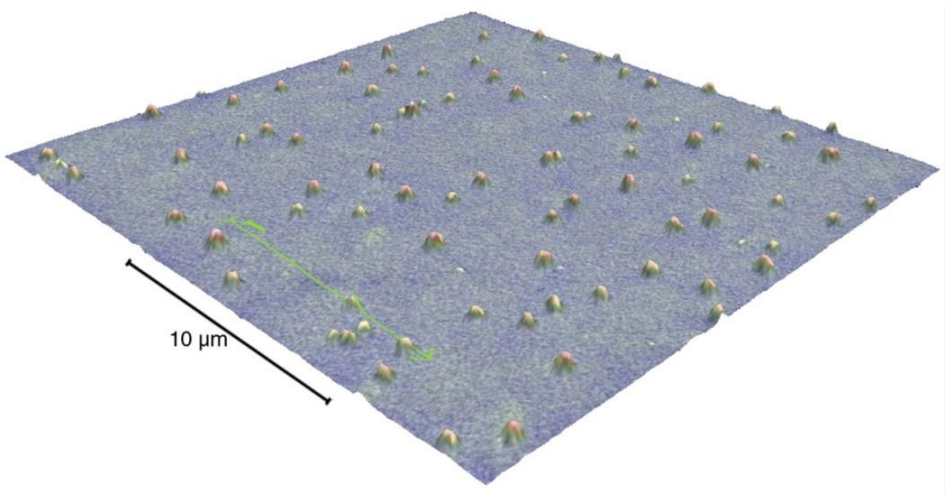

Fig. 31 3D SEM surface reconstruction of auto-catalytic Ag nucleation after 30 m without irradiation

In contrast to the control sample, other substrate samples were also immersed in the plating solution and irradiated for times increasing from 30 s to 60 min. A clear trend of increased Ag deposit with time was observed, Fig. 32. All irradiated samples produce considerably more Ag deposition than the 30 min dark control sample, again demonstrating the ability of TiO_2 in photocatalytically initiating metal deposition.

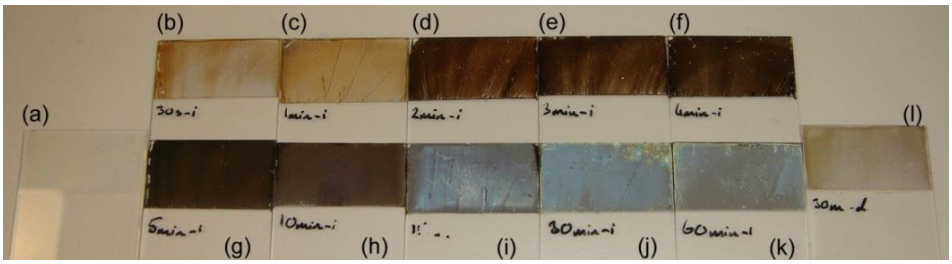

Fig. 32 (a) Blank m-TiO_2; Ag deposits after irradiation for (b) 30 s, (c) 1 min, (d) 2 min, (e) 3 min, (f) 4 min, (g) 5 min, (h) 10 min, (i) 15 min, (j) 30 min & (k) 60 min; (l) Ag deposit after 30 min in darkness

Irradiation times of 30 s to 5 min show rapidly increasing Ag nucleation with the sample becoming increasingly brown and opaque as greater amounts of Ag are deposited. At these irradiation times all samples remain non-conductive as the Ag deposit has not formed a coherent layer. SEM images emphasise the immediacy of the photocatalytic initiation as a large quantity of nucleation sites become visible after only 30 s, Fig. 33. This again provides stark contrast to the amount of metal nucleation observed over 30 min the absence of irradiation, Fig. 31, so demonstrating the strength of photocatalysis in driving metal reduction.

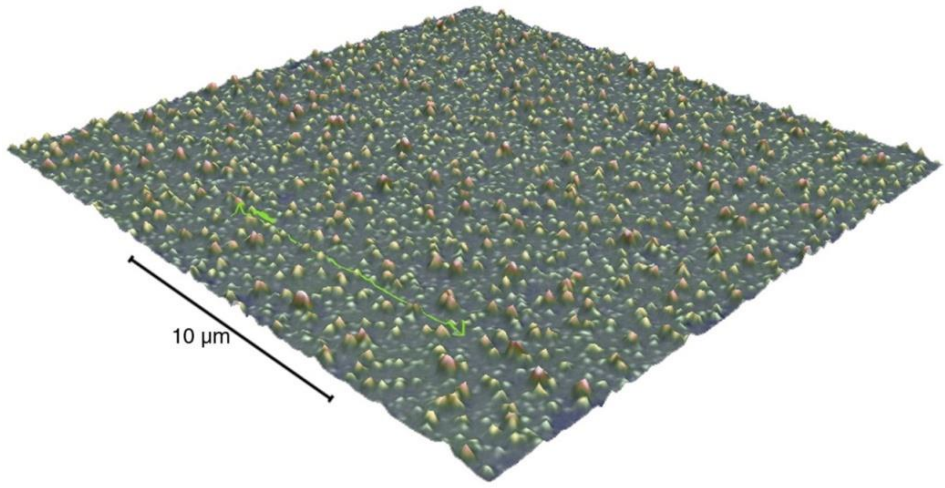

Fig. 33 3D SEM surface reconstruction of photocatalytic Ag nucleation after 30 s irradiation

After a 5 min irradiated immersion, Ag nucleation has continued from that seen after 30 s with metal deposition sites now covering the majority of the semiconductor surface, Fig. 34.

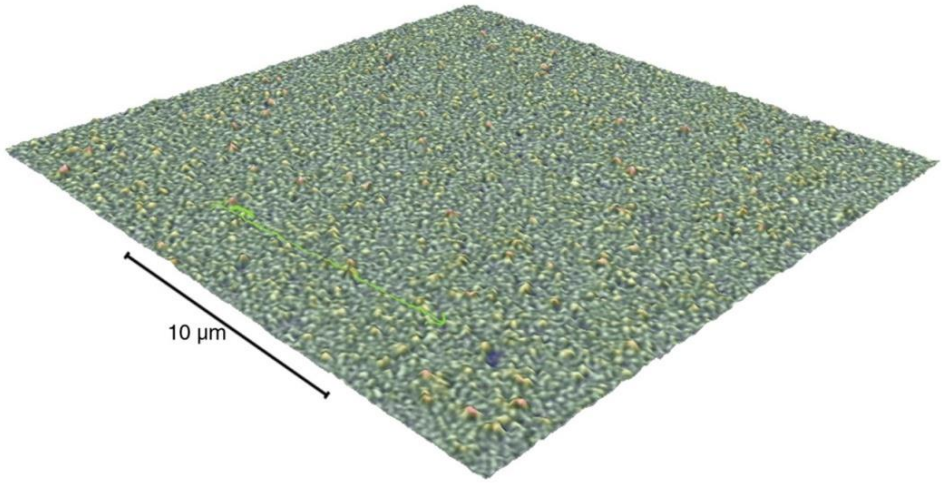

Fig. 34 3D SEM surface reconstruction of photocatalytic Ag nucleation after 5 min irradiation

Interestingly, this Ag deposit, produced in 5 min with the presence of a reducing agent, potassium sodium tartrate, is comparable to that seen after 60 min without, Fig. 35. This represents a significant increase in deposition rate as the reductant not only facilitates Ag reduction itself but also acts as a hole scavenger, so leading to the accumulation of photogenerated electrons within the semiconductor. As more electrons are then accessible to solution, the rate of metal reduction (nucleation and growth) by the TiO_2 is enhanced.

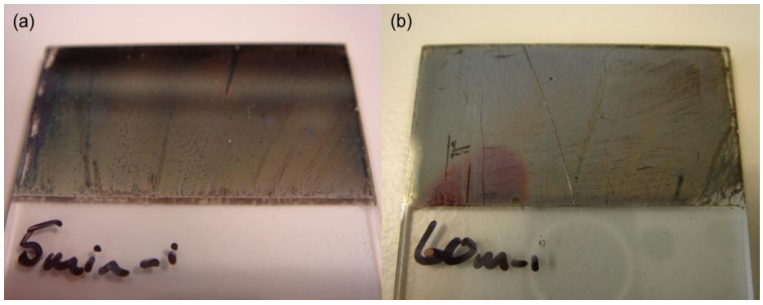

Fig. 35 Ag deposit on m-TiO_2 sensitised glass; (a) 5 min with reductant; (b) 60 min without reductant

After a 10 min irradiation the Ag deposit begins to display a metallic surface appearance, Fig. 36 (a), and becomes conductive across small areas. The conductivity does not range across the entire sample area as the Ag deposit remains incomplete having not yet conglomerated all nucleation sites. This can be most readily appreciated by viewing light transmitted through the sample via LED backlighting, Fig. 36 (b).

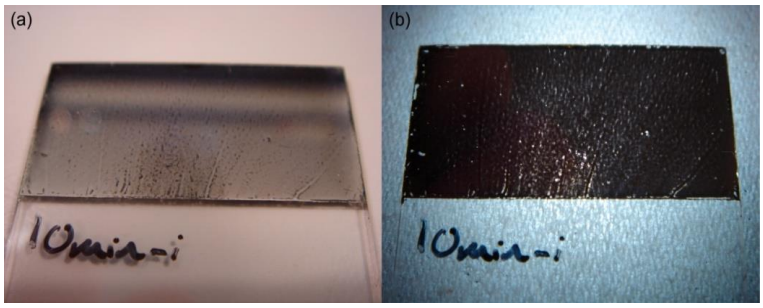

Fig. 36 Ag deposit after 10 min irradiation; (a) viewed normally, (b) with backlighting

Deposition times of 15 min and greater result in fully conductive and metallic Ag coatings. The consistency and lustre of these deposits improves with time as nucleation sites grow into islands, eventually merging into one complete layer as further Ag deposition occurs. While the Ag layer deposited after a 15 immersion is conductive across all areas, backlit viewing demonstrates the presence of some incompletely covered areas appearing as translucent brown patches, Fig. 37 (a). After 30 min these areas are fully coated with the only remaining defects in the Ag layer being those corresponding to areas of inconsistency in the m-TiO_2 coating, Fig. 37 (b). These isolated spots lacking in Ag are gradually covered by further deposition as the auto-catalytic process grows the metal deposit over these small un-sensitised areas Fig. 37 (c).

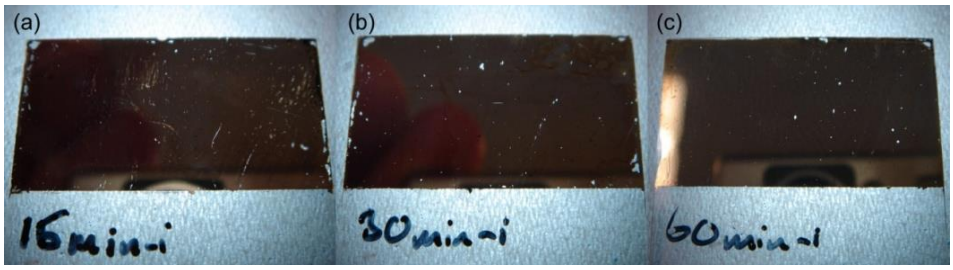

Fig. 37 Ag deposits after (a) 15 min, (b) 30 min & (c) 60 min viewed with LED backlighting

Conductive metal layers retain the microstructure previously observed as lateral and vertical growth of all nucleation sites occurs to form a coherent granular film, Fig. 38.

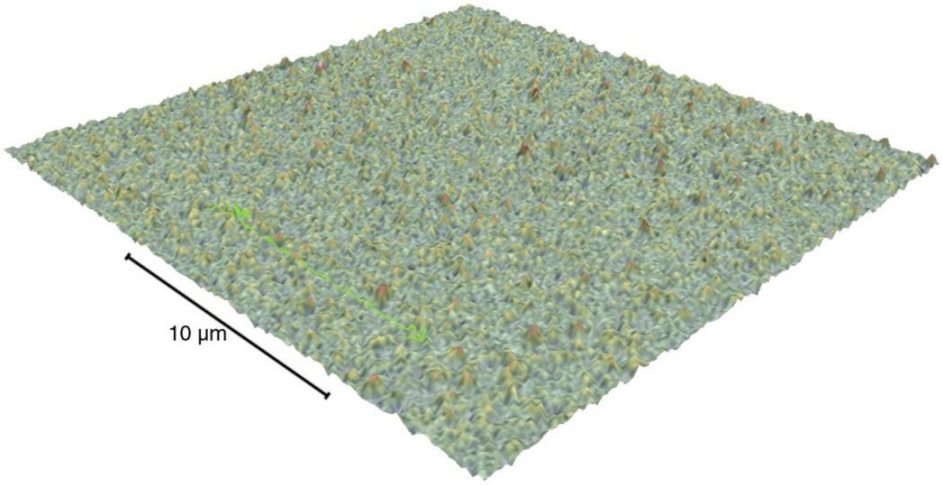

Fig. 38 3D SEM surface reconstruction of Ag after 30 m irradiation

A further measure of the quality of metal deposit is provided by measurement of the sheet resistivity which offers a value of electrical resistance over the plane of the thin metal layer.

Irradiation	0-5 min	10 min	15 min	30 min	60 min
Sheet Resistivity	–	653 Ω / sq	0.6 Ω / sq	0.2 Ω / sq	0.2 Ω / sq

Table 6 Sheet resistivity measurements after extending irradiated immersion times

Table 6 shows how sheet resistivity decreases with longer irradiated immersion times indicating a more conductive metal layer. At irradiated immersion times of 5 min or less, the Ag layer shows no conductivity. After 10 min, the metal layer becomes conductive though only in small areas, as represented by a high resistivity value, while immersion times of ≥15 min produce wholly conductive layers and very low sheet resistivity values. The small areas of incomplete coverage remaining after 15 min probably contribute to the slightly higher sheet resistivity measurement observed at this time compared to the values recorded from samples immersed for longer time periods and with consequently larger metal layer thickness. Those samples displaying a sheet resistivity of ≤0.2 Ω / sq are considered to be fully conductive.

As would be expected, a longer deposition time results in a thicker deposit as the auto-catalytic deposition continues in all available directions, not merely laterally. This means that, once initiated the metal deposition will continue until halted by one of the following; the substrate is removed from the electroless plating bath; the metal precursor is depleted; the

reducing agent is depleted; the bath loses stability and undergoes spontaneous decomposition. These factors offer further opportunities for process control – meaning that not only can the onset of metal deposition be controlled with PIED but also the extent of coverage and depth of the resulting metal deposit.

3.6.4 Photocatalytic Initiation and Auto-Catalytic Deposition

3.6.4.1 Photocatalytic Period of 15 Minutes

Again from the perspective of process control, it would be useful to separately understand the dynamics of the two constituent processes of PIED – photocatalytic metal deposition (primarily responsible for metal nucleation) and subsequent auto-catalytic electroless deposition (primarily responsible for nucleate growth). Therefore, to further investigate these processes individually, m-TiO_2 sensitised quartz slides were exposed to Ag electroless plating solution for varying periods of sequential irradiated and non-irradiated immersion periods. As above, only a very small amount of nucleation occurred on samples that had undergone non-irradiated immersion only. From earlier experiments (*vide supra*), an irradiated immersion time of 15 min is able to produce a conductive Ag layer, albeit with incomplete coverage of the entire m-TiO_2 sensitised area. Continued irradiated immersion produces increasingly coherent and lustrous layers though the roles of photo and auto-catalysis in this period are not differentiated.

By immersing substrates in a plating bath for 15 min with irradiation before removing the light source for continued deposition in darkness, it is possible to assess the role of the auto-catalytic deposition alone during this period. The 15 min initiation time was selected for these experiments as it produces a comparable starting point of a metallic coating with visually detectable margins for improvement.

By using a 15 min irradiated immersion period for sample preparation, post-irradiation immersion experiments were conducted as a function of time. Continued immersion in

darkness clearly shows further deposition as the metal layer becomes more complete and lustrous with longer periods of dark growth, *Fig. 39*.

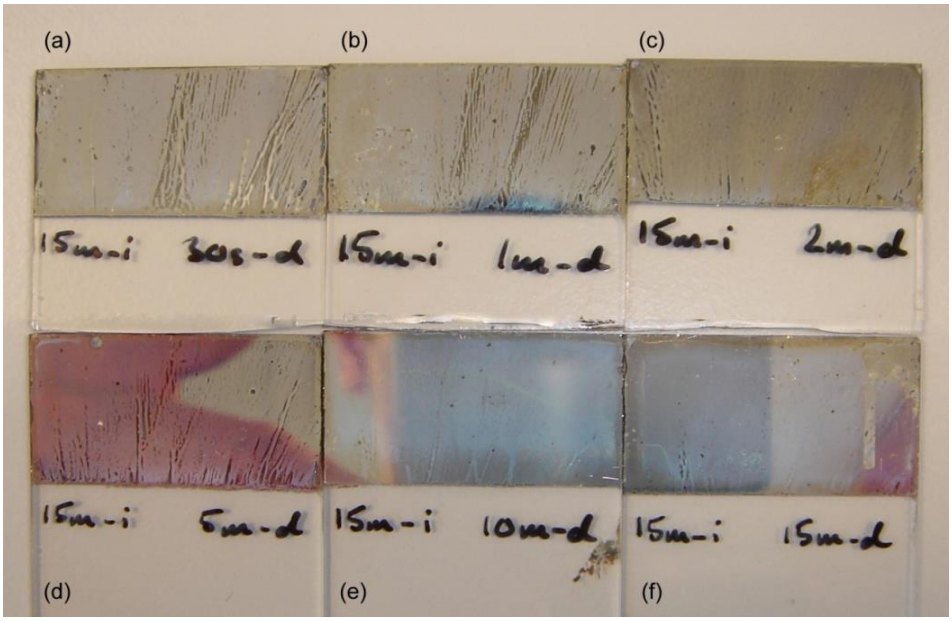

Fig. 39 Ag deposits after 15 min irradiation plus dark growth of (a) 30 s, (b) 1 min, (c) 2 min, (d) 5 min, (e) 10 min & (f) 15 min

After 15 min irradiated immersion and just 30 s further non-irradiated immersion the deposit is not fully conductive and shows considerable faults across the metal layer. These areas of poor deposition appear to be a direct translation of the macroscopic features within the TiO_2 layer beneath. As previous experiments have shown, a 15 min irradiated immersion is sufficient to produce a conductive layer and this suggests that the overall conductivity is largely affected by the quality, or lack of, of the TiO_2 coating. A TiO_2 layer with coverage deficiencies, and hence areas of poor sensitisation, produces a comparably poor metal deposit as nucleation on the incompletely covered areas is reduced. While the 15 min photocatalytic deposition lays down enough metal to produce a catalytic surface on those areas of the substrate with effective m-TiO_2 coverage and so sensitisation, after just 30 s there has been insufficient auto-catalytic deposition to cover the poorly m-TiO_2 covered / sensitised areas. As seen in *Fig. 39*, these areas are gradually encroached upon by continued auto-catalytic deposition with a surface of uniform appearance being visible after a further 10 and 15 min immersion. The deposits for these combined immersion times of

25 and 30 min are comparable to that seen after a 30 min fully irradiated immersion, Fig. 37 (b). Further evidence of the improving quality of this metal layer with dark immersion time is again provided by sheet resistivity measurements, Table 7, a resistivity value of 0.2 Ω / sq denoting full conductivity. Generally speaking, resistivity decreases with dark immersion time, any deviations from this trend being attributable to the inhomogenous nature of a metal coating that does not, as yet, cover the entire substrate – again due to incomplete substrate sensitisation by m-TiO_2.

Irradiation	15 min	15 min	15 min	15 min	15 min
Dark growth	1 min	2 min	5 min	10 min	15 min
Sheet Resistivity	1.6 Ω / sq	0.6 Ω / sq	0.8 Ω / sq	0.2 Ω / sq	0.2 Ω / sq

Table 7 Sheet resistivity measurements after 15 min irradiated immersion plus additional periods of deposition during non-irradiated, dark immersion

3.6.4.2 Photocatalytic Period of 5 Minutes

The results of the preceding section clearly demonstrate that a 15 min initiation period followed by auto-catalytic deposition in darkness can produce a metal layer of equal quality to that achieved by full irradiation over the same period of time. Therefore it is now known that electroless deposition is able to continue independently after successful photocatalytic initiation. However, the above experiments involve the use of an initial irradiation period that is itself known to produce a conductive layer as a basis for studying subsequent deposition in the dark. Therefore, in order to better observe the effect that the auto-catalytic process has on deposit quality, the initial irradiated immersion time was reduced to 5 min, a period which has been shown to only produce partial surface coverage with a non-conductive layer. Nonetheless, this offers a well nucleated base layer for further, auto-catalytic deposition to occur onto without the samples showing prior conductivity. As above, after the initial irradiation period, further deposition was observed after continued immersion in the electroless plating bath in the dark, Fig. 40.

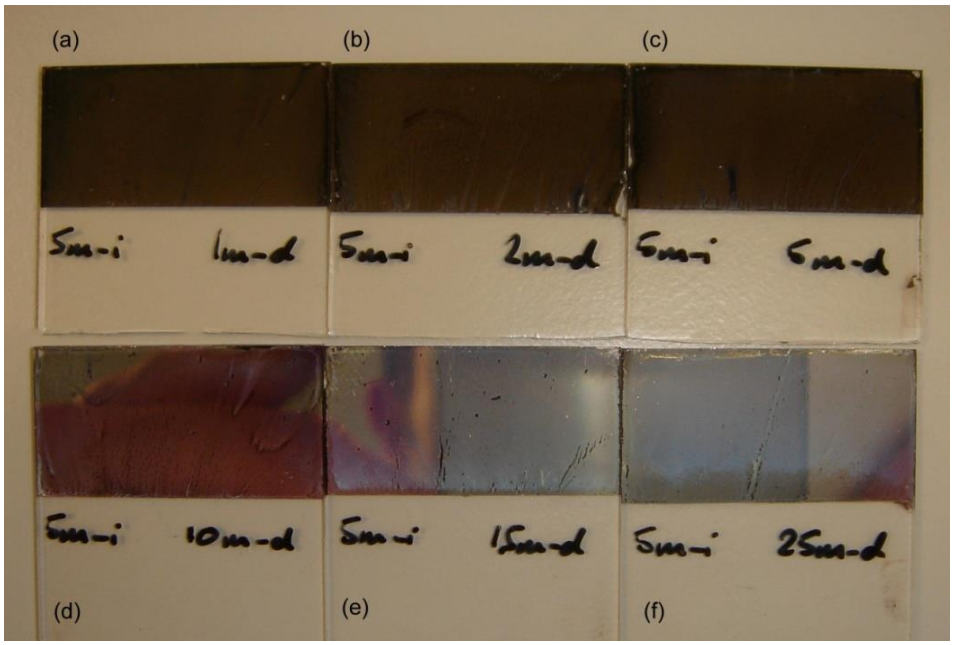

Fig. 40 Ag deposits after 5 min irradiation and dark growth of (a) 1 min, (b) 2 min, (c) 5 min, (d) 10 min, (e) 15 min & (f) 25 min

The metal deposits of Fig. 40 are clearly seen to progress from a brown to metallic appearance in the same pattern as all previous observations (Fig. 22, Fig. 32 & *Fig.* 39). Dark immersion periods of 1, 2 & 5 min all produce brown Ag deposits with increasing opacity though no conductivity. After a 10 min period of dark immersion, corresponding to a total immersion time of 15 min, Fig. 40 (d) it can be seen that a metallic finish has formed and, although there are some areas of transparency, Fig. 41 (b), the sample becomes conductive and finite sheet resistance can be measured, Table 8. This again corresponds with the previously observed minimum 15 min overall deposition time required to produce a sample with partial conductivity.

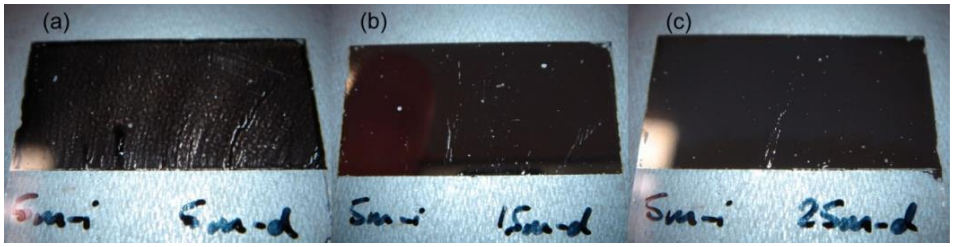

Fig. 41 Ag deposits after 5 min irradiation and dark growth of (a) 5 min, (b) 15 min & (c) 25 min viewed with LED backlighting

Irradiation	5 min	5 min	5 min	5 min	5 min
Dark growth	1 min	5 min	10 min	15 min	25 min
Sheet Resistivity	–	–	1.7 Ω / sq	0.3 Ω / sq	0.2 Ω / sq

Table 8 Sheet resistivity measurements after 5 min irradiated immersion plus extending dark growth periods

Further extension of the dark immersion period again demonstrates the presence of a continued auto-catalytic process as a 25 min dark immersion period and overall immersion period of 30 min produces a coherent and apparently uniform Ag layer, Fig. 40 (f), with full conductivity and associated low sheet resistance, Table 8. The metallic lustre is comparable to that produced from a 30 min irradiated immersion, Fig. 32 (j), as well as that from a 15 min irradiation with 15 min dark growth period, *Fig. 39* (f). Similarly, the microstructure of a sample produced by 5 min irradiated and 25 min non-irradiated immersion appears comparable to these previous results when viewed with SEM, Fig. 42.

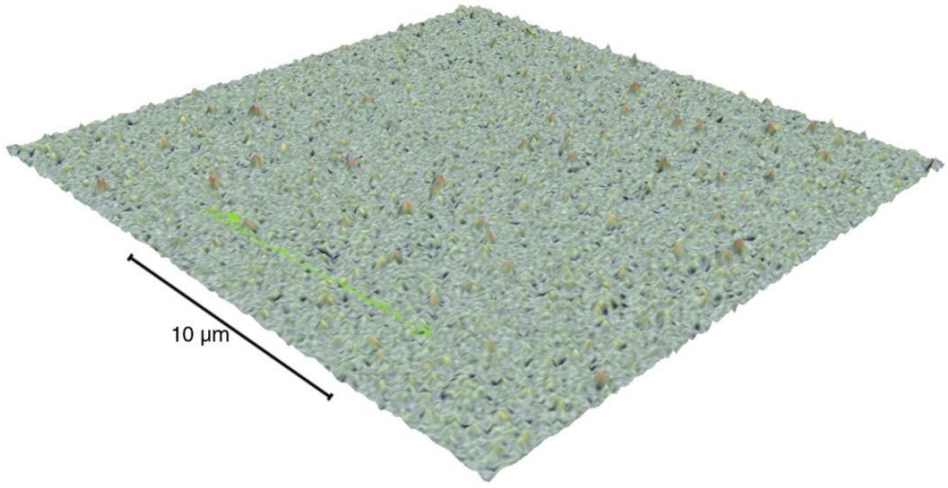

Fig. 42 3D SEM surface reconstruction of Ag after 5 m irradiation and 15 min dark growth

This further suggests that the auto, rather than the photocatalytic, deposition is the driving force beyond the first 5 min and that, a comparable metal layer can be produced with or without full irradiation given that sufficient photocatalytic nucleation has taken place.

Considering that the principle of PIED is to photocatalytically initiate electroless deposition rather than photocatalytically drive metal deposition throughout the whole immersion period, these results are as expected. Importantly, we have already demonstrated that as little as

30 s irradiation is sufficient to produce Ag nucleation. Thus, again in an attempt to gain greater insight into the respective importances of photocatalytic nucleation and auto-catalytic growth during the early stages of the immersion period, this minimal nucleation time was used to produce a pre-conductive layer on which to study auto-catalytic deposition, again for increasing periods of time. This study is the subject of the next section.

3.6.4.3 Photocatalytic Period of 30 Seconds

Samples irradiated for 30 s followed by dark growth periods of 1 - 5 min display increasingly brown Ag deposits, Fig. 43 (a, b & c), though these are noticeably lighter in pigmentation than those obtained for similar dark growth periods on samples subjected to 5 min irradiated immersion. This is most probably due to a reduced level of Ag deposit compared to those samples seen in Fig. 40 which were generated a longer, 5 min irradiation period.

After a 10 min period of subsequent non-irradiated immersion, and associated auto-catalytic deposition, the Ag layer begins to appear metallic although remains non-conductive and transparent to backlighting. Conductivity over small areas occurs after 15 min of dark deposition but to a lesser extent than usually seen from other 15 min net immersion period protocols (see sections 3.6.3, 3.6.4.1 & 3.6.4.2 above). Visually, the metal surface produced using a 30 s initial irradiation period followed by a net 15 min immersion is also more granular and inconsistent than that produced by a net 15 min immersion with a longer initial irradiated period. Only after 30 min of dark deposition is a fully conductive, visually complete, metallic layer produced though this is less lustrous than those produced with longer irradiation periods.

Sheet resistivity measurements support these observations with no finite value being obtained at times less than 15 min. The partially conductive sample achieved after 15 min deposition in the dark has a significantly higher resistivity, Table 9, than comparable immersion times with longer irradiation periods. This indicates a lower quality of Ag deposit being obtained due to the shorter period of irradiation. However, 30 min immersion in the

dark after an initial 30 s period of irradiation still produces a fully conductive metal layer with low resistivity.

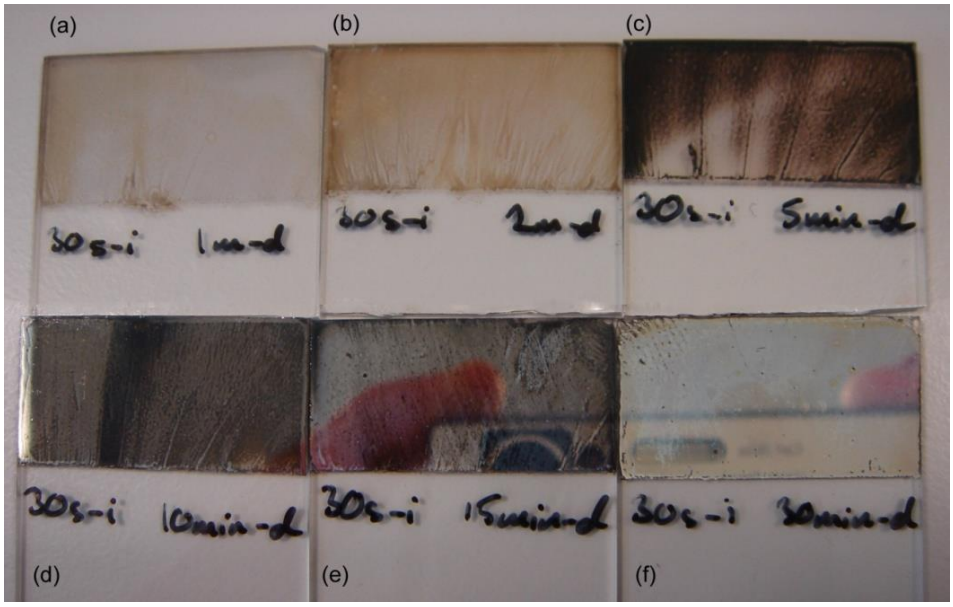

Fig. 43 Ag deposits after 30 s irradiation and dark growth of (a) 1 min, (b) 2 min, (c) 5 min, (d) 10 min, (e) 15 min & (f) 30 min

Irradiation	30 s	30 s	30 s	30 s
Dark growth	1-5 min	10 min	15 min	30 min
Sheet Resistivity	–	–	1,800 Ω / sq	0.2 Ω / sq

Table 9 Sheet resistivity measurements after 30 s irradiated immersion plus extending dark growth periods

It is known that an irradiation time of 30 s produces nucleation sites which, while comparatively few in comparison to those formed by longer irradiation, are numerous and capable of growth into a conductive metal layer. SEM images reveal that the early removal of irradiation and the resulting switch to an auto-catalytic process focuses Ag deposition onto the larger nucleation sites, increasing their size and forming several, disproportionately large Ag particles, Fig. 44.

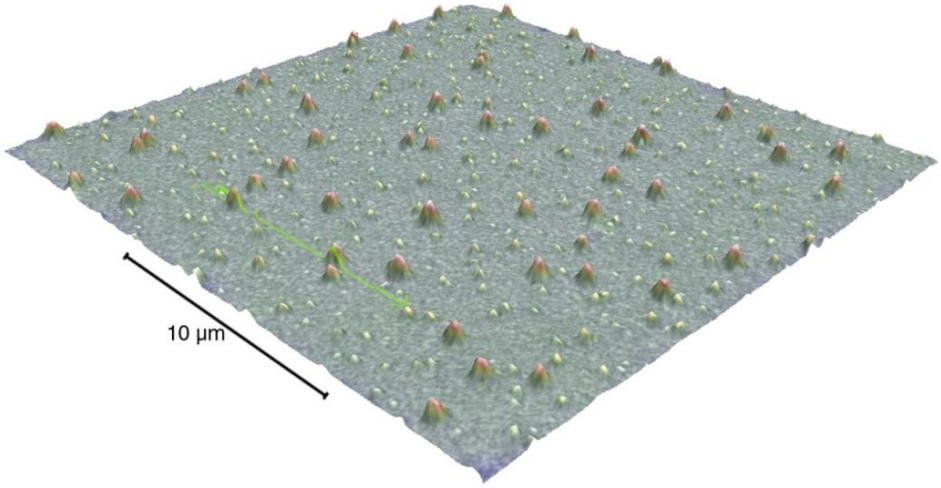

Fig. 44 3D SEM surface reconstruction of Ag after 30 s irradiation and 2 min dark growth

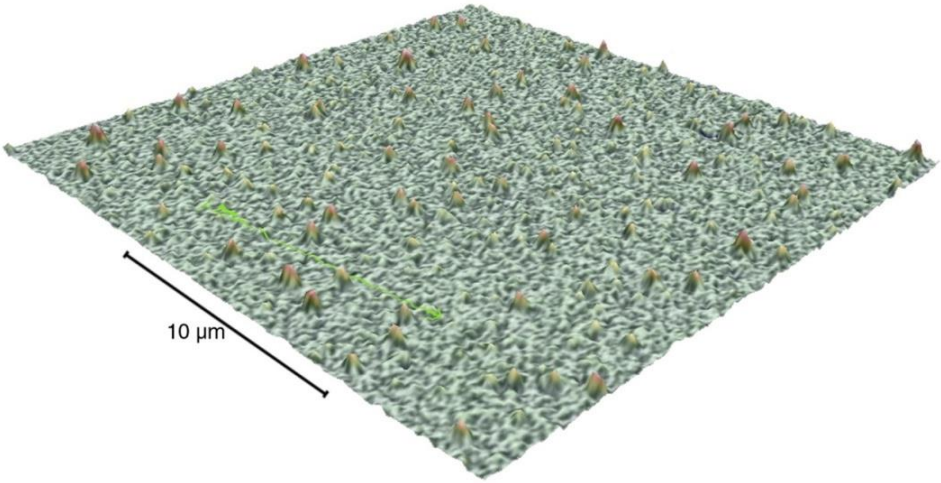

Fig. 45 3D SEM surface reconstruction of Ag after 30 s irradiation and 15 min dark growth

With continued immersion, Ag is auto-catalytically deposited onto all existing nucleation sites, the lateral growth of which ultimately forms a conductive metal layer; however, the reduced number of nuclei means that more auto-catalytic deposition is require at each nucleation site before a conductive metal layer is formed. The impact of this on the microstructure of the layer is that large Ag particles persist and give the metal a coarse granularity, Fig. 45, when compared with the microstructure of a deposit resulting from a longer initial irradiation period, Fig. 42.

The findings of these time dependent studies can be summarised as follows. The initial irradiated immersion period promotes the formation of Ag nuclei on the TiO_2 surface. Longer initial irradiation periods and, by implication larger surface concentrations of metal nuclei,

lead to metal deposits with finer granularity and a more reflective appearance, whilst shorter initial irradiation periods, and hence fewer nuclei, result in coarser and more granular deposit structure. While an irradiation of 30 s is capable of producing a fully conductive and metallic Ag layer, longer irradiation / nucleation times are needed for higher quality metal deposits and a more efficient process.

3.6.4.4 Conductivity Summary

Table 10 summarises the results of the sheet resistivity / conductivity measurements of the Ag layers produced during this study. Conductivity is indicated by a resistivity measurement of 0.2 Ω / sq or lower; samples designated as exhibiting partial conductivity show conductivity in small areas of the sample in question while typically recording a higher or wide variation in resistivity across the sample as a whole. Conducting layers were consistently produced when the combined immersion times of irradiated plus non-irradiated immersion periods exceeded 20 min. At times shorter than this, conductive metal layers are produced, though not completely homogenous across the entire sample area.

Irradiation Period	0.5 min	1 min	2 min	3 min	5 min	15 min	30 min	60 min
Dark 0 min	x	x	x	x	x	o	✓	✓
Dark 1 min	x	x	x	x	x	o	✓	✓
Dark 2 min	x	x	x	x	x	o	✓	✓
Dark 5 min	x	x	x	x	x	o	✓	✓
Dark 10 min	x	x	o	o	o	✓	✓	✓
Dark 15 min	o	o	o	o	✓	✓	✓	✓
Dark 30 min	✓	✓	✓	✓	✓	✓	✓	✓

Table 10 Summary of conductivity of PIED Ag layers on m-TiO_2 coated quartz

x = non-conducting, o = partially conducting, ✓ = conducting

3.6.5 Control of Deposition

While PIED is a highly flexible technique, able to be applied to a range of different metals and substrates, the process also offers several means of controllability and hence process advantages. Traditional modifications to electroless plating baths are able to yield improved stability or increased deposition rates but typically the electroless process lacks control in

aspects such as initiation onset and area of coverage. PIED affords much greater control with particular benefits in these areas.

As the process involves photocatalysis, the initiation of metal deposition is dependent on the presence of a suitable photocatalyst and irradiation of this photocatalyst with ultra-band gap light energy. The dependency of process initiation on each of these factors means that both provide a means to control PIED with metal deposition being prevented by the lack of either. The effect of these and other influencing factors is discussed below.

3.6.5.1 Sensitisation Area

As discussed above, photocatalytic initiation cannot take place unless the substrate has been first sensitised with a photo-active compound, in this case TiO_2. Clearly this offers simple control over special specificity of the metallisation process by virtue of whether the substrate surface is sensitised with TiO_2 or not. A wide variety of TiO_2 sensitisation methods are possible beyond the spin and dip coating techniques described above, including sputter coating [130], oxidative hydrolysis [131,132] and thermal spraying [133]. Spin and dip coating themselves can be restricted to a desired area by simply masking the substrate prior to TiO_2 coating. This produces sensitised areas which are to be subsequently metallised and non-sensitised areas onto which no metal deposition occurs and hence, selective metal coverage.

3.6.5.2 Irradiation Period

In addition to the presence of a photocatalyst, PIED also depends on the application of sufficient light energy to produce a catalytic effect. In the case of wide band gap metal oxides such as TiO_2, SnO_2 etc, this energy is provided by UV light and metal deposition onto the TiO_2 does not begin until the sample is irradiated. This light-switchable initiation provides a significant improvement over traditional sensitisation methods which decorate a substrate with catalytic metal nucleates prior to electroless deposition. In such traditional sensitisation methods, the electroless deposition process will enter the auto-catalytic stage immediately

on immersion of the sensitised sample within the plating bath. In contrast, a TiO_2 sensitised sample remains inactive when immersed in an electroless bath until it is irradiated. This means that the initiation of metal deposition can be easily controlled and that stability is maintained in the early stages of deposition, crucial to the quality of the final metal layer.

In addition to direct onset control, irradiation continues to drive photocatalytic nucleation and hence the length of the irradiated period can be seen to affect the properties of the produced metal layer. Very short irradiation times, such as 30 s, provide enough nucleation for continued auto-catalytic deposition and can produce a complete, conductive metal film; however, a noticeable difference in the auto-catalytic deposition rate and metal quality is seen as the initiating irradiation period is varied. The small amount of nucleation produced in short times is an effective initiation for electroless deposition but the number of sites available for auto-catalytic deposition is restricted, leading to a more granular deposit. By applying irradiation for a longer time, the photocatalytic nucleation process is driven for longer and hence produces more nucleation sites. The greater amount of metal nucleation makes the following auto-catalytic deposition occur at a higher rate and onto more sites producing a metal layer with finer granularity and hence a smoother, more reflective surface.

3.6.5.3 Immersion Time

Just as the period of irradiated immersion has a direct consequence on the amount of nucleation, the total time that a sample is immersed in the electroless plating bath, in light and dark, determines the maximum extent of metal deposition. Once auto-catalytic deposition begins, metal will continue to deposit onto the nucleated area until the substrate is removed from the electroless bath or the bath constituents are depleted. Bath constituents are typically plentiful for a lengthy deposition and can also be replenished throughout the process; immersion time therefore becomes the controlling influence with longer times producing thicker metal layers. Therefore, metal layers of predictable thickness can be formed as deposition can be easily halted before the metal growth extends beyond a desired point.

3.6.5.4 Spatial Restriction

While PIED is dependent on the sample being sensitised with a photocatalyst and irradiated, further control of the spatial specificity of deposition can be achieved even when both are present. A fully sensitised substrate can be selectively metallised by masking any areas required to remain free from metal. This masking can be achieved by the application of a physical barrier layer such as a clear varnish in order to prevent access of the metal precursor to the photocatalyst, so disabling metal deposition without affecting metallisation of non-masked areas. Masking with an opaque material may also be used to restrict the sample area receiving irradiation and hence prevent photocatalytic metal reduction in masked regions. Similarly, controlling the area of irradiation by use of either a beam spot or a patterned irradiation field may be used to restrict the incident light impinging selected areas, in turn restricting the areas of the photocatalyst sensitised substrate on which metal nucleation can occur. Coating-based masking offers the most effective restriction as metal deposition is physically prevented. However, this does involve the application of an additional material to the substrate surface and may present difficulties in removal; a masking layer may be easily removed from a glass substrate but may be less readily peeled away from other insulating substrates such as a flexible polymer membrane. Local irradiation avoids the need to apply any such material but lacks the absolute restriction of metal deposition beyond the area of intended metallisation. This is because, irrespective of how precisely the irradiation is applied, the nature of PIED and particularly the auto-catalytic growth of the deposit make it highly likely that metallisation will occur laterally across the substrate surface, beyond the irradiated area.

3.7 Conclusions

The scope for the application of metal deposition onto insulating substrates remains wide for modern research and industry though the traditionally utilised electroless plating methods hold several disadvantages. These include narrow restrictions on the types of materials

which may be metallised, extensive and laborious sensitisation methods and a lack of control over the deposition process and the resulting metal layer.

Through photocatalysis, the use of chemically and photochemically stable, wide band gap semiconductor materials, such as TiO_2, as surface sensitisers allows for metal to be deposited onto an extensive range of substrate materials by photochemically initiated means. Upon irradiation with ultra-band gap light energy, the photogenerated electrons within the semiconductor are able to partake in local redox reactions, where thermodynamically viable. Such reactions include the reduction of metal ions from solution resulting in the direct metallisation of the semiconductor particle. TiO_2 has proven to be particularly applicable to such a scenario with a broad band gap in the near UV (so avoiding adventitious process initiation by ambient light) and a conduction band edge that is more negative than the redox potential of a range of metal ions.

Photocatalytic metal deposition, as opposed to PIED, is long established but due to the thinness and granular nature of the deposit has not been exploited as a coating technology. Confirming earlier results from other groups, our own studies show that photocatalytically generated Ag and Pd nucleation can be observed in the absence of any other reductant. This shows that the photocatalyst alone is capable of reducing metal ions directly from solution. However, the deposition rate and, in the case of Pd, the required energy input are uneconomical. In light of this, we have demonstrated and developed PIED as an effective method for the metallisation of a range of materials with several different metals.

In PIED, photocatalytic metal deposition is used to generate metal nucleates. These are then subjected, either simultaneously or sequentially, to an auto-catalytic growth stage by exposure to an electroless deposition bath containing an appropriate metal precursor / reductant mixture. Metal layers formed through this combined process are smooth and reflective with conductivity after as little as 15 min immersion in the electroless bath, a significant increase in deposition rate and efficiency in comparison to photocatalytic metal reduction in the absence of a chemical reductant. Importantly we see that metal deposition

does not begin onto an immersed, photocatalyst sensitised substrate until it is photo initiated with ultra-band gap irradiation. Furthermore, the metal deposition occurs exclusively onto semiconductor sensitised areas, and then only those areas also subject to ultra-band gap irradiation. Hence PIED offers considerable control over when and where metal deposition takes place.

Timed deposition studies show that PIED produces thicker, more coherent metal layers as immersion time increases via a combination of photo and auto-catalytic deposition processes. The roles of these separate component processes may be further understood through varying the periods of irradiated and non-irradiated immersion. These studies show that a conductive metal deposit can be formed following an initiating irradiation period of as little as 30 s. However, the period of irradiation has further influence on the properties of the deposit beyond simple initiation. The nature of electroless deposition dictates that grain size, and hence roughness of the final metal deposit is determined by the balance between the surface density of nucleation sites and the rate of growth by auto-catalytic deposition. A higher density of nucleation sites and a slower growth rate result in a smoother metal deposit with a finer grain and *vice versa*. In PIED, the nucleation stage is controlled by semiconductor photocatalysis and hence the density of nucleation sites, and consequently the properties of the resulting metal layer, is determined by the length and effectiveness of the photocatalytic initiation period. While an irradiation period of 30 s is sufficient to produce a conductive metal layer, the density of nucleation sites so produced is smaller than that produced during longer irradiation periods with larger metal grain sizes arising post-growth. Significant improvements in layer quality (smaller grain size) are seen when the photocatalytic initiation period is extended by as little as 5 min.

Overall, PIED represents a highly effective application of semiconductor photocatalysis to metal deposition technology. PIED retains the inherent benefits of electroless deposition in that it can be used to metallise non-conducting materials but also has several process advantages. The deposition of metal directly onto the semiconductor obviates the need for other, more extensive sensitisation and surface preparation methods and hence offers

improved product purity. Meanwhile, the combination of metal nucleation and growth into a single process provides immediate advantages in time and cost. In addition to this, the technique offers multiple means by which the deposition process can be tailored and controlled while remaining highly flexible and versatile. PIED can be applied to many different material types, conducting and non-conducting, organic and inorganic, while allowing for the metallisation of specific areas of the substrate material through selective sensitisation or irradiation. Furthermore, it can be used to produce metal layers of varying thickness by simple control over rate and duration of deposition.

It is clear then, that semiconductor photocatalysis is a powerful and oft overlooked tool for applications in metal deposition. While branch applications include heavy metal recovery, semiconductor doping and the formation of metal nano-particles, photocatalysis can also be incorporated as an integral part of efficient and novel metal deposition processes.

3.8 Acknowledgements

We would like to thank The Royal Society of Chemistry (RSC), The Engineering and Physical Sciences Research Council (EPSRC) and The Lloyd's Register Educational Trust (LRET) for their support and funding towards this research.

CHAPTER 4

METHOD FOR FORMATION OF POROUS METAL COATINGS

International Patent Application PCT/GB2011/001402, Pub. No. WO/2012/042203, 2011

Michael A. Bromley, Colin Boxall*

Engineering Department, Lancaster University, Lancaster LA1 4YR, UK

"Lister, if you must know, I submitted a discourse on porous circuitry that was too... radical, too unconventional, too mould-breaking for the examiners to accept."

Arnold J. Rimmer

4.1 Publication Summary

- Published patent application for the method of forming porous metal films on insulating surfaces
- The claimed novelty and innovation of porous metallisation through PIED are defined

4.2 Author Contributions

- M.A.B.: designed and performed all experiments, analysis and characterisation; co-author of the application and of various responses to prior art searches
- C.B.: conceived and supervised the study; co-author of the application and of various responses to prior art searches
- Additional authorship from Research & Enterprise Services at Lancaster University for drafting of application format and determining claims

4.3 Abstract

A method of forming a metal layer on an electrically insulating substrate comprises depositing a photocatalyst layer onto the substrate and depositing a mask layer comprising voids on the substrate, such as a layer of latex microparticles with voids between them, to give an open pore structure to the mask. An electroless plating solution is then provided on the photocatalyst layer, and the photocatalyst layer and electroless plating solution are irradiated with actinic radiation whereby deposition of metal from the electroless plating solution to form a metal layer on the photocatalyst layer is initiated whereby the metal deposits in the voids of the mask layer. The mask layer is subsequently removed to leave a porous metal layer on the substrate.

The method allows for deposition of porous metal films with controlled thickness and excellent adhesion onto electrically insulating substrates. The method is suitable for providing metal layers with controlled, regular porosity.

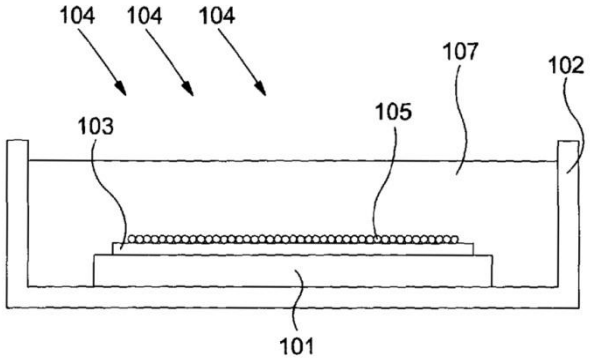

Fig. 46 Schematic cross-sectional view through a substrate prepared for metal deposition

4.4 Method of Metal Deposition

The present invention is concerned with methods of depositing metal onto substrates from an electroless plating solution. In particular, it relates to the deposition of metal layers, particularly porous metal layers, onto insulating substrates.

4.4.1 Background

Substrates having one or more metal layers deposited on one or more of their surfaces have many industrial uses. For instance, insulating films having a metal layer or layers on one or more surfaces are of use in separation processes, fuel cells, super-capacitors, electrolytic cells for splitting water into hydrogen and oxygen, and for catalysis.

Electroplating (also known as electro-deposition) is a well known industrial process that uses electrical current to reduce ionic precursors of a desired material (usually a metal) from a solution (aqueous or non-aqueous) in order to coat a conductive substrate with a layer of the desired material. The electrically conductive substrate may be suitably used as one of the electrodes in an electrochemical cell whereby the electrical current causing electroplating is provided, effecting the electroplating. US patent publication 6,203,925 (Attard *et al*) [53] and international patent application Publication WO 99/00536 (Bartlett *et al*) [52] disclose the production of porous metal films on electrically conducting substrates by electro-deposition from a liquid crystalline phase.

US patent publication 2,532,283 (Abner & Riddell) [8] discloses electroless plating. Electroless plating is an auto-catalytic reaction used to deposit a coating of a desired material (usually a metal) from an electroless plating solution (usually an aqueous solution) onto a substrate (usually a conducting substrate). In contrast to electroplating, electroless plating does not require application of an electric current. Instead, deposition proceeds as a chemical reaction at the surface of the substrate.

Once deposition by electroless plating has been initiated, the electroless reaction is typically self-sustaining until either: a) the electroless plating solution is exhausted, b) the substrate is

removed from the electroless plating solution, or c) the composition of the solution is adjusted to terminate plating. Electroplating is suitable for use with electrically conducting substrates. Electroless plating offers the advantage of allowing deposition of material by plating onto electrically insulating substrates.

Prior electroless plating methods require substantial preparation of the substrate prior to commencement of plating. Typically, prior to commencement of electroless plating, a catalytic metal such as Pd is first deposited onto the substrate as a seed or nucleation layer, most usually in a two step process, for example: (i) priming of the substrate with an acidic $SnCl_2$ solution is carried out, this resulting in adsorption of Sn^{2+} ions onto the surface from the solution to provide a primed surface; (ii) treatment of the primed surface with a solution of $PdCl_2$ in hydrochloric acid whereby Sn^{2+} ions adsorbed in step (i) reduce Pd (II) ions in solution to form deposits of metallic Pd on the substrate surface.

These Pd deposits subsequently act as nucleation sites during electroless plating of the desired metal, which may be Pd or which may be a different metal. It is also known, in the prior art, to combine the metal ions for priming and those used for providing nucleation sites on the surface to be treated in a single pre-treatment solution. This may result in initial adsorption of Sn-Pd particles onto the surface of the substrate, with the Sn subsequently removed by treatment with concentrated hydrochloric acid to leave Pd deposits on the surface to act as nucleation sites for electroless deposition. However, irrespective of which pre-preparation method is used to provide a substrate ready for electroless deposition, the pre-preparation method may have to be repeated up to ten times in order to achieve a surface adequately modified to act as a template for electroless deposition.

This is both costly and time consuming. Also, lengthy surface preparation, involving cleaning, etching and neutralising, may be required, prior to electroless plating and / or prior to pre-treatment. This is in order to promote adhesive bonding of the electroless metal layer to the substrate surface upon which it is deposited. Furthermore, the resulting metal deposit, generated by electroless plating, will contain Pd and may include Sn, this latter metal being a

particularly troublesome and undesirable impurity if the substrate upon which the metal layer has been deposited is for subsequent use in electrochemical applications.

Photocatalytic deposition of metals onto semiconductors is a mature technology in the prior art. In particular, TiO_2 is known as a photocatalyst for use in the reductive deposition of noble metals such as Pd and Pt onto semiconductor surfaces. During irradiation of TiO_2, using actinic radiation such as ultra-violet radiation having a photon energy in excess of the band gap of the TiO_2, electrons may be excited and drive redox reactions, catalysed by the TiO_2 particles and leading to deposition of metal from a treatment solution onto the semiconductor surface.

However, such processes typically result in either:

a) a layer of deposited nano-particles of metal with a granular structure and highly disordered porosity, or

b) a coherent monolayer of metal, the formation of which results in cessation of the plating process once the surface and its photocatalyst layer are masked.

There is no control of layer thickness afforded in either instance.

It is also known to use photo-catalysis such as TiO_2 in etching of surfaces as well as deposition. US patent publication 7,067,237 [134] and US patent application publication 2006-0019076-A [135] disclose modification of surfaces using a photocatalyst followed by electroless deposition onto the modified surface. The processes disclosed in these documents comprise separate, discrete process steps for photoexcitation, primer metal nucleation and then electroless metal deposition.

Hence, there is a need for electroless methods of deposition of metal layers onto substrates which obviate the complex substrate treatment regimes required in the prior art and which eliminate the need for primer or nucleation metals to be present in or below deposited layers.

4.5 Summary of the Invention

It is one object of the invention, amongst others, to provide electroless methods of deposition of metal layers onto electrically insulating substrate surfaces which obviate the complex substrate treatment regimes required in the prior art. In particular, it is an object of the invention to provide methods which do not require deposition of primer or nucleation metals prior to electroless deposition. It is a further object of the invention to provide methods which ensure that the metal layers deposited are strongly adhered to the substrate surface upon which they are formed. It is a further object of the invention to provide methods for deposition of porous metal layers onto substrate surfaces. Another object of the invention is to provide methods for depositing metal layers wherein the thickness of the deposited metal layer is easily controllable during the deposition method. A further object of the invention is to provide simpler methods than those of the prior art, for instance requiring fewer process steps or obviating the need for deposition of a primer metal onto a surface prior to electroless deposition of a metal.

The invention provides, in a first aspect, a method of forming a porous metal layer on an electrically insulating substrate, the method comprising:

a) depositing a photocatalyst layer onto the substrate,

b) depositing a mask layer comprising voids, on the photocatalyst layer,

c) providing an electroless plating solution on the mask layer and photocatalyst layer,

d) irradiating the photocatalyst layer, mask layer and electroless plating solution with actinic radiation whereby deposition of metal from the electroless plating solution to form a metal layer on the photocatalyst layer is initiated, whereby deposition of the metal occurs within the voids, and

e) removing the mask layer following deposition of the metal to provide a porous metal layer.

In a second aspect, the invention provides a method of forming a porous metal layer on a substrate, the method comprising:

a) depositing a mask layer comprising voids on the substrate, wherein the mask layer is a layer of microparticles, the voids being the spaces between the microparticles,

b) depositing metal onto the substrate, whereby the metal deposits in the voids of the mask layer, and

c) removing the mask layer to leave a porous metal layer on the substrate, wherein the metal is deposited by electroless plating from an electroless plating solution.

4.6 Detailed Description of the Invention

Throughout this specification, the term “comprising” or “comprises” means including the component(s) specified but not to the exclusion of the presence of others. The term “consisting essentially of” or “consists essentially of” means including the components specified but excluding other components except for materials present as impurities, unavoidable materials present as a result of processes used to provide the components, and components added for a purpose other than achieving the technical effect of the invention. Typically, a composition consisting essentially of a set of components will comprise less than 5% by weight, typically less than 3% by weight, more typically less than 1% by weight of non-specified components, where % weight is used to define a composition. Where g / dm^3 is used to define levels of components in a composition, the composition consisting essentially of a set of components will typically comprise less than 50 g / dm^3, typically less than 30 g / dm^3, more typically less than 10 g / dm^3 of non-specified components.

Whenever appropriate, the use of the term “comprises” or “comprising” may also be taken to include the meaning “consists essentially of” or “consisting essentially of”, or “consisting of”.

By actinic radiation is meant radiation, typically electromagnetic radiation, capable of inducing chemical reaction when used to irradiate the photocatalyst layer. Typically, the actinic radiation will be ultraviolet radiation.

The method of the first aspect of the invention comprises, in step (a), depositing a photocatalyst layer onto the substrate. The photocatalyst layer comprises or consists essentially of a photocatalyst, for instance TiO_2 or the like, for instance in particulate form, which is capable of inducing reductive deposition of a metal from an electroless plating solution when suitably irradiated with actinic radiation. Suitably, the photocatalyst layer is deposited directly onto the substrate (*i.e.* without any binder or primer layer being used).

The photocatalyst layer may comprise any suitable photocatalyst which may typically be present as colloidal particles (having a volume mean particle size say from 1 to 1000 nm). The photocatalyst may comprise or consist essentially of a semiconductor, and suitably may comprise or consist essentially of a particulate semiconductor. For instance the photocatalyst may be selected from semiconducting single, binary and ternary metal oxides with band gaps corresponding to photon energies in the visible, near and middle ultraviolet UV spectral regions (say 1.5 to 6.0 eV), or doped versions thereof, regardless of crystalline phase (e.g. for TiO_2 - anatase, rutile or brookite may be employed) or of crystalline habit (spheres, needles, etc.). Suitably, the band gap may be 3.5 eV or less, such as 3.2 eV or less.

Examples of suitable semiconductor photocatalysis include; single metal oxides: WO_3, SnO_2, alpha and gamma Fe_2O_3, TiO_2, indium oxide, $BiVO_4$, ZnO; binary metal oxides: $BaTiO_3$, $SrTiO_3$, $FeTiO_3$; ternaries: $In_{0.9}Ni_{0.1}TaO_4$. Mixtures of such catalysts may also be used.

Preferably, the photocatalyst layer may comprise or consist essentially of TiO_2, suitable to act as photocatalyst for electroless deposition of metal. Preferably, the TiO_2 may be in particulate form. The TiO_2 may, for instance, be deposited onto the substrate surface as colloidal particles or as a mesoporous film, for instance prepared by sol-gel deposition, such as set out in J. Mater. Chem., 2004, 14, 1187-1189 [136].

The method of the invention comprises, in step (b), depositing a mask layer comprising voids, the mask layer provided on the photocatalyst layer, whereby deposition of the metal occurs within the voids. The mask layer is removed (e.g. by its dissolution) in step (e), following deposition of the metal, whereby the metal layer is a porous metal layer.

The mask layer is a porous mask layer with voids forming the pore space of the mask layer and may be formed or provided by any suitable method. The porous mask layer is deposited on the substrate prior to application of the electroless plating solution in the subsequent process step (c). One method to form such a mask layer is to deposit a layer of microparticles, the voids being provided by the spaces between the microparticles. The mask layer is suitably of an open porous structure whereby the electroless plating solution is in fluid contact with the substrate through the open pore structure of the mask layer. Preferably, the layer of microparticles is substantially a monolayer when shallow, 2-dimensional porosity is required, allowing the electroless plating solution to efficiently contact the photocatalyst layer through voids between the microparticles, but may also be of 2 or more layers where 3-dimensional porosity is required. By microparticles is meant particles having a mean diameter (volume mean diameter as measured by light scattering particle sizing apparatus such as a Malvern Mastersizer™) from 50 to 1000 nm. The particle may have any shape but preferably may be spheroidal or more preferably substantially spherical in shape. The shape of the microparticles generates the shape of the resulting pores, after removal of the microparticles. Hence microparticles of different sizes and / or geometries may be suitably chosen to produce layers suitable for different applications.

Suitably, the microparticles may be polymer latex particles. These may be deposited from a latex solution onto the substrate surface on the photocatalyst layer to provide deposition of the mask layer. A suitable volume of latex solution to provide a substantial monolayer of microparticles may be used to provide the porous mask layer by depositing a calculated volume onto the substrate and evaporating the liquid to leave the latex particles deposited as a substantial monolayer on the surface. The volume of latex solution or the latex concentration of that solution may be increased to a suitable level to produce multiple layers of microspheres on the surface.

Suitable polymers for the latex microparticles include polystyrene, natural or synthetic rubbers, polyethylene or the like, as are well known and readily commercially available.

Suitably, the microparticles may be substantially monodisperse in diameter.

As electroless deposition of metal from the electroless plating solution onto the photocatalyst layer is initiated and proceeds, metal is deposited in the voids of the mask layer and cannot form where the mask layer skeleton is present. For instance, for a layer of microparticles, the metal is deposited in the voids between the microparticles.

Once metal deposition has been stopped, for instance by exhaustion of the electroless plating solution or by removal of the substrate from the electroless plating solution, the mask layer may be removed, for instance by dissolution using a suitable solvent, whereby a porous metal layer is left deposited on the substrate surface, the pore space of the metal layer being formed by voids left behind when the mask layer is dissolved and removed.

In step (c), an electroless plating solution is provided on the photocatalyst layer, on the substrate. The electroless plating solution may be any suitable electroless plating solution. Suitably, an aqueous solution may be used, meaning that the electroless plating solution comprises at least 700 g / dm^3 by weight of water in addition to other components making up the balance of the electroless plating solution. Details of electroless plating methods and solutions are found in “Electroless plating: fundamentals and applications” – Mallory and Hadju – 1990 [7].

Other components of the electroless plating solution may include a metal salt, typically from 0.5 to 20 g / dm^3 of metal salt, for instance from 1 to 10 g / dm^3, say from 1 to 5 g / dm^3. The metal salt or precursor is a source of ions for the metal to be deposited, such as $AgNO_3$ for Ag deposition or $PdCl_2$ for Pd deposition. There may also be included a complexant, such as a chelating agent, for instance ethylenediamine, EDTA (ethylene diamine tetra-acetic acid) di-sodium salt or the like. The complexant may suitably be present at a level from 1 to 200 g / dm^3, for instance from 2 to 100 g / dm^3. Stabiliser such as 3,5 di-iodotyrosine, ammonium hydroxide or the like may also be included. This stabiliser may be typically at a level from 0.001 to 150 g / dm^3.

The role of the complexant and / or stabiliser is to stabilise the electroless plating solution by reducing the concentration of free metal ions, preventing or reducing precipitation of undesirable basic metal salts and also may act as a buffer to prevent rapid decrease in pH as electroless plating progresses.

A further ingredient which may be present in the electroless plating solution is a reducing agent, reductant and / or scavenger such as potassium sodium tartrate, hydrazine or the like. The scavenger is a hole scavenger and may be the same chemical as the reducing agent or reductant. The reducing agent acts as electron donor for the auto-catalytic stage of metal reduction. Other examples of suitable reducing agents include sodium hypophosphite and ethanol. Typically these may be present at a level from 0.5 to 50 g / dm^3, say 0.6 to 15 g / dm^3.

By hole scavenger is meant a compound which donates electrons to fill in hole-type (as opposed to electron) conductors which may form on photocatalysts such as TiO_2 upon photoexcitation of electrons. The use of a hole scavenger may enhance the capability of the photocatalyst to reduce the metal ions and make them more available in solution. If holes remain un-scavenged, an electron accumulation layer may form, inhibiting further deposition.

Step (d) involves irradiating the photocatalyst layer and electroless plating solution with actinic radiation whereby deposition of metal from the electroless plating solution to form a metal layer on the photocatalyst layer is initiated.

The actinic radiation is typically ultraviolet radiation. For instance the ultraviolet radiation has a photon energy sufficient to excite electrons across the band gap of the photocatalyst whereby reduction reactions are catalysed.

The deposition of the metal onto the photocatalyst layer means that a layer of the metal is deposited onto the substrate, on the photocatalyst layer. Steps (a), (b), (c) and (d) are applied sequentially but other steps may be carried out between them. Once the deposition of metal from the electroless plating solution has been initiated, it may then continue auto-

catalytically in the absence of further irradiation with suitable actinic radiation. The deposition of metal within the voids may be self-sustaining following initiation by irradiation with actinic radiation. The deposition of metal within the voids may be sustained by electroless deposition to achieve a desired or required thickness.

The method of the invention may be used in selective deposition of metal layers onto different parts of a substrate surface, so that some portions of a substrate are provided with a metal layer, and other parts are free of deposited metal.

For instance the method of the invention may comprise selecting a first portion of surface upon which the metal layer is formed and a second portion which remain free of metal layer by irradiating the first portion but not the second portion with the actinic radiation.

In another embodiment, the method of the invention may comprise selecting a first portion of surface upon which the metal layer is formed and a second portion which remains free of metal layer by depositing the photocatalyst layer on the first portion and no photocatalyst layer on the second portion.

The method of the invention is for use with a substrate of an electrically insulating material, as electroless deposition does not require an electrically conductive substrate. By electrically insulating is meant a material having a conductivity of less than 1 S / m.

The metal may suitably be Ag or Pd. Electroless plating of these methods is known in the prior art and electroless plating solutions are readily available.

In a second aspect, the invention provides a method of forming a porous metal layer on a substrate, the method comprising:

a) depositing a mask layer comprising voids on the substrate, wherein the mask layer is a layer of microparticles, the voids being the spaces between the microparticles,

b) depositing metal onto the substrate, whereby the metal deposits in the voids of the mask layer, and

c) removing the mask layer to leave a porous metal layer on the substrate, wherein the metal is deposited by electroless plating from an electroless plating solution.

As with the first aspect of the invention, the substrate may be an electrically insulating substrate.

For the avoidance of doubt, the optional features set out for the first aspect of the invention are also applicable, where appropriate, to the second aspect of the invention.

Specific embodiments of the invention will now be described further by reference to the following, non-limiting examples. Reference will also be made to the accompanying Fig. 46 which shows a schematic cross-sectional view through a substrate prepared for metal deposition using an embodiment of the method of the first aspect of the invention.

4.7 Examples

All reagents used were AnalaR™ grade or better, and purchased from Sigma Aldrich, Gillingham, Dorset, UK. All water used was Ultrapure from a Direct-Q 3 UV Millipore water purification system (Millipore (U.K.) Limited, Watford, UK) to a resistivity of 18.2 MΩ / cm. The PVDF (polyvinylidene fluoride) membranes were purchased from Millipore, the pore size was 200 nm.

4.7.1 Deposition of TiO_2 Photocatalyst onto Glass Slides by Spin Coating

Mesoporous films of colloidal TiO_2 were prepared using a modified reverse micellar sol-gel method. Firstly, triton X-100 (26g) and cyclohexane (150 ml) were mixed to form the reverse micellar solution. Water (1.08 g), titanium isopropoxide (23 g) and acetylacetone (10 ml) were added. The resultant sol-gel was applied to substrates by spin-coating for 5 seconds at 2900 rpm. The substrates were then fired in a furnace at 770 K for 1 hour. The substrates were stored in the dark at room temperature before use.

4.7.2 Deposition of TiO_2 Photocatalyst onto Glass Slides by Dip Coating

A colloidal suspension of TiO_2 was prepared by adding 0.3258 g of TiO_2 powder (commercial grade P25 ex Degussa) to 40 ml of deionised distilled water. After vigorous shaking the solution was sonicated for 200 seconds at an amplitude of 6 µm using a cycle of 10 seconds on and10 seconds off. The sonicator used was an MSE Soniprep 150. The substrates were then dip-coated manually in the colloidal suspension and allowed to dry under ambient conditions. The coating / drying cycle process was repeated 5 times. The coated substrates were stored in the dark at room temperature before use.

4.7.3 Deposition of TiO_2 Photocatalyst onto PVDF Membrane by Dip Coating

PVDF membrane (Millipore UK) with pore size 200 nm was manually dip-coated twice in a nanoparticulate TiO_2 / methanol suspension. The TiO_2 particles (Sigma Aldrich, UK, particle diameter = 25 - 75 nm) constituted 2 % by weight of the suspension with the balance being methanol. Before each coating step, the solution was sonicated (MSE Soniprep 150 sonicator), for 2 minutes at 6 µm amplitude and the coated layer was allowed to dry before re-coating. The final coated substrate was then allowed to dry for 1 hour in the dark before use.

4.7.4 Depositing A Mask Layer by Deposition of Microparticles

Polystyrene microspheres of 1 micron diameter (ex Alfa Aesar) as a 2.5 wt% suspension in water were used as microparticles. For preparation purposes this commercial latex was further diluted to 1.0 wt% with distilled water to form a microparticle suspension.

Substrates comprising a photocatalyst layer prepared according to examples 4.5.1, 4.5.2 or 4.5.3 as set out above were further prepared for deposition of the microparticles by irradiating with UV light for 60 minutes. This was to ensure that the photocatalyst layer has a hydrophilic surface in order to facilitate deposition of the microparticles as a close packed array.

A tapered PTFE ring was adhered to the photocatalyst layer on the substrate surface with silicone grease, to provide a seal impermeable to liquid leakage. The substrate was then placed on a level surface to prevent gravitational bias in deposition of microparticles. Where monolayer microparticle coverage is required, the amount of microparticle suspension deposited into the ring was calculated to ensure a substantial monolayer of microparticles using the following equation

$$\text{Quantity of 1.0 wt\% suspension } (\mu l) = \text{Area } (mm^2) \times 0.13 \quad (8)$$

Following application of the microparticle suspension, substrates were left undisturbed for 12 hours in an enclosed environment to ensure that evaporation is not accelerated by air currents. Once the water had evaporated, the PTFE ring was removed and the substrate with photocatalyst layer and mask layer (monolayer of microparticles) was ready for deposition of metal by electroless plating.

Turning to Fig. 46, this shows a substrate 101 having a photocatalyst layer 103 and a mask layer of microparticles 105 placed into an electroless plating solution 107 in vessel 102 for deposition of the metal layer. The microparticles 105 may be in a random or preferably in an ordered, close packed arrangement. Actinic (UV / visible) radiation 104 is shone onto the substrate 101 through the electroless plating solution 107 to initiate deposition of metal. Examples of plating solutions are given below in Table 11 and Table 12.

Electroless Ag plating solutions were prepared to the composition given in Table 11. All components were added to a small quantity of distilled water in the order listed, ensuring full dissolution with each addition. The completed solution was made up to volume with distilled water and purged with nitrogen for 20 minutes to deoxygenate it. The pH of the solution was 11.5 and photo-initiated electroless deposition was carried out at 298 K. Electroless plating solutions were freshly made immediately prior to use. As $AgNO_3$ is light sensitive, Ag solutions were prepared and stored in amber flasks in darkness.

Role	Component	Concentration
Metal precursor	Silver Nitrate	1.496 g / dm^3 (8.8 mmol / dm^3)
Complexant	Ethylenediamine	3.245 g / dm^3 (54 mmol / dm^3)
Stabiliser	3,5-diiodotyrosine	0.017 g / dm^3 (39.2 µmol / dm^3)
Reducing agent / scavenger	Potassium Sodium Tartrate	0.7356 g / dm^3 (26 mmol / dm^3)
pH	-	11-12
Temp	-	298 K

Table 11 Composition of Ag electroless plating solution

Electroless Pd plating solutions were prepared to the composition given in Table 12. $PdCl_2$, di-sodium EDTA and ammonium hydroxide (28% by weight ammonia in water) were added and, to ensure formation of a Pd-amine complex, stirred with gentle heating until the solution cleared. The resulting clear solution was cooled and hydrazine reducing agent added. The solution was then made up to volume with distilled water and purged with nitrogen for 20 min. The electroless plating solution was prepared immediately before use.

Role	Component	Concentration
Metal precursor	Palladium Chloride	3.60 g / dm^3 (20.3 mmol / dm^3)
Complexant	Ammonium Hydroxide (28%)	350.0 ml / dm^3 (5.2 mol / dm^3 NH_3)
Stabiliser	Di-sodium EDTA	62.4 g / dm^3 (167.7 mmol / dm^3)
Reducing agent / scavenger	Hydrazine (65%)	11.0 ml / dm^3 (216.7 mmol / dm^3)
pH	-	11-12
Temp	-	298 K

Table 12 Composition of Pd electroless plating solution

Each substrate, with its photocatalyst film as formed in examples 4.5.1, 4.5.2 or 4.5.3, was placed into the electroless plating solution and irradiated for 20 min with UVA light (wavelength 315 nm). After this irradiation time, a coherent, conducting layer of metal was produced, the thickness of which was controllable by selection of immersion time.

The metal layers formed were found to be highly adhesive to the substrate, and were found to be compliant with British Standard metal adhesion test BS EN ISO 2819:1995.

During photo-initiated electroless deposition, metal is deposited only on the part of the surface which is both coated with photo-catalyst and subjected to suitable actinic radiation.

Virtually no deposition at all occurs in un-irradiated areas or in areas not coated with photo-catalyst. Consequently the area of deposition of metal layer may be demarcated using techniques such as;

physically masking the deposition of the photo-catalyst to leave uncoated areas,

physically masking part of the area previously prepared with photo-catalyst,

optically masking part of the area irradiated to prevent irradiation with actinic radiation, or

selectively irradiating the area using a scanned beam of actinic radiation.

Once the substrate has been irradiated for about five minutes with the actinic radiation, electroless plating will have been sufficiently initiated for auto-catalytic plating then to continue, even in the absence of further irradiation with actinic radiation, whereby a bright, reflective, coherent, conducting layer of metal may be formed.

In the case of PVDF membranes that have been dip-coated as set out above in example 4.5.3, the opposed faces of the membrane may be provided with a metal layer simultaneously without through-plating of the pores of the membrane.

Following deposition of the metal layer, the microparticles may be dissolved in an appropriate solvent chosen to dissolve the microparticles but not the substrate. For these Examples, toluene was employed for dissolution of the mask layer of microparticles to leave a porous metal layer.

The invention provides a method for manufacturing metal films with controlled thickness and excellent adhesion on substrates, particularly electrically insulating substrates. The method is suitable for providing metal layers with controlled, regular porosity by use of a mask layer as set out hereinbefore.

4.8 Claims

1. A method of forming a porous metal layer on an electrically insulating substrate, the method comprising:

a) depositing a photocatalyst layer onto the substrate,

b) depositing a mask layer comprising voids, on the photocatalyst layer,

c) providing an electroless plating solution on the mask layer and photocatalyst layer,

d) irradiating the photocatalyst layer, mask layer and electroless plating solution with actinic radiation whereby deposition of metal from the electroless plating solution to form a metal layer on the photocatalyst layer is initiated, whereby deposition of the metal occurs within the voids, and

e) removing the mask layer following deposition of the metal to provide a porous metal layer.

2. A method according to claim 1 wherein the mask layer is a layer of microparticles, the voids being the spaces between the microparticles.

3. A method according to claim 2 wherein the layer of microparticles is substantially a monolayer.

4. A method according to claim 2 or claim 3 wherein the microparticles are polymer latex particles.

5. A method according to any one of claims 2 to 4 wherein the microparticles are substantially monodisperse in diameter.

6. A method according to any preceding claim wherein the photocatalyst layer comprises or consists essentially of a semiconductor material.

7. A method according to any preceding claim wherein the photocatalyst layer comprises or consists essentially of particles of a semiconductor material.

8. A method according to any preceding claim wherein the photocatalyst layer comprises or consists essentially of TiO_2.

9. A method according to claim 8 wherein the photocatalyst comprises or consists essentially of particles of TiO_2.

10. A method according to any preceding claim wherein the actinic radiation is ultraviolet radiation.

11. A method according to any preceding claim comprising selecting a first portion of surface upon which the metal layer is formed and a second portion which remains free of metal layer by irradiating the first portion but not the second portion with the actinic radiation.

12. A method according to any preceding claim comprising selecting a first portion of surface upon which the metal layer is formed and a second portion which remains free of metal layer by depositing the photocatalyst layer on the first portion and no photocatalyst layer on the second portion.

13. A method according to any preceding claim wherein the metal is Ag or Pd.

14. A method of forming a porous metal layer on a substrate, the method comprising:

a) depositing a mask layer comprising voids on the substrate, wherein the mask layer is a layer of microparticles, the voids being the spaces between the microparticles,

b) depositing metal onto the substrate, whereby the metal deposits in the voids of the mask layer, and

c) removing the mask layer to leave a porous metal layer on the substrate, wherein the metal is deposited by electroless plating from an electroless plating solution.

CHAPTER 5

THE NANOPOROUS METALLISATION OF INSULATING SUBSTRATES THROUGH PHOTOCATALYTICALLY INITIATED ELECTROLESS DEPOSITION

Cambridge University Press, Cambridge UK, *MRS Proceedings*, Volume 1409, Article mrsf11-1409-cc05-20, (2012)

DOI:10.1557/opl.2012.392

Michael A. Bromley, Colin Boxall*

Engineering Department, Lancaster University, Lancaster LA1 4YR, UK

"Show us this "the wheel.""

Prof. Hubert J. Farnsworth

5.1 Publication Summary

- MRS Proceedings paper to accompany the first presentation of the deposition of porous metal films through PIED
- Highly regular and predictable nanostructure demonstrated through the inclusion of a microsphere template

5.2 Author Contributions

- M.A.B.: designed and performed all experiments, analysis and characterisation; primary author of the manuscript from first draft to final proof
- C.B.: conceived and supervised the study; co-author of manuscript through review of draft

5.3 Abstract

We report the novel use of semiconductor photocatalysis for the deposition of metal onto insulating surfaces and the in-process formation of nano-structured porosity within this metal. In the process of Photocatalytically Initiated Electroless Deposition (PIED) we have developed a controllable, spatially selective and versatile metallisation technique with several advantages over traditional, non-photocatalytic techniques such as enhanced controllability and purity of the deposit as well as reduced operational costs and environmental impact. With the addition of a self-assembled, hexagonally close packed microparticle template to the substrate prior to metal deposition, PIED can be used to fabricate thin metal films with highly ordered porosity on the nano-scale. Nanoporous metallisation in this way is able to produce substrates with potentially wide applications such as membrane and separation technology, energy storage and sensors – especially surface enhanced resonance Raman spectroscopy (SERRS).

5.4 Introduction

The metallisation of non-conducting materials is typically performed through a process known as electroless plating. This involves the chemical reduction of metal ions from solution in order that they be deposited onto the substrate surface in metallic form [7]. While independent of electrical current, electroless plating does require the catalysis of metal ion reduction by the substrate surface and traditionally involves extensive sensitisation steps with Sn-Pd catalysts before the deposition process can take place. Semiconductor particles, such as TiO_2, SnO_2, WO_3, can act as efficient photocatalysts for a range of processes [12] and, as such, present an alternative means of metal ion reduction which may be employed as part of an electroless plating process, providing a more efficient and cost-effective method for the sensitisation and subsequent metallisation of insulating substrates.

Photocatalysis is a multi-step process, initiated by the absorption of ultra-band gap light energy to generate electron-hole pairs. These photogenerated electron-hole pairs may undergo recombination or, given appropriate conditions, can be sufficient to drive redox reactions with species, such as metal ions, on the semiconductor surface or in local solution if the process is thermodynamically viable. We have appropriated these reactions in the development of a novel metallisation technique known as Photocatalytically Initiated Electroless Deposition (PIED), a novel process in which semiconductor photocatalysis is used to nucleate and fully metallise insulating substrate materials via submersion in a typical electroless plating bath [137-139]. The deposition process is initiated photocatalytically by irradiation of the semiconductor with ultra-band gap light energy. The photocatalytic effect is such that metal nanoparticles are generated directly on the semiconductor surface from metal precursor ions in solution, Fig. 47 (i); once sufficient metal nucleation sites have been formed by photocatalytic means then, in the presence of an appropriate reductant, further deposition may occur onto those nucleate sites by conventional electroless deposition reaction Fig. 47 (ii). These are the principal processes of PIED.

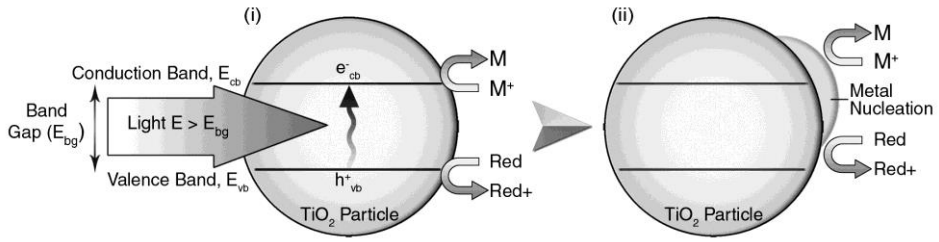

Fig. 47 Two stages of PIED: (i) photocatalytic process derived from interfacial electron transfer at photoexcited semiconductor particle; (ii) autocatalytic electroless deposition process

PIED has been successfully utilised in the deposition of various metals, including Ag and Pd, so demonstrating both 1 and 2 electron reduction processes, and has been applied to a range of substrate materials, including glass and polymers [137-139]. In all cases, PIED is able to produce conductive, metallic films with a strong adhesion to the substrate. In this basic embodiment, the resulting metal film takes the form of a single coherent layer and is free from any artificially induced structure. However, with the addition of a nanoparticle template, assembled prior to metal deposition and subsequently removed by dissolution, PIED can be used to fabricate thin metal films with highly ordered porosity on the nano-scale. We will now discuss the experimental processes involved in this fabrication and examine the extent to which the nanoporous metallisation of insulating substrates has been achieved.

5.5 Experimental

In order that the substrate material possessed the necessary photocatalytic properties, TiO_2 sensitisation was performed separately as a pre-sensitisation stage via either (a) sol-gel spin coating and annealing at 773 K, producing a robust mesoporous TiO_2 film [140]; or (b) deposition of pre-formed, commercially available TiO_2 nanoparticles by spin or dip coating techniques.

Where PIED was to be carried out without induced porosity, the TiO_2 sensitised substrate was subjected to the metallisation process; where induced porosity was required, a microparticle template was first arranged on the substrate surface. A typical microparticle template consists of polystyrene microspheres of a selected size, e.g. 1 μm. The template was arranged through controlled evaporation from an aqueous microsphere suspension to

produce a self-assembled, hexagonally close packed (HCP) microsphere array [55,56]. This process relies on the substrate surface being suitably hydrophilic in order that the microsphere suspension is able to spread across the surface, an essential precursor step for microsphere assembly into a close packed array to occur. Here, the pre-established TiO_2 layer on the substrate surface offers further process advantage; it is known that, under UV irradiation, TiO_2 exhibits a super-hydrophilic effect that results in water drop spreading [59]. Hence, a 30 – 60 min period of UV irradiation was found to greatly assist in the application of the microsphere suspension and assembly of the microsphere array.

TiO_2 sensitised substrates, with or without a microsphere template as required, were placed directly into freshly prepared electroless plating solutions consisting of a metal precursor, complexant, stabilizer and reducing agent [137,139]. This immersion was performed in a quartz reaction vessel for improved UV transmittance, ensuring efficient irradiation of the semiconductor. A N_2 stream was bubbled through the plating solutions during deposition in order to purge the solution of oxygen that can compete with metal ions for reduction at the semiconductor surface, and provide a source of agitation to prevent local depletion of metal ions at the substrate surface. Ultra-band gap irradiation was then provided in the form of 315 nm UV light. A thermostatically controlled water supply, passed through an incorporated jacket of the quartz vessel by means of a peristaltic pump, was used to maintain a constant plating solution temperature for the purpose of additional process control.

Post deposition, the substrate was removed from the plating solution, rinsed with doubly deionised water (DDW) and dried in air. Where no microsphere template was used, no further treatment is required; where a microsphere template was in place, the substrate was immersed in toluene for dissolution of the microspheres. No adverse effect on the deposited metal was observed during this step. The microstructures of the resultant metal layers were characterised using scanning electron microscopy (FEI Phenom, Lambda Photometrics Ltd, UK).

5.6 Discussion

Previously, we have successfully used PIED to produce layers of various metals including Ag and Pd on glass, quartz and polymer substrates [137-139]. The resultant metal layers were coherent and conductive with a reflective, metallic finish whilst displaying strong adhesion and resistance to delamination. Metal deposition was found to occur exclusively onto those areas both sensitised with an appropriate semiconductor and irradiated with ultra-band gap light energy, so making the PIED process spatially selective and highly controllable. Coherent and conductive metal coatings may be produced across the whole TiO_2 sensitised area in deposition times of 15 min. As might be expected, thicker, more robust films were obtained after deposition periods greater than this, typically 60 min or more.

The period of irradiation, and hence the extent of photocatalytic nucleation, was found to be important in determining the quality of the final metal film. A longer period of photocatalytic metal deposition results in a greater number of nucleation sites and, consequently, a denser, more efficient auto-catalytic deposition. An irradiation period of as little as 30 sec was found to be sufficient to initiate PIED and achieve a conductive metal film through subsequent auto-catalytic deposition though the resulting metal was a notably granular structure, Fig. 48 (i). An extended irradiation period, of several minutes, produced more nucleation sites and, as a result, a smoother and less granular metal deposit, Fig. 48 (ii).

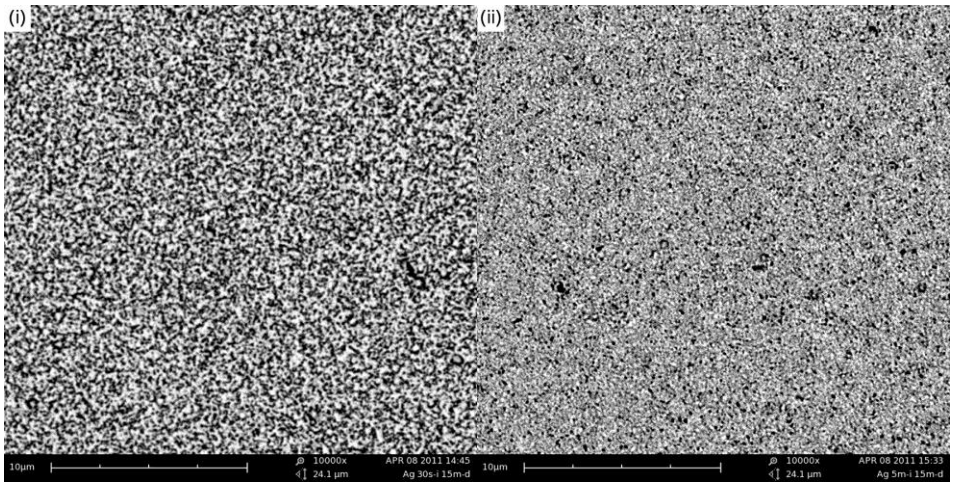

Fig. 48 SEM images of metal surface: (i) granular metal deposit resulting from short irradiation time, (ii) less granular metal deposit resulting from longer irradiation time

Our more recent work has focused on the introduction of controllable micro and nanoporosity to PIED generated metal layers. With a microsphere template in place on the substrate, we found that PIED metallisation occurs by much the same mechanism as observed on a non-templated substrate; an initial photocatalytic stage drives metal nucleation and subsequent auto-catalytic deposition enables continued growth to form a coherent metal film. PIED remains possible through HCP microsphere templates as the arrays contain regular interstitial spaces. It is these spaces which allow access to the semiconductor for both UV irradiation and electroless bath constituents. Photocatalytic metal nucleation occurs directly onto the TiO_2 surface and auto-catalytic deposition continues the metal growth upwardly throughout the aforementioned interstices, Fig. 49. In this way, the deposited metal forms around the microsphere template without dislodging or disrupting any of the individual microspheres to produce a conductive metal film with regular nanostructure. Importantly, metal deposited throughout a microsphere template in this way, remains adhered to the substrate upon dissolution of the spheres, thus confirming the fact that metal deposition occurs directly onto the TiO_2 rather than onto the microspheres themselves.

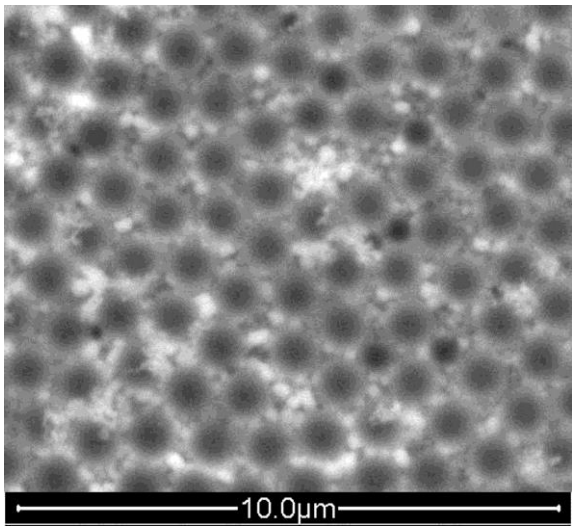

Fig. 49 Ag growth in interstitial spaces of 1 µm microsphere template

However, the rate of metal deposition observed within HCP microsphere templates is reduced from that seen on a non-templated sample. While a period of 15 – 60 min is sufficient to produce a conductive, non-porous metal film, the same period of time is

insufficient where a microsphere template is in place. This suggests that the microsphere array acts as a partial physical barrier; reducing the UV irradiation reaching the TiO_2, so compromising the photocatalytic effect; and restricting access of the electroless plating bath to the TiO_2 leading to localised depletion of the metal precursor and reductant. If the photocatalytic initiation stage is inhibited, less nucleation occurs and hence fewer sites for continued auto-catalytic deposition are provided. In addition to this, reduced mass transport of the bath constituents will have the effect of both reducing nucleation and slowing the subsequent auto-catalytic deposition. Despite this reduction in the rate of metal deposition, it is not completely inhibited and, as such, the effect can be easily compensated for with an extension of the deposition period, typically to around 120 min to achieve conductivity.

Once the microsphere template is removed, the resulting metal film displays regular, ordered nanoporosity which maintains the hexagonal arrangement of the microsphere array, Fig. 50 (i). The pore centre to centre distance is measured to be 1 μm, consistent with the size of the polystyrene microspheres used in the template. This demonstrates that the microsphere template is not affected by the metallisation process, retaining original size and position, and also that no metal shrinkage or expansion occurs post-deposition or during the microsphere template removal process.

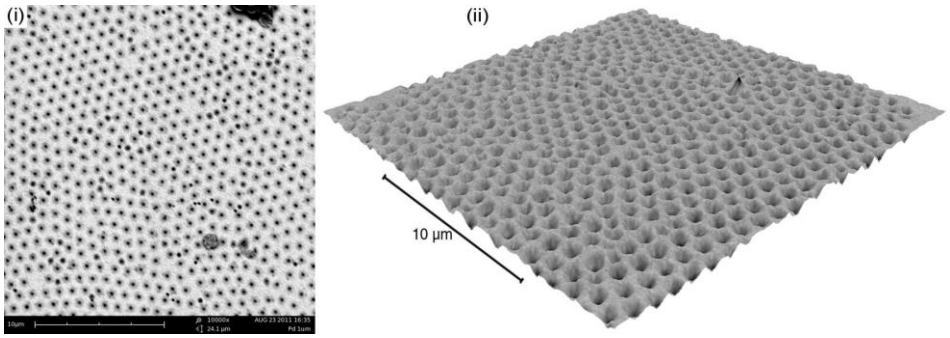

Fig. 50 Nanoporous Pd produced by PIED using a 1 μm polystyrene microsphere template: (i) 2D SEM image, (ii) 3D surface reconstructive SEM image

Particularly noticeable when viewed 3-dimensionally, Fig. 50 (ii), is the consistent height of the upper metal surface across the sample, indicative of a controlled and homogenous growth pattern. Furthermore, the nanoporosity can be seen to consist of a series of

hemispherical recesses within the smooth metal layer, formed as the depositing metal takes shape around the microsphere template. Within each of these hemispheres lies a smaller pore which is open to the surface below and formed by the prevention of metal deposition at the point of contact between each microsphere and the substrate surface. The size of these pores results directly from this contact area and in the case of 1 μm diameter microspheres, the resulting pore size is <200 nm. With polystyrene microspheres commercially available at 50 nm diameter, a pore size of approximately 10 nm is feasible with careful control of the metal deposit thickness. This observed nanostructure means that the metal layer not only possesses greatly increased surface area but also retains through-porosity and, as such, has wide potential for applications such as membrane technologies.

5.7 Conclusions

We report a novel photocatalytically initiated electroless deposition (PIED) process that allows for the photogeneration of coherent and conducting metal layers on semiconductor-sensitised insulator surfaces. The process is highly controllable, spatially selective and obviates the need for Sn-Pd activation catalysts to provide reduced operational costs and an environmentally cleaner alternative to the traditional techniques of dielectric plating.

With the addition of a microparticle template, the deposited metal can also be induced with nanoporosity through a highly regular and predictable nanostructure. The coverage and pore diameter of this is again controllable as it is directly dictated by the coverage and particle diameter of the template.

The fabrication of nanoporous metal by this novel method adds a conductive and permeable metallic structure of high surface area to an otherwise electrically insulating surface. Such metallised insulating materials have potentially wide applications in membrane and separation technology, desalination, electrode/solid electrolyte composites for fuel cells, energy storage and sensors – especially surface enhanced resonance Raman spectroscopy (SERRS).

5.8 Acknowledgements

The authors wish to thank the organizers of the 2011 MRS Fall Meeting for the invitation to submit this paper. The authors also wish to thank the Royal Society of Chemistry UK and the Lloyds Register Educational Trust for financial support. The Lloyds Register Educational Trust is an independent charity working to achieve advances in transportation, science, engineering and technology education, training and research worldwide for the benefit of all.

CHAPTER 6

PHOTOCATALYTICALLY INITIATED ELECTROLESS DEPOSITION OF MACROPOROUS METAL FILMS ONTO INSULATING SUBSTRATES

Electrochemistry Communications, 23, (2012), 87-89

DOI: 10.1016/j.elecom.2012.07.015

Michael A. Bromley, Colin Boxall*

Engineering Department, Lancaster University, Lancaster LA1 4YR, UK

"That was an important speech, sir, and it needed to be made. Might I suggest, however, that the rest of this discourse is continued by those with brains larger than a grape?"

Kryten 2X4B-523P

6.1 Publication Summary

- Research communication accepted into Electrochemistry Communications
- 5-year Impact factor: 4.950
- Urgent communication of the photocatalytically initiated electroless deposition of porous Ag and Pd films onto insulating substrates
- The increase in metal film thickness as a function of deposition period is demonstrated
- First report of the deposition of porous Ag films on PVDF membrane

6.2 Author Contributions

- M.A.B.: designed and performed all experiments, analysis and characterisation; primary author of the manuscript from first draft to final proof
- C.B.: conceived and supervised the study; co-author of manuscript through review of draft

6.3 Abstract

By use of Photocatalytically Initiated Electroless Deposition (PIED) we have deposited macroporous metal films with highly ordered arrays of sub-μm (hemi) spherical pores directly onto the surface of insulating substrates for the first time. This has been achieved by sensitisation of the target substrate with TiO_2 photocatalyst followed by PIED of the target metal into the interstitial spaces of a template comprised of hexagonally close packed polystyrene microspheres.

6.4 Introduction

Metal materials with an ordered, sub-μm scale pore structure interfaced directly with an insulating substrate are attractive for use in clean energy production (fuel cells [45]), energy storage [46,47], sensors (especially surface enhanced resonance Raman techniques [48,49]) and separation science [50]. Metal layers, including structured metal layers, are most conveniently and cost effectively formed by electrodeposition although this remains applicable only to conducting substrates. From a processing perspective, it would be convenient if an electroless deposition-based fabrication route existed whereby porous metals could be formed directly onto insulator surfaces. To date, no such route exists.

In contrast, a number of routes exist by which such porous metals may be deposited onto the surfaces of conductors. Of these, the most practical and simple is perhaps the method first reported by Bartlett *et al* [54] wherein metal films with ordered arrays of sub-μm spherical voids are prepared by electrodeposition into the interstitial spaces between polystyrene (PS) spheres assembled on metal electrode surfaces. The spheres are then removed, by dissolving in THF or toluene, to leave a porous metal film with regular inter-connected cavities. Using our recently reported insulator metallisation process of Photocatalytically Initiated Electroless Deposition (PIED) [137-139], we have developed a novel method to allow for the deposition of such porous films onto non-conducting substrates, something we believe to be a world first.

The metallisation of non-conducting materials is typically performed through electroless plating. While independent of electrical current, electroless plating does require extensive and repetitive sensitisation of the substrate surface with expensive Sn-Pd catalysts before metal ion reduction can take place [7]. Semiconductor materials such as TiO_2, SnO_2, WO_3can act as photocatalysts, generating electron-hole pairs upon the absorption of ultra-band gap light energy. As described in reference [137],we have appropriated the photogenerated electrons for metal ion reduction within the PIED process, so producing a metallisation

technique that is both more controllable and cost-effective than conventional electroless deposition [137-139]. Metallisation through PIED is comprised of two main steps:

(i) Irradiation of the semiconductor with ultra-band gap light energy (λ = 315 nm) to generate conduction band electrons. These electrons reduce metal precursor ions in solution, forming metal nuclei on the semiconductor surface, Fig. 51 (i).

(ii) Once sufficient nucleation sites have been photocatalytically generated, these begin to grow independently of irradiation through an auto-catalytic electroless deposition reaction, driven by the electroless plating bath reductant, Fig. 51 (ii), the growing nuclei eventually coalescing to form a coherent metal layer. This second step can occur both in the presence and absence of light, the latter being particularly advantageous for producing thick, non-transparent metal layers.

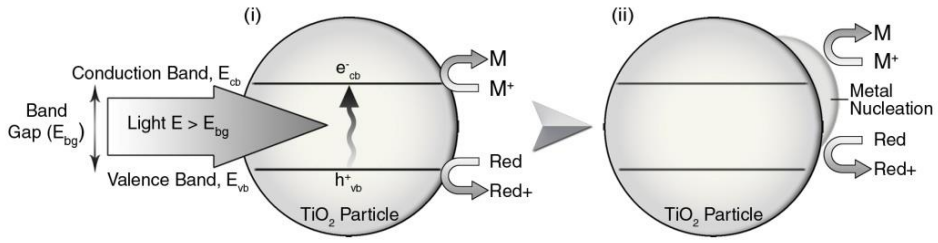

Fig. 51 Two stages of PIED: (i) photoreductive metal nucleation on irradiated photocatalyst; (ii) auto-catalytic electroless deposition process

In the above, the resulting metal film has no artificially induced structure. However, this paper is concerned with the deposition of metals with highly ordered nano-scale porosity by PIED, something that we have achieved through the assembly of a polystyrene microsphere template at the photocatalyst-sensitised insulator surface in a manner similar to that described by Bartlett *et al* for templated electro- (as opposed to electroless) deposition [54].

6.5 Experimental

PIED of non-porous metals has been described in detail in a previous communication from this laboratory [137] to which the interested reader is referred. Here we present a summary of the process and the modifications made to induce a porous structure in the deposited

metal. For PIED to occur, the surface of the insulating substrate to be metallised is first sensitised with a photocatalyst, such as TiO_2. This is applied by either (a) sol-gel spin coating and annealing [140]; or (b) spin or dip coating of commercially available TiO_2 nanoparticles, in each case without the use of molecular linkers required during photocatalytic patterning techniques [62]. Remaining post-metallisation, the chemically inert, mesoporous TiO_2 layer causes no adverse physical or chemical effects.

Microsphere templates are self-assembled on the substrate surface to produce a hexagonally close packed (HCP) array [55]. Briefly, this is achieved by incubator-controlled evaporation of a thin layer of a 1 wt % suspension of 1 μm diameter PS spheres, a process that requires the microsphere suspension to spread across the surface. Here, the presence of a sensitising TiO_2 layer on the substrate surface offers further process advantage; under UV irradiation, TiO_2 is rendered super-hydrophilic, resulting in water drop spreading [59,141]. Hence, 30–60 min of UV irradiation prior to application of the microsphere suspension was found to greatly assist in microsphere array assembly.

TiO_2 sensitised substrates, either with or without microsphere template, are immersed in a freshly prepared electroless plating solution, consisting of a metal precursor, complexant, stabilizer and reducing agent [137,139] within a UV-transparent quartz reaction vessel. Metal deposition is initiated by irradiation with 6 x 8 W UV lamps arranged in a hemi-cylindrical array facing towards the target substrate. Solutions are purged with N_2 for 20 min before irradiation and throughout the deposition process.

Post deposition, substrates are simply rinsed with doubly deionised water (DDW) and dried in air. The microsphere template is then removed by dissolution in toluene.

6.6 Results and Discussion

Using PIED, both Ag and Pd have been deposited around 1 μm diameter PS microsphere templates on TiO_2 sensitised glass substrates. SEM images of such deposits pre- and post-template removal are shown in Fig. 52 for both metals, the films can be seen to be coherent

and are conducting (surface resistivity, R_s, ~0.2 Ω / sq), so demonstrating both 1 and 2 electron reduction processes. Deposited films are strongly adhered to the substrate, demonstrated by compliance with adhesion test BS-EN-ISO-2819:1995.

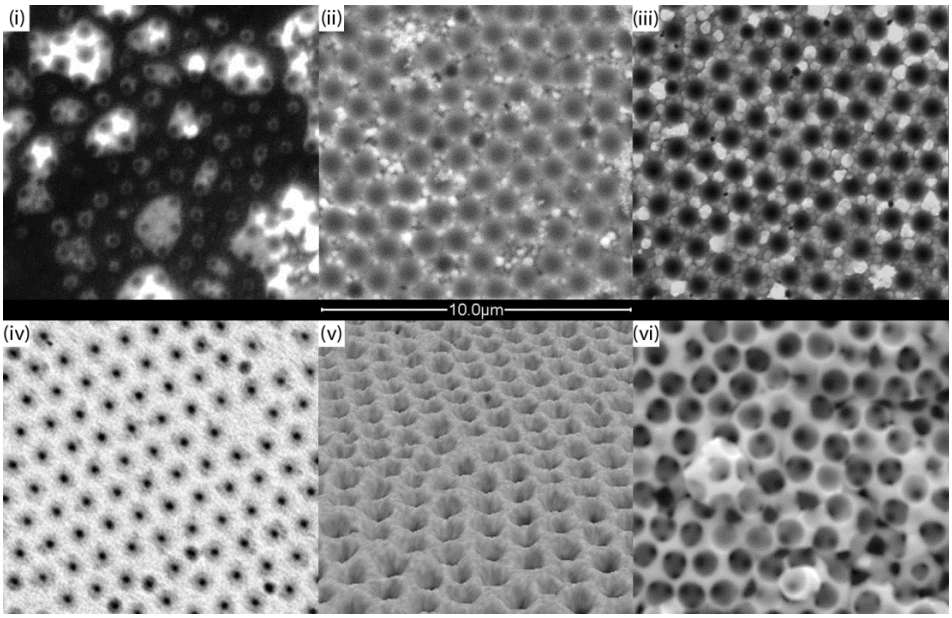

Fig. 52 SEM images of (i) Photo-generated Ag nucleation; (ii) PIED generated Ag layer with 1µm microsphere template still present; (iii) same deposit after template removal (iv) nanoporous Pd deposit on glass after template removal; (v) 3D 'shape from shading' surface reconstruction of same Pd deposit; (vi) multi-layer porosity in Pd

Whilst the general mechanism by which PIED occurs, Fig. 51, would be expected to be the same on templated and non-templated substrates, the rate of metal deposition on the former is found to be reduced with respect to the latter. Thus, whilst a period of 15 min is sufficient to produce a non-porous metal film that is conducting with an R_s of 0.2 Ω / sq, 60–120 min is required to achieve the same R_s with a template in place. This suggests that the template acts as a partial physical barrier, restricting access of the initiating UV irradiation and electroless plating bath constituents to the TiO_2 beneath. However, the regular interstitial spaces of the HCP microsphere array allow sufficient access to the underlying semiconductor for PIED to occur. An initial photocatalytic stage drives metal nucleation directly onto the TiO_2 sensitised substrate, Fig. 52 (i), and subsequent auto-catalytic deposition continues the metal growth upwardly throughout the aforementioned interstices, Fig. 52 (ii), forming a metal film around the base of the microsphere template.

Post template-removal, the resultant metal film displays ordered nano-scale porosity consisting of hemispherical voids mirroring the shape of the now removed microspheres, Fig. 52 (iii) & (iv). At the base of each hemispherical void lies a smaller hole which is open to the substrate below and forms at the point of contact between the microspheres and the substrate surface. In the case of ∅ = 1 μm microspheres, each hole has ∅ < 200 nm.

Throughout the sample, the porosity maintains the hexagonal arrangement of the microsphere array and, in the most ordered regions, pore centre to centre separation can be measured to 1 μm ± 10 nm. This is consistent with the size of the microspheres used and demonstrates that the template is not affected by the PIED process, retaining original size and position, and also that no metal shrinkage or expansion occurs post-deposition or during template removal. Particularly noticeable when viewed 3-dimensionally, Fig. 52 (v), is the consistent height of the upper metal surface across the sample, indicative of controlled and homogenous growth. The metal layer thickness is represented by the sagitta of each hemispherical pore. Using the diameter of the templating microsphere and the measured diameter of the pore upper opening, the sagitta, and so layer thickness, is found to be 137 and 120 nm for the Ag and Pd samples of Fig. 52, each with a deposition times = 60 min, the thickness of the metal deposit being affected by the deposition time. As the thickness of deposits produced with irradiation throughout the deposition are similar to those produced through part irradiated, part dark deposition periods [137], the overall deposition period can be used as a control parameter analogous to the use of coulombic charge passed during electrodeposition.

Where the template consists only of a monolayer of microspheres, the thickness of the deposited metal must be restricted to less than the diameter of one microsphere. If metal is deposited to a thickness greater than this, the nanoporosity is occluded as the metal growth spreads over the upper surface of the microspheres. We have found that the use of a multi-layer microsphere template allows for the deposition of layers with a thickness greater than one microsphere diameter and results in a metal film with an interlinked, multi-layer nanoporosity, Fig. 52 (vi).

Demonstrating its utility for a range of insulating substrates, PIED has also been used to deposit porous Ag, Fig. 53, and Pd onto nanoparticulate TiO_2 sensitised 0.2 μm pore size polyvinylidene fluoride (PVDF) membranes. In both instances, the deposited metal layers are found to be conducting and of metallic appearance. However, the roughness of the substrate surface partially disrupts the microsphere array self-assembly; as a result, the templates show less two-dimensional order than those produced on smooth glass substrates although remain suitable for the induction of widespread porosity in the deposited metal film.

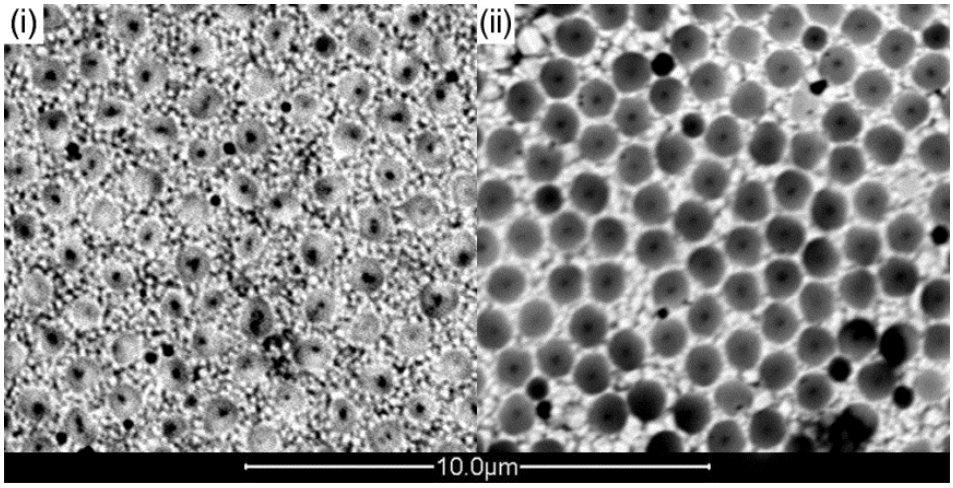

Fig. 53 Nanoporous Ag on PVDF deposited to a thickness of (i) 138 nm in 60 min and (ii) 344 nm in 120 min

Similarly, the holes at the pore base, formed at the contact points between spheres and substrate, are less consistent in shape and diameter, ranging from <50 nm to 250 nm, attributable to an irregular contact area between microspheres and the rough PVDF surface. However, spatially consistent metal deposition is observed; the upper opening diameters of the hemispherical pores is measured at 690 nm ± 25 nm after 60 min deposition time, Fig. 53 (i), and 950 nm ± 25 nm after 120 min, Fig. 53 (ii). These equate to metal film thickness of 138 nm and 344 nm respectively, demonstrating that, as on glass, thicker layers are formed with increased deposition time. We have found that deposition can be applied to a single side of the membrane by selective sensitisation through spin coating of the TiO_2, or on both sides by full sensitisation through dip coating. In the case of the latter, no through membrane deposition or conductivity is observed, so providing two individual porous metal

films on either side of the same membrane. This may be applicable to thin layer polymer electrolyte fuel cells or electrochemically assisted membrane separation processes.

6.7 Conclusions

We have presented the first reported electroless deposition of metals with highly ordered nanometre scale porosity on insulating substrates. We also provide the first reported use of electroless deposition with a controllable onset in the creation of ordered nanoporous metals on any kind of support, be it insulator, semiconductor or metal.

The novel PIED process allows for controllable photo-initiation of the metallisation process whilst facilitating continued auto-catalytic electroless deposition to produce coherent porous metal films, the thickness of which is determined by the total deposition time. The resulting metal deposits can be induced with single or multi-layer nano-scale porosity with a highly regular and predictable order with coverage and pore diameter being determined by the spatial application and particle diameter of the template array. This has been achieved with a variety of metals and onto both organic and inorganic insulator substrates.

Insulating materials metallised with PIED have potentially wide applications in membrane and analytical separation technology, desalination, electrode/solid electrolyte composites for fuel cells, energy storage and sensors – especially surface enhanced resonance Raman spectroscopy (SERRS).

6.8 Acknowledgements

We thank the Royal Society of Chemistry UK, EPSRC (Award No EP/I002928/1) and The Lloyds Register Educational Trust (LRET) for financial support. The LRET is an independent charity working to achieve advances in transportation, science, engineering and technology education, training and research worldwide for the benefit of all.

CHAPTER 7

THE METALLISATION OF INSULATING SUBSTRATES WITH NANOSTRUCTURED METAL FILMS OF CONTROLLABLE PORE DIMENSION

Journal of Materials Chemistry A: Chemistry, 1, 20, (2013), 6152-6161

DOI: 10.1039/C3TA10421D

Michael A. Bromley*, Colin Boxall

Engineering Department, Lancaster University, Lancaster LA1 4YR, UK

"Nothing is impossible! Not if you can imagine it. That's what being a scientist is all about!"

Prof. Hubert J. Farnsworth

7.1 Publication Summary

- Research article accepted into the Journal of Materials Chemistry A: Chemistry
- 5-year Impact factor: 6.101
- Detailed report of the specific nucleation and growth patterns occurring during metal deposition around a microsphere template on glass
- Investigation of the effects of temperature on PIED of Pd
- Report of the difficulties encountered and overcome in developing PIED of nanoporous Pd
- Report of the formation of metal films of both 2-dimensional monolayer and 3-dimensional multi-layer porosity
- Demonstration of the control of pore dimensions through variation of template microsphere diameter.

7.2 Author Contributions

- M.A.B.: designed and performed all experiments, analysis and characterisation; primary author of the manuscript from first draft to final proof
- C.B.: conceived and supervised the study; co-author of manuscript through review of draft

7.3 Abstract

By use of Photocatalytically Initiated Electroless Deposition (PIED) we have deposited nanoporous metal films with both single and multi-layer, highly ordered arrays of sub-μm spherical pores directly onto the surface of insulating substrates. This has been achieved by sensitisation of the target substrate with a TiO_2 photocatalyst followed by the self-assembly of a hexagonally close packed polystyrene microsphere template, assisted by the photogenerated hydrophilicity of the TiO_2 sensitiser. Metal is then deposited through PIED into the interstitial spaces of a template and directly onto the TiO_2 sensitised substrate surface. The dimensions of the resultant pores in the deposited metal are determined by the size of the microspheres used to for the template while metal film thickness may be controlled by the deposition period.

7.4 Introduction

Metal materials with an ordered, sub-μm scale pore structure interfaced directly with an insulating substrate are attractive for use in clean energy production (fuel cells [45]), energy storage (supercapacitors [46,47]), sensors (especially surface enhanced resonance Raman techniques [48]) and separation science (membranes [50]). Metal layers, including structured metal layers, are most conveniently and cost effectively formed by electrodeposition although this remains applicable only to conducting substrates. From a materials processing perspective, it would be convenient if an electroless deposition-based fabrication route existed whereby the porous metal could be formed directly onto the insulator surface. The first report of such a route was made in our previous communication [142], in which we developed a novel method to prepare porous metal films with ordered arrays of sub-μm spherical voids on non-conducting substrates using our insulator metallisation process of Photocatalytically Initiated Electroless Deposition (PIED) [137-139]. These films are prepared by electrolessly depositing metal into the interstitial spaces of a hexagonally close packed polystyrene (PS) microsphere array. The microspheres are removed post-deposition, by dissolving in toluene, to leave a porous metal film with a regular nanostructure.

Building on our earlier work, this paper is concerned with the formation of nanoporous Ag and Pd films on TiO_2 sensitised glass and the control of pore dimensions within the deposited metal through variation of the primary microsphere diameter. The use of photo-induced super-hydrophilicity on TiO_2 to assist in the self-assembly of the templating microsphere array is described and the mechanism of metal film nucleation and growth is discussed.

7.5 Background

The metallisation of non-conducting materials is typically performed through electroless plating. This involves the chemical reduction of metal ions from solution in order that they be deposited onto the substrate surface in metallic form. While independent of electrical current, electroless plating does require extensive and repetitive sensitisation of the substrate surface

with expensive Sn-Pd catalysts before metal ion reduction can take place [7]. Semiconductor materials such as TiO_2, SnO_2, WO_3 can act as photocatalysts, generating electron-hole pairs upon the absorption of ultra-band gap light energy. These charge carriers may undergo recombination or may be used to drive useful redox reactions with species, such as metal ions, on or at the semiconductor surface [12,143]. As described in our earlier work [137], we have appropriated the electrons photogenerated within semiconductor photocatalysts for metal ion reduction within the PIED process, so producing a metallisation technique that is both more controllable and cost-effective than conventional electroless deposition [137-139]. Metallisation through PIED is comprised of two main steps:

(i) Irradiation of the semiconductor with ultra-band gap light energy (λ = 315 nm) to generate conduction band electrons. These electrons reduce metal precursor ions in solution, forming metal nuclei on the semiconductor surface, Fig. 54 (i).

(ii) Once sufficient nucleation sites have been photocatalytically generated, these begin to grow independently of irradiation through an auto-catalytic electroless deposition reaction, driven by the electroless plating bath reductant, Fig. 54 (ii), the growing nuclei eventually coalescing to form a coherent metal layer. This second step can occur both in the presence and absence of light, the latter being particularly advantageous for producing thick, non-transparent metal layers.

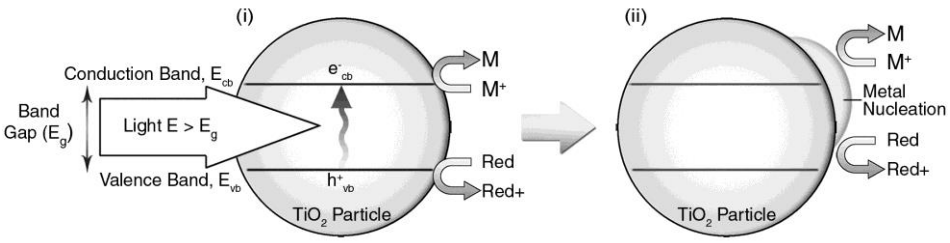

Fig. 54 Two stages of PIED: (i) photoreductive metal nucleation on irradiated photocatalyst; (ii) auto-catalytic electroless deposition process

In this basic embodiment, the resulting metal film has no artificially induced structure. In order to produce a metal film with a nanostructure, the metal deposition must take place around some form of template. A number of possibilities exist for the formation of a template

around which metal deposition can take place, the most applicable of which are; liquid crystalline phases formed by lyotropic surfactants; and a self-assembled monolayer of polystyrene microspheres. Use of the former has been demonstrated by Attard *et al* in the electrodeposition of nanostructured Pt in the interstitial spaces of normal hexagonal (H_1) liquid crystalline phase surfactants [51]. The use of the latter was reported by Bartlett *et al* [54] in the preparation of porous metal films with ordered arrays of sub-μm spherical voids by electrodeposition into the interstitial spaces between polystyrene spheres assembled on metal electrode surfaces; Haginoya *et al* [144] in the fabrication of nanostructured Pt-Pd through sputter coating; and Takeyasu *et al* [145] in the electroless deposition of Au onto the internal regions of microsphere structures inside capillary tubes.

The use of surfactant micelles in the plating bath allows for extremely small theoretical pore sizes, of the order of <10 nm, although this requires highly specific conditions to maintain the correct phase type and orientation. Such conditions are not conducive to the use of electroless plating baths and hence, microsphere arrays assembled on the substrate surface provide a more suitable option. Microspheres do not interfere with the electroless plating solution and provide fixed and stable templates with highly predictable and reproducible structures. Furthermore, polystyrene spheres are commercially available in many sizes from 50 nm to 3 μm, potentially allowing for the production of metal films with a wide range of pore sizes using the same deposition technique.

In light of the above, we have chosen to use hexagonally close packed PS microsphere arrays as a template material with which to introduce porosity into metal films produced through PIED. The results of this process for Ag and Pd, as examples of one and two electron metal precursor reduction processes, are the subject of the remainder of this paper.

7.6 Experimental

7.6.1 Materials and Reagents

All reagents used are AnalaR grade or higher, and purchased from Sigma Aldrich (Gillingham, Dorset, UK) or Alfa Aesar (Heysham, Lancashire, UK) with the exception of nanoparticulate TiO_2 sol (TiPE® G502/O502, TitanPE Technologies Inc., Shanghai, China). All water used is Ultrapure doubly deionised water from a Direct-Q 3 UV Millipore water purification system (Millipore (U.K.) Limited, Watford, UK) to a resistivity of 18.2 MΩ / cm. Nitrogen Whitespot grade is provided by BOC Ltd., Guildford, Surrey, UK.

7.6.2 Substrate Sensitisation with TiO_2

Prior to PIED, substrates were first sensitised with TiO_2 in order that they be photocatalytically active. This was achieved with the preparation of a reverse micellar sol-gel was prepared by vigorously mixing Triton X-100 (26.0 g) and cyclohexane (150 ml) to form a reverse micellar solution. After 30 min, water (1.08 g) was added and the solution appears turbid. This turbidity clears upon addition of titanium (IV) isopropoxide (99.999%) (23.0 g). The solution was then stirred for 60 min at 293 K, so forming a colloidal suspension of TiO_2 nanoparticles. Acetylacetone (10 ml) was added to stabilise the solution.

The resultant sol-gel was applied to glass or quartz substrates by spin coating for 5 seconds at 2900 rpm using an inverted model 636 rotating disk electrode system (Princeton Applied Research, Tennessee, USA). Prior to coating with sol-gel, the substrates were cleaned by washing first with acetone and then by doubly distilled water. Coated substrates were then fired in a furnace at 773 K for 1 hour to anneal the titania and produce a resilient mesoporous TiO_2 (m-TiO_2) coating composed of interconnected, mono-dispersed primary particles approximately 15 nm in diameter with a predominantly anatase structure [137]. Sensitised substrates were stored in darkness at room temperature prior to use.

7.6.3 Polystyrene Microsphere Template Formation

PS microsphere arrays were arranged on TiO_2 sensitised substrates in order to provide a template material around which subsequent metal deposition, through PIED, takes place. PS microspheres of a range of diameters (1 μm 400 nm, 269 nm, 149 nm) were purchased from Alfa Aesar as a 2.5 wt% solution in water. For template preparation purposes this was further diluted to 1.0 wt% with doubly deionised water. TiO_2 coated surfaces exhibit super-hydrophilicity upon irradiation with UV light [59], a phenomenon that we have explored for optimising the self-assembly of ordered microsphere arrays. In this, TiO_2 sensitised substrates were irradiated with UV light for 60 min prior to the application of the microsphere solution, the photo-induced substrate hydrophilicity facilitating an even spreading of that solution (see below). 12.35 μl of the microsphere solution was applied to the substrate via micro-pipette inside an 11 mm diameter PTFE ring with tapered inner edge Fig. 55. This ring was sealed to the substrate surface with silicone grease to ensure there is no solution leakage while the tapered edge creates a permanent concave meniscus on the liquid surface, essential for the ordered template self-assembly process, again shown in Fig. 55. Upon application of the sphere solution, substrates were left undisturbed for 12 hours on a level surface (to prevent gravitational bias) and in an enclosed environment (to ensure no uneven evaporation is caused by local air currents). Ordered template self-assembly then occurs through the capillary action of the surface tension force of the evenly evaporating liquid meniscus on the component microspheres, Fig. 55.

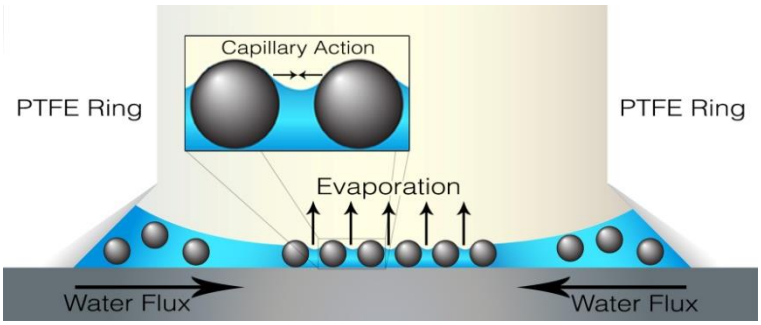

Fig. 55 Self-assembly of polystyrene microsphere template

7.6.4 Preparation of Ag & Pd Electroless Plating Baths

Electroless Ag and Pd plating solutions to be used with PIED were prepared according to the compositions given in Table 13 and Table 14 (see sections 7.S2 & 7S3) as previously developed in these laboratories [137]. All components are added to a small volume of distilled water (~10 ml) in the order listed, ensuring full dissolution with each addition. The completed solutions were made up to volume with doubly deionised water and purged with N_2 for 20 min to deoxygenate. Electroless plating solutions were freshly made immediately before use for optimum performance.

7.6.5 Photocatalytically Initiated Electroless Deposition

TiO_2 sensitised, microsphere template coated substrates were placed directly into freshly prepared electroless plating solutions in order to be metallised. A quartz reaction vessel was used for optimal UV transmittance and plating solutions were bubbled with N_2 during deposition in order to purge the solution of oxygen which can compete with metal precursor ions for reduction at the photocatalytic surface. The N_2 stream also provides a source of agitation to prevent local depletion of the metal ion concentration at the substrate surface. The reaction vessel is then placed inside a photoreactor (Lidam Scientific, Dartford, UK) comprised of two hemi-cylinders, each containing 6 x 8W UVA lamps. A thermostatically controlled water supply, passed through the incorporated jacket of the quartz vessel by means of a peristaltic pump, allowed the plating solution to be maintained at a constant temperature. The immersed substrates were exposed to UV light for varying irradiation periods during which PIED occurs.

7.6.6 Polystyrene Microsphere Template Removal

Post-PIED, the microsphere template was removed to reveal the porous metal film. This was achieved by immersing the substrate in a toluene bath to dissolve the polystyrene spheres. Dissolution is rapid, with typical immersion times being in the order of 30 seconds leaving a

structure of ordered (hemi) spherical voids within the deposited metal; no adverse effects are observed on the deposited metal such as shrinkage, cracking or delamination.

7.6.7 Metal Deposit Characterisation

Nanoporous metal layers formed through PIED into the interstitial spaces of a PS microsphere template were characterised by scanning electron microscopy (FEI Phenom, Lambda Photometrics Ltd, UK). Both conventional 2D and reconstructed 3D "shape from shading" surface images were acquired.

7.7 Results and Discussion

7.7.1 Polystyrene Microsphere Array Formation

Methods described by Denkov *et al* for the formation of 2D close packed microsphere arrays on horizontal substrates [55] formed the basis of the method employed here for the self-assembly of the microsphere templates to be used to introduce porosity into PIED generated metal layers. This method requires the microsphere suspension to be evenly spread across a preferably hydrophilic substrate surface. An insufficiently hydrophilic substrate can impact upon the formation of a well-organised microsphere array by inhibiting the spreading of the microsphere suspension. Such inhibition can result in the formation of alternating concentric rings of thick (multi-layer) and sparse (sub-monolayer) microsphere coverage due to the contact angle hysteresis of the liquid front during evaporation (see ESI).

The assembly of PS microspheres into hexagonally close packed arrays is well documented [54-56,146-149]. However, the presence here of a sensitising TiO_2 layer on the substrate surface offers a novel process advantage; under UV irradiation, TiO_2 is rendered super-hydrophilic to produce an extremely wettable surface [59,141,150]. As all substrates are sensitised with TiO_2 prior to microsphere template formation and a 30–60 min period of UV irradiation prior to application of the microsphere suspension was found to greatly assist in microsphere array assembly. The suspension is readily dispensed over the hydrophilic sample area and water flux is able to occur uninhibited from the edge of the drop towards

the area of maximum evaporation at the centre of the drop, Fig. 55, so facilitating the template self-assembly process.

The resulting microsphere templates show large regions of monolayer arrays with vibrant iridescence due to optical interferences with the template layer, demonstrating the ability of light to penetrate the template, a significant factor for successful PIED. SEM images show hexagonal packing of the templating spheres across the majority of the surface, although these also show that some dislocations and defects remain in the array, Fig. 56. These defects are largely attributable to the roughness of the underlying m-TiO_2 surface which causes minor disruptions to the receding liquid front, and thus template self-assembly, during evaporation.

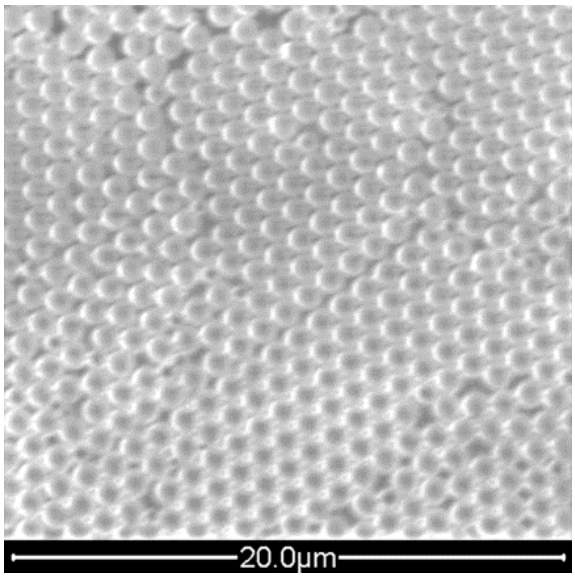

Fig. 56 Monolayer array of 1 µm polystyrene microspheres on m-TiO_2 sensitised glass generated by photo-induced super-hydrophilic self-assembly

7.7.2 PIED of Nanoporous Ag

The microsphere array coated, m-TiO_2 sensitised substrates prepared as described above were treated by PIED to create porous metal films. Microsphere array coated substrates were immersed in the electroless deposition bath given in Table 13 and irradiated with light of energy greater than the band gap of TiO_2 via 6 x 8W UVA lamps in order to induce metallisation with Ag. As described in our previous communication, the extent of the metal

deposition, as measured by deposit thickness, is found to depend upon the deposition period [142]. During the initial 30 min, the metallisation process occurs largely through photocatalytic metal nucleation [137,139]; the Ag deposited in this time persists after the removal of the microsphere template, confirming that deposition occurs directly onto the m-TiO_2 through photocatalytic means. Ag nucleation on the TiO_2 sensitised substrate occurs primarily around the point of contact between individual microspheres and the substrate surface, forming isolated rings of Ag with a diameter of <200 nm, Fig. 57 (i). The possible origins of this effect include: (i) multiple reflections of PIED initiating light between the substrate and microsphere surfaces in the vicinity of sphere-surface contact, effectively increasing the local light intensity, and hence photocatalytic effect at this point; and (ii) concentration of metal nucleation due to a catalytic spillover effect [151] between the TiO_2 and microsphere surfaces, this effect diminishing with increasing distance from the sphere-substrate point of contact.

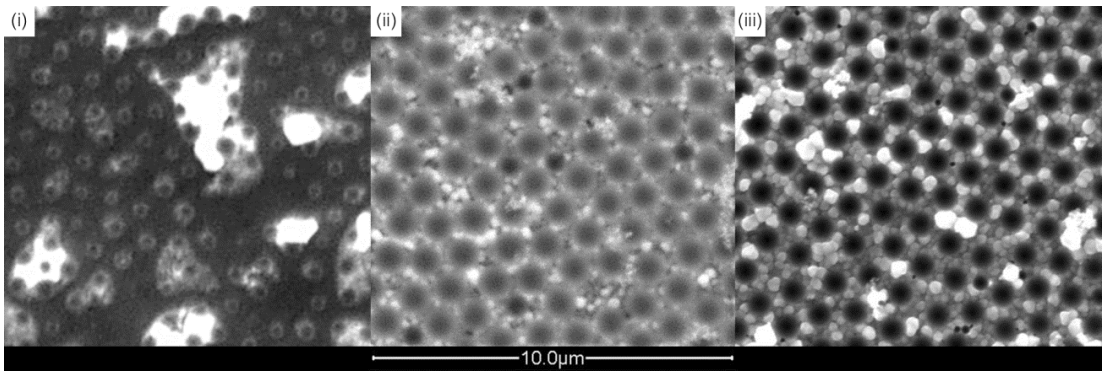

Fig. 57 SEM images of (i) photocatalytically generated Ag nucleation and island growth around (removed) 1 µm microsphere template; (ii) Ag growth in interstitial spaces of 1 µm microsphere template (still present); (iii) ordered porous structure of Ag deposited on glass after microsphere template removal

As PIED continues, auto-catalytic lateral growth of these nucleation rings occurs until the advancing Ag metal front associated with a single ring meets that of another nearby. As several rings coalesce, small islands of Ag are formed containing several small circular pores, again Fig. 57 (i). More extensive deposition leads to the merging of these islands in the same way, forming larger and more expansive Ag layers until a single cohesive Ag film is formed. Subsequent auto-catalytic deposition continues the metal growth upwardly

throughout the interstitial spaces in the microsphere array, forming a metal film around the base of the template Fig. 57 (ii). An irradiated deposition period of 60 min using the same light source produces a fully conductive, porous Ag layer with a surface resistivity, R_s, of ~0.2 Ω / sq with metal deposition occurring throughout the aforementioned interstices without overgrowing the 1 μm template.

After removal of the microsphere template by 30 s dissolution in toluene, the Ag film appears reflective and metallic though also displays a vivid iridescence, comparable to that seen on commercial holographic materials. This effect, produced by the interference of light passing through the sub-micron voids at varying incident angles, provides a direct visual indication of a porous structure present in the deposited metal. This structure is confirmed directly through SEM analysis, revealing a widespread organised nanoporous structure across the templated region, Fig. 57 (iii), and demonstrating the feasibility of creating porous metal layers by templated PIED of simple, 1 electron reduction-based metal systems. The resulting pores have a centre to centre separation of 1 μm, consistent with the size of the polystyrene microspheres used in the template, demonstrating that little or no metal shrinkage or expansion occurs post-deposition or during the microsphere template removal process. The resultant layer of porous Ag remains adhered to the substrate, the strength of that adherence (i) being demonstrated by compliance of the Ag layer with adhesion test BS-EN-ISO-2819:1995; and (ii) confirming that metal deposition occurs directly onto the m-TiO_2 rather than onto the microspheres themselves.

The growth processes described above are comparable to those observed in PIED in the absence of a microsphere template [139]. However, the rate of metal deposition is notably lower when a microsphere template is in place. From our earlier studies of PIED [137,139], the time to produce a non-porous, conductive Ag layer (R_s of ≤0.2 Ω / sq) in the absence of a microsphere template, using the plating bath composition of Table 13 and irradiated with 6 x 8W UVA lamps, is found to be ~15 min. Through a microsphere template, however, significantly less metal is deposited during this time and a deposition period of at least 60 min is required to produce a conductive, porous Ag film with an R_s of ≤0.2 Ω / sq. This

suggests that the microsphere array acts to inhibit the metal deposition through: (i) restricting the access of the electroless plating constituents bath to the underlying m-TiO_2 layer; and / or (ii) attenuating the intensity of the UV irradiation reaching the TiO_2, so reducing the photocatalytic effect and the number of nucleation sites formed. Despite these inhibiting effects, the deposition of nanoporous Ag films through PIED is demonstrated and, as deposited metal film thickness increases with deposition time [142], the reduced rate of metal deposition can be easily compensated for with an increased immersion time in the Ag plating bath.

While the above results were achieved with ultra-band gap irradiation throughout, it is known from our earlier studies on non-templated metal deposition [139] that PIED does not require irradiation throughout the whole immersion period with deposition continuing auto-catalytically after an initial period of photo-initiation. To assess the auto-catalytic activity with a microsphere template in place, the 60 min fully irradiated Ag deposition described above was repeated with a photo-initiation period of 30 min followed by a 30 min period of dark growth. As already shown, an irradiated 30 min deposition through a microsphere template is insufficient to produce a complete Ag layer. Thus, the additional 30 min period of auto-catalytically driven deposition is required if the Ag layer is to develop beyond the partial coverage formed during the initial irradiated stage. It is found that Ag films produced through both fully and partially irradiated deposition periods are comparable, with upper pore diameters of 625 nm and 673 nm respectively (not shown). Geometric analysis of the upper pore diameter (see ESI) allows for the layer thicknesses to be calculated, values for the two samples being found to be similar at 110 nm and 130 nm respectively. Therefore, as with non-templated PIED, irradiation is not required once the metal deposition has been photocatalytically initiated on microsphere templated samples; auto-catalytic Ag deposition then driving metal film formation for the rest of the immersion period.

7.7.3 PIED of Nanoporous Pd

Having demonstrated the generation of a highly ordered nanoporosity in metal films via the single electron reduction associated with the deposition of Ag, the same method was applied to the deposition of Pd, a two electron metal ion reduction process. Accordingly, TiO_2 sensitised glass substrates coated with a 1 μm microsphere template were immersed in the hydrazine based bath developed in house for Pd PIED, Table 14, for 60 min at an operating temperature of 303 K with 315 nm UV irradiation throughout provided by 6 x 8W UVA lamps.

During the initial 30 min, the rate of Pd nucleation appears to be slower than that observed in the Ag deposition discussed above, producing fewer nucleation sites with some areas of the sample exhibiting no nucleation sites at all. However, where Pd nucleation does occur, the same growth pattern exhibited by the Ag system is observed, *i.e.* nucleation rings formed at the base of each microsphere, Fig. 58. As with Ag, this small amount of Pd persists after the removal of the microsphere template and it may therefore be concluded that it is photocatalytically generated directly on the m-TiO_2 surface.

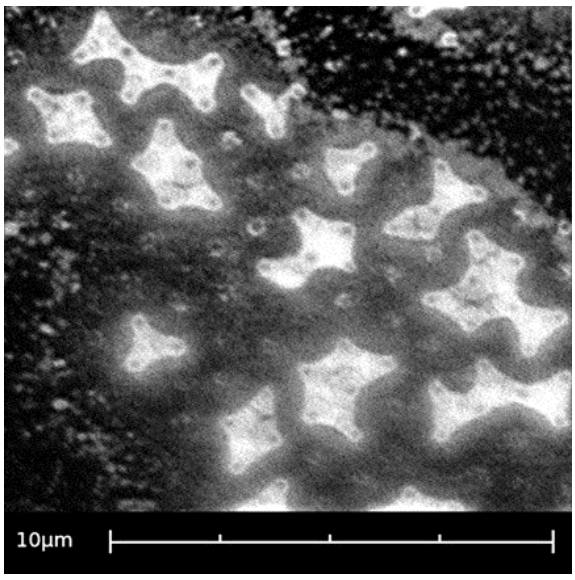

Fig. 58 SEM image of photocatalytically generated Pd nucleation around 1 μm microsphere template

The reduced rate of photocatalytic nucleation in the Pd system, compared to the Ag system, may be explained by consideration of previous potentiometric studies of non-templated PIED [137]. These indicate that a larger potential drop / greater band bending occurs within the

TiO_2 matrix in the Ag PIED system than in the Pd PIED system, with the bands bending upwards towards the surface in the former and being near flat band in the latter. The Ag system therefore exhibits greater photogenerated charge carrier separation and less recombination of conduction band electrons and valence band holes, thus resulting in a greater availability of holes at the TiO_2 surface. In both instances, the electroless bath reductant (potassium sodium tartrate in the case of Ag; hydrazine in the case of Pd) acts as a hole scavenger and hence increases the availability of photogenerated electrons to drive metal deposition. In the absence of a microsphere template, mass transport of the reductant / hole scavenger is unimpeded and hole scavenging occurs efficiently. However, with a microsphere template present, mass transport of all bath constituents is inhibited (*vide supra*), including the reductant / hole scavenger, thus reducing hole scavenging efficiency and the consequent availability of photocatalytically generated electrons. As the Pd system has a lesser population of holes at the TiO_2 surface to begin with, due to lower band bending / greater recombination, it may be expected to show greater sensitivity to hole scavenger availability; hence the rate of photocatalytic nucleation in the Pd system is lower than that in the Ag system when a microsphere template is in place.

However, this effect notwithstanding, photocatalytic nucleation is still observed with the Pd system and thus it should be expected that a greater amount of Pd deposition can be achieved by simply extending the deposition period. After a 60 min irradiated immersion using the same light source, a metallic Pd deposit is visible throughout the microsphere template and remains adhered to the substrate after microsphere removal. However, subsequent SEM analysis reveals that, while considerable amounts of Pd were deposited, there is little evidence of a coherent Pd film spanning laterally across the substrate surface (as would normally be expected in a non-porous Pd deposit) or within interstitial spaces (as previously observed in porous Ag deposits); instead Pd deposition has occurred only over the microsphere surfaces, wholly encapsulating each sphere within a fine metal casing or shell Fig. 59 (i).

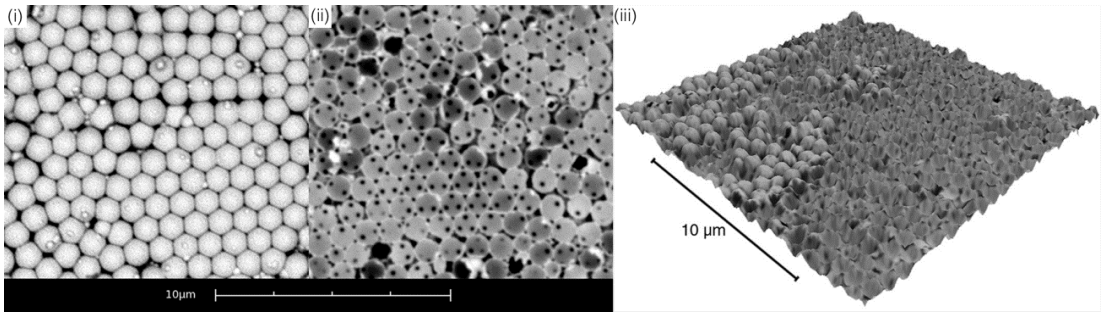

Fig. 59 (i) monolayer of 1 µm polystyrene microspheres coated with fine Pd film; (ii) Pd hemispheres formed throughout a multi-layer microsphere template with sub-pore interconnectivity between layers; (iii) 3D surface reconstruction of Pd film formed in neighbouring monolayer (left) and multi-layer (right) microsphere templates

When deposited throughout a multi-layer microsphere template, Fig. 59 (ii), the upper surface of the Pd deposit can be seen to have formed a series of well defined hemispherical "bowls", visible after removal of the microspheres. Within each bowl, a triangular arrangement of three sub-pores is observed, characteristic of metal which has formed around close packed microsphere arrays of two or more layers in depth. In the same way as a single sub-pore is formed at the point of contact with each microsphere and the m-TiO_2 sensitised substrate surface, these three sub-pores form at the contact points between upper layer microspheres and the three contacting microspheres beneath. However, each hemispherical bowl / spherical shell remains individually formed and linked to neighbouring bowls / shells by virtue of direct contact rather than by Pd deposition within the interstices to form a unified metal layer.

In both Fig. 59 (i) and (ii) it is clear that the locality of Pd deposition is being influenced by the microsphere surfaces. However, it does not appear that this Pd deposition has occurred randomly over the microsphere surfaces through spontaneous auto-catalytic nucleation and subsequent deposition. Should this be the case, irregular coverage of the individual spheres by the metal would be expected and a large proportion of this deposited Pd would then be removed upon dissolution of the microspheres onto which it was adhered. In fact we observe adhesion of these Pd shell structures to the m-TiO_2 sensitised substrate after microsphere removal as well as evidence of metal growth in a consistent direction *i.e.* upwardly from the substrate surface. Fig. 59 (iii) shows a 3D surface reconstructed "shape from shading" SEM

image of a Pd film formed on a template comprised of neighbouring domains of monolayer and multi-layer microsphere arrays. In the monolayer regions, the Pd film fully encapsulates the spheres and preserves their underlying structure in the topography of its upper surface, as in Fig. 59 (i); in multi-layer regions, the upper Pd surface retains open porosity as the second microsphere layer continues to template the Pd growth but without the microspheres being completely encapsulated, as in Fig. 59 (ii). Across the sample, the Pd film thickness demonstrates remarkable consistency with the formed structure only being dependent on the number of microsphere layers.

As Fig. 59 provides no evidence of spontaneous auto-catalytic nucleation onto the upper microsphere surfaces distal from the underlying TiO_2-coated substrate, it would appear that the Pd deposition has originated from photocatalytic nucleation on the m-TiO_2 surface with subsequent directed auto-catalytic deposition occurring uniformly with a steadily advancing growth front over the polystyrene microsphere surfaces. It seems apparent then, that the polystyrene surface is exerting a directing influence on the auto-catalytic Pd deposition following photocatalytic initiation.

The polystyrene microspheres used in this work carry an anionic charge from surface-bound stabilising sulphate groups. The negative charge of these groups may result in coulombic attraction of Pd^{2+} cations towards the surface of the microspheres with a consequent greater effective concentration of Pd^{2+} in the electrical double layer of the microsphere than in the solution bulk (including the bulk solution permeating the interstitial spaces of the template). After photocatalytic initiation, auto-catalytic Pd deposition then occurs most readily at the triple point between the deposited metal front, the electroless plating solution and the (semi) partitioned Pd ion layer, thus resulting in the formation of Pd shells around microspheres as described above. This phenomenon is not observed in the Ag PIED system as Ag^{+} ions are less significantly affected by coulombic attraction towards the microsphere surface, and hence undergo less partitioning between the electrical double layer of the microsphere and the solution bulk, than the more positively charged Pd^{2+} ions.

In order to counteract the coulombic partitioning of Pd^{2+} ions at the surface of the microspheres by the negatively charged sulphate groups, the electroless Pd bath in Table 14 was modified with an excess of inert cations in the form of Na^{+} (0.1 M). These Na^{+} ions would be expected to have a twofold effect, both competing for sulphate sites on the microsphere surface and coulombically shielding their associated charge from solution, so suppressing Pd^{2+} partitioning into the microspheres electrical double layer and resulting in Pd deposition occurring throughout the interstitial spaces of the template.

After 60 min and 90 min irradiated immersion periods, using the same light source as above, in this Na^{+} modified bath at an operating temperature of 303 K, conductive porous Pd films with filled interstices are successfully produced. SEM imagery, Fig. 60, confirms the highly ordered nature of the porous structure with pore centre to centre separation remaining at 1 μm, consistent with the size and arrangement of the microsphere template. As with Ag PIED, this demonstrates that the metal film does not undergo any appreciable expansion / shrinkage post-deposition or during the microsphere removal process. The bias towards Pd deposition onto the microsphere surfaces appears to have been eliminated through the addition of Na^{+} ions as the metal deposition has occurred throughout the interstitial spaces, forming a coherent and conductive Pd film comparable to the structure of the PIED generated Ag films, Fig. 57 (iii). Each Pd deposit displays a smooth upper surface and shows consistent thickness across the sample, indicative of a controlled and homogenous growth pattern. Particularly visible in Fig. 60 (i) are 200 nm sub-pores, formed at the contact point between each microsphere and the substrate surface, within the larger hemispherical voids formed by the base of each microsphere.

For the Pd film shown in Fig. 60 (i), deposited over a 60 min period, we measure an average upper hemispherical void diameter of ~650 nm, equating to a metal thickness of 120 nm; comparable to that of Ag layers formed within the same time period. For the Pd film shown in Fig. 60 (ii), deposited over a 90 min period, an increase in the upper pore diameter to ~900 nm is observed, this equates to a metal layer thickness of approximately 282 nm.

Thus, as previously reported for the Ag system [142], we also observe an increase in Pd film thickness with increasing deposition period.

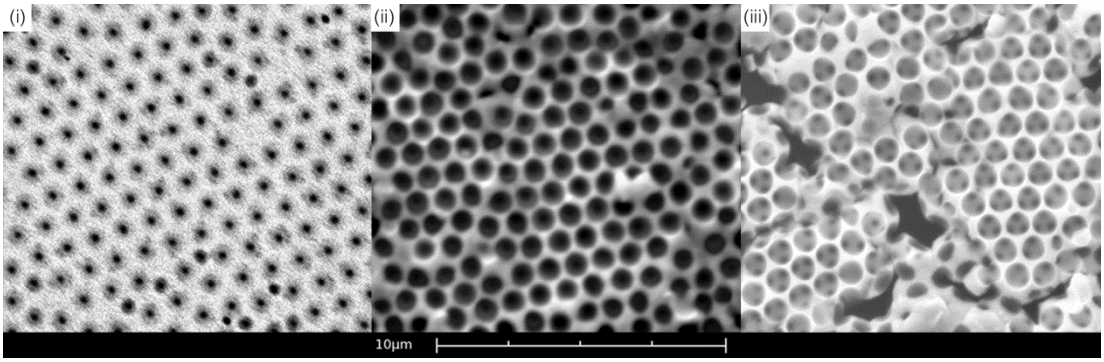

Fig. 60 Pd deposit with organised, monolayer porosity after deposition periods of (i) 60 min and (ii) 90 min; (iii) Pd deposit with interlinked, multi-layer porosity after deposition period of 120 min

In the context of monolayer microsphere templates, as used in Fig. 60 (i) & (ii), it is important to consider the potential eventuality of the deposition time being long enough that the spheres are completely plated over, occluding the porosity of the metal deposit. Where a monolayer template is in place, the maximum metal thickness which may be deposited before the induced porosity becomes so-occluded is less than one microsphere diameter. However, as seen in Fig. 59, microspheres can be arranged in multiple hexagonally close packed layers. Here, at high Na^+ concentration, the use of auto-catalytic deposition over extended periods permits the formation of a metal film with multi-layered porosity where metal deposition has occurred throughout the template interstices. Fig. 60 (iii) shows such a metal film, produced using PIED and a deposition time of >120 min. An upper layer of ordered nanoporosity in the form of hemispherical voids is clearly seen, comparable to that already observed in the monolayer based samples of Fig. 60 (i) & (ii). Also seen are the characteristic features of three interconnecting sub-pores in a triangular arrangement within each void. The deposit therefore displays multi-layer porosity in the form of a network of interconnected spherical and hemispherical voids within a fully conductive Pd film. The formation of such films serves to display another level of versatility in the porous structures which can be achieved using PIED and polystyrene microsphere templates.

7.7.4 The Effect of Elevated Temperature on PIED of Nanoporous Pd

Operating temperature has a direct influence on the rate of conventional electroless deposition [128], suggesting that an increase in operating temperature during PIED may reduce the deposition period required for the formation of a conducting Pd film. Immersion of a TiO_2 sensitised substrate in the Pd bath detailed in Table 14 at 318 K for a fully irradiated period of 60 min results in the deposition of a quantity of Pd which demonstrates adhesion to the m-TiO_2 sensitised substrate upon microsphere removal. However, SEM analysis reveals a structure to the deposited metal that differs from that seen at lower temperature (Fig. 60); rather than a coherent film, the deposited Pd takes the form of an array of large nodules which are 3 – 4 μm in diameter, Fig. 61 (i). This observation is consistent with increased auto-catalytic deposition, as opposed to photocatalytic nucleation, at elevated temperature and is compounded by the low rate of photocatalytic nucleation in the Pd system through a microsphere template (see above). The resultant low density of nucleation sites and accelerated auto-catalytic deposition rate means that significant auto-catalytic growth occurs at each nucleation site before the deposited metal merges with that of other nearby advancing growth fronts.

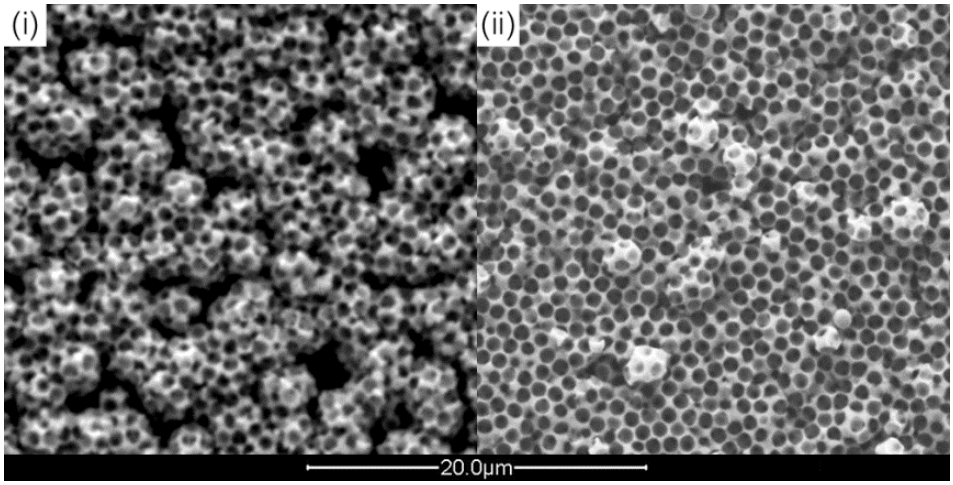

Fig. 61 Pd growth in a 1 μm microsphere template at 318 K after (i) 60 min and (ii) 90 min

While the Pd film produced in this way after 60 min is not fully coherent, an extended deposition period of 90 min results in further auto-catalytic deposition and the agglomeration of these growth nodes into a coherent Pd film, Fig. 61 (ii). The Pd deposit now forms one

continuous and conductive layer though evidence of the nodular growth pattern remains with an undulating upper surface to the Pd film. It is noteworthy that the Pd film produced after 90 min at 318 K displays multi-layer porosity, a feature which requires a deposition period of >120 min at 303 K. Thus, despite a reduction in evenness of film thickness, an increased Pd bath temperature does appear to reduce the immersion period over which the formation of conductive Pd films of multi-layer porosity occurs.

Investigation of temperatures higher than 318 K reveals an operational limitation arising from the use of a polystyrene microsphere template to induce porosity in the electrolessly deposited metal. At temperatures of ≥333 K widespread lifting and dispersion of the template is observed, Fig. 62, most likely due to the thermal expansion of the polystyrene microspheres leading to buckling of the array and its consequent disassembly.

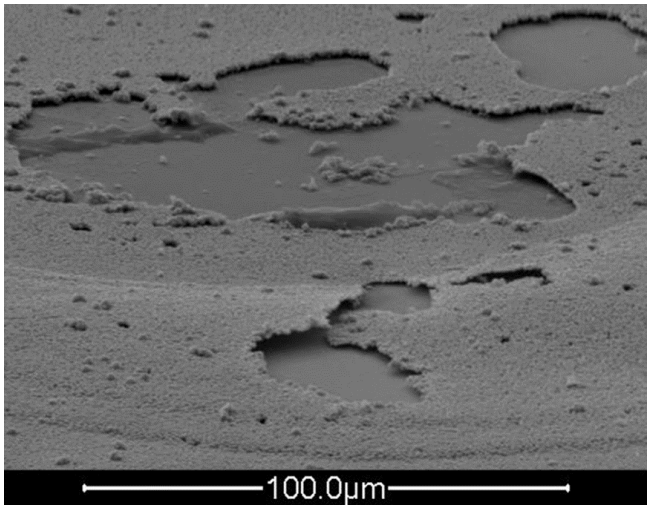

Fig. 62 SEM image at 70° viewing angle of microsphere template lifting due to elevated temperature

7.7.5 Templated PIED with Reduced Microsphere Diameter

While the PIED process can be used on a range of metals, generating both single and multi layer structures, the use of microsphere templates also affords direct control over the pore dimensions within the deposited metal. PS microspheres are commercially available in a wide range of sizes, from 50 nm to 3 µm in diameter; hence it is possible to induce the same range of primary pore sizes into PIED generated metal films.

The results of Fig. 57 - Fig. 61 were obtained using 1 μm diameter microspheres. However, for many envisaged technological applications, it is desirable to induce porosity on a smaller scale, e.g. in the case of the deposited metal being used as an electrode material to facilitate membrane based separation processes, the use of a smaller diameter microsphere template increases the number of pores per unit area within the resultant metal deposit, rendering the deposition of the electrode less detrimental to the permeability of the membrane. Furthermore, the more numerous, smaller pores also serve to increase the surface area of the metal deposit / electrode, resulting in a greater overall triple phase boundary (electrode / membrane / electrolyte) at which electrochemically controlled ion transfer into the membrane may occur. Therefore, PIED has been performed with a range of microsphere templates of component microsphere diameters less than 1 μm, assembly performed as above.

Studies of Ag PIED through a 400 nm diameter microsphere template show that the deposit growth follows the same patterns as observed with 1 μm templates. Nucleation rings form at the base of each microsphere and coalesce through lateral growth into small metal islands, Fig. 63 (i).

As might be expected, the pores arising from the contact point between microspheres and substrate are now smaller in diameter, 100 – 120 nm, compared with ~200 nm for a 1 μm microsphere template (see above). As with Ag PIED around a 1 μm microsphere template, a conductive, coherent and well ordered nanoporous metal film is formed after a 60 min irradiated immersion period using the same light source as above, Fig. 63 (ii). The average upper diameter of the hemispherical voids is measured to be 385 nm which, for a 400 nm template, equates to a metal thickness of approximately 146 nm, a thickness similar to that of 110 - 130 nm produced over the same 60 min irradiated immersion period using a 1 μm diameter microsphere template. Also comparable is the evenness of the upper metal front, again demonstrating steady, controlled Ag deposition across the sample area. A minimum pore centre-to-centre separation of 400 nm is observed, indicating both that the template is hexagonally close packed and that no metal shrinkage has occurred during deposition and

template removal. This separation exhibits values of up to 480 nm in other areas, attributable to local disorder in microsphere packing rather than post-deposition expansion of the metal film.

Thus, a 400 nm diameter microsphere template produces a structure identical to that produced using a 1 μm diameter microsphere template save for the pore size being smaller. Analogous results are obtained using 269 nm and 149 nm diameter microsphere templates, Fig. 63 (iii) & (iv). However, while metallisation occurs via the same growth patterns as observed in Fig. 57 & Fig. 63, a reduction in deposition rate is observed.

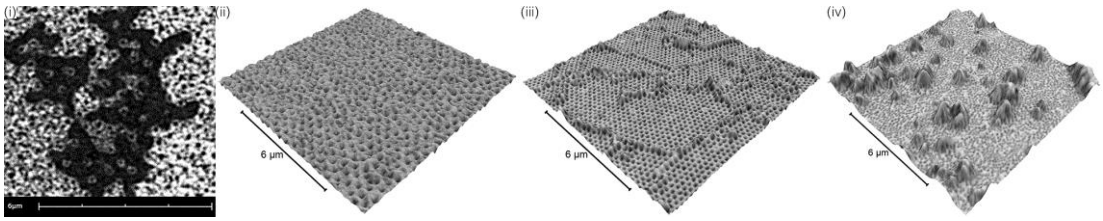

Fig. 63 (i) SEM image of Ag nucleation; and 3D surface reconstructions of nanoporous Ag film formed around (ii) 400 nm (iii) 269 nm and (iv) 149 nm diameter polystyrene microsphere templates

After a 60 min deposition period around a 269 nm diameter microsphere template, a metal film is formed with an average hemispherical void diameter of 190 nm. For this microsphere diameter, this equates to a metal film thickness of 39 nm, considerably less than that of an Ag film produced in the same time period using larger microspheres. It is likely that the reduced size of the interstitial spaces associated with these spheres causes an increased restriction on the mass transport of bath constituents to the substrate surface and therefore reduces the metal deposition rate. Significantly though, the upper surface of the metal deposit again shows areas of even metal growth, Fig. 63 (iii). As demonstrated above with Pd, this represents a deposition process consisting of abundant photocatalytic nucleation and slow auto-catalytic deposition. It can therefore be concluded that, while the smaller microspheres do indeed cause a further restriction on mass transport, the photocatalytic initiation is relatively unaffected with sufficient UV light being able to reach the TiO_2 surface to generate an even coverage of nucleation sites. Interestingly, peaked ridges are also observed across the Ag deposit, Fig. 63 (i). These appear to form along the length of

packing dislocations within the HCP microsphere array where the spacing between adjacent spheres is increased. It is therefore likely that less inhibition of bath constituent mass transport, and consequently of the auto-catalytic deposition process, occurs at these locations thus enabling a greater thickness of Ag to be deposited within the same immersion period.

Similar observations are made when the microsphere diameter is further reduced to 149 nm. While an Ag film is formed after a 60 min deposition period, the metal thickness is a mere 22 nm, again representing a slower metal deposition rate than that observed with a larger microsphere template. Microspheres of this size also show less HCP organisation than their larger counterparts as the array formation is proportionally more susceptible to disruption by imperfections on and the roughness of the substrate surface. This leads to more significant gaps in the microsphere array and contrasting deposition rates at these gaps and throughout the microsphere template. As a consequence, proportionally large protrusions on the upper Ag surface are formed as auto-catalytic deposition occurs with less mass transport-based restriction at breaks in the microsphere coverage, Fig. 63 (iv). More efficient assembly of HCP microsphere arrays of this diameter and smaller may potentially be achieved through alternate formation methods such as Langmuir-Blodgett deposition. Work on this is ongoing within our laboratories.

Despite this, these results represent the smallest nanoporosity induced in PIED generated metal to date with 106 nm primary pores in a metal film of 22 nm thickness. Through this, and the series of results above, we have demonstrated the highly controllable and convenient manipulation of the nanostructure dimensions through simple choice of the template particle size.

7.8 Conclusions

We have reported the photocatalytically initiated electroless deposition of metals with highly ordered nanometre scale porosity on TiO_2 sensitised insulating substrates. This novel process allows for controllable photo-initiation of the metallisation process whilst facilitating

continued auto-catalytic electroless deposition to produce coherent porous metal films, the thickness of which is determined by the total deposition time. Metallisation is demonstrated with both one electron, Ag, and two electron, Pd, metal ion reductions and the initial nucleation and growth patterns of the produced metal films have been described. The resulting metal deposits can be induced with 2-dimensional monolayer or 3-dimensional multi-layer nano-scale porosity with a highly regular and predictable order. The dimensions of this porosity are conveniently controlled via the particle diameter of the microsphere template.

PIED of metals with induced porosity therefore represents a flexible yet controllable method for the fabrication of nano-structured metal films with predictable dimensions on the surface of otherwise electrically insulating substrate materials. Such metallised materials have potentially wide applications in membrane and analytical separation technology, desalination, electrode/solid electrolyte composites for fuel cells, energy storage and sensors – especially surface enhanced resonance Raman spectroscopy (SERRS).

7.9 Acknowledgment

We would like to thank the RSC Analytical Division (Award No 07/G61) and the EPSRC (Award No EP/E062261 and EP/I002928/1) for funding. We also thank The Lloyds Register Educational Trust (LRET) for financial support. The LRET is an independent charity working to achieve advances in transportation, science, engineering and technology education, training and research worldwide for the benefit of all.

APPENDIX

SUPPLEMENTARY INFORMATION

7.S1 Microsphere Array Formation

Ordering through controlled evaporation is achieved by slow evaporation of water from a microsphere solution on the substrate surface. This solution must be maintained in a constant meniscus for effective organisation. A meniscus is induced by a PTFE ring with tapered inner edge which is sealed onto the substrate allowing the sphere solution to be placed within. It is known that in sufficient liquid depths the microspheres are mobile and undergo Brownian motion and that this occurs until evaporation results in the liquid depth at the meniscus centre becoming approximately equal to sphere diameter. At this point there is a transition from disorganisation and spheres begin to deposit on the substrate surface at this central point. As liquid depth is insufficient to maintain free suspension, spheres settle on the substrate and miniature menisci form between them Fig. 64.

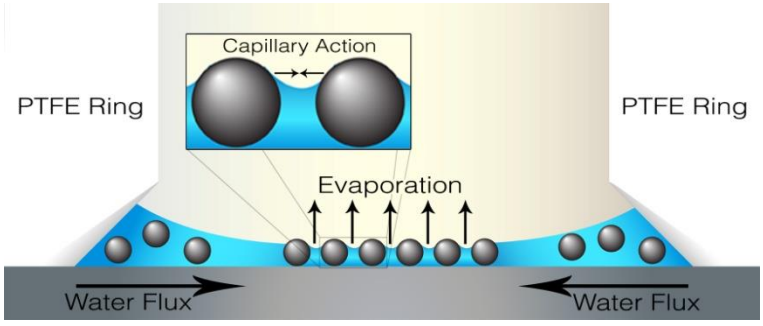

Fig. 64 Mechanism of formation of microsphere template

As evaporation continues lateral capillary forces between individual spheres draw them closer together to form a hexagonally close packed nucleus. Organisation continues outwards from the central nucleus as more spheres are transported by water flux within the evaporating meniscus. Spheres reaching the edge of the ordered array are deposited and packed by the same lateral capillary forces resulting in areas of ordered monolayers of the latex spheres.

The ordered array is usually ringed by a thicker multi-layer deposit formed where the angle of the liquid meniscus becomes greater due to closer proximity to the PTFE wall. Defects within the ordered region are also common and may be caused by defects on the substrate, poorly controlled evaporation or the formation of gas bubbles in the microsphere solution. Slower evaporation allows for improved organisation and closer packing making a controlled humidity environment desirable. Microsphere organisation is also more efficient on a hydrophilic surface which allows the sphere solution to spread evenly across the substrate.

7.S2 Preparation of Ag Electroless Plating Baths

Electroless Ag plating solutions were prepared according to the composition given in Table 13 as developed in our laboratories [137]. All components are added to a small volume of distilled water (~10 ml) in the order listed, ensuring full dissolution with each addition. The completed solution was made up to volume with doubly deionised water and purged with N_2 for 20 min to deoxygenate. The pH of the solution was 11.5 and PIED was carried out at 298 K. Electroless plating solutions were freshly made immediately before use for optimum performance. As $AgNO_3$ is light sensitive, Ag solutions are prepared and stored in amber coloured flasks in the darkness before use.

Role	Component	Concentration
Metal precursor	Silver Nitrate	1.496 g / dm^3 (8.8 mmol / dm^3)
Complexant	Ethylenediamine	3.245 g / dm^3 (54 mmol / dm^3)
Stabiliser	3,5-diiodotyrosine	0.017 g / dm^3 (39.2 µmol / dm^3)
Reducing agent / scavenger	Potassium Sodium Tartrate	0.7356 g / dm^3 (26 mmol / dm^3)
pH	-	11-12
Temp	-	298 K

Table 13 Composition of Ag electroless plating solution

7.S3 Preparation of Pd Electroless Plating Baths

Electroless Pd solutions, also developed in these laboratories [137], were prepared to the composition given in Table 14. $PdCl_2$, di-sodium EDTA and ammonium hydroxide (28% NH_3 in water) were added and, to ensure formation of the Pd-amine complex, stirred

with gentle heating until the solution cleared. The solution was cooled and hydrazine reducing agent added. The solution was then made up to volume with doubly deionised water and purged with N_2 for 20 min. Electroless plating solutions were made immediately before use for optimum performance.

Role	Component	Concentration
Metal precursor	Palladium Chloride	5.0 g / dm^3 (28 mmol / dm^3)
Complexant	Ammonium Hydroxide (28%)	100.0 ml / dm^3 (1.5 mol / dm^3 NH_3)
Stabiliser	Di-sodium EDTA	20.0 g / dm^3 (53.8 mmol / dm^3)
Stabiliser	Thiourea	1.2 mg / dm^3 (15.8 µmol / dm^3)
Reducing agent / scavenger	Hydrazine (65%)	0.3 g / dm^3 (6 mmol / dm^3)
pH	-	11-12
Temp	-	298 K

Table 14 Composition of Pd electroless plating solution

7.S4 Geometric Determination of Metal Deposit Thickness

The thickness of the deposited porous metal layer can be determined by considering the geometry of the microspheres and resulting metal pores, Fig. 65. When considered in cross section, it can be seen that the deposited metal forms an arc around the lower portion of each microsphere, the sagitta (s) of this arc corresponding to the depth of the metal deposit. The size of s can be calculated using equation (9) where r = sphere radius and l = ½ chord length, the latter corresponding to the measured radius of the upper opening of the pore / hemispherical void, as determined by scanning electron microscopy.

$$s = r - \sqrt{r^2 - l^2} \tag{9}$$

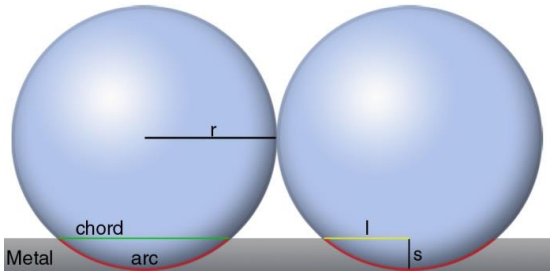

Fig. 65 Microsphere template and templated metal pore geometry for determination of metal film thickness

This equation calculates a metal depth which is only applicable to a deposit formed around a single microsphere layer. Where the metal thickness covers multiple microsphere layers, the overall thickness must include the depth of each fully covered lower microsphere layers as well as the partial coverage of the uppermost layer. The nature of hexagonal close packing dictates that the horizontal pitch, the distance between neighbouring sphere centres, is equal to twice the sphere radius, 2r. However, the vertical pitch is a smaller distance as spheres on the upper layer sit within the hollows formed between neighbouring spheres on the layer beneath. This vertical pitch distance can be calculated using equation (10).

$$\left(\sqrt{6}\times\frac{2r}{3}\right) \tag{10}$$

The horizontal and vertical pitch in hexagonally close packed spheres is shown in Fig. 66. While the vertical pitch is described as the centre to centre distance between vertically stacked spheres, it can also be interpreted as the distance between the basal points of these spheres. Given that equation (9) provides the distance from the base of the uppermost microsphere to the upper surface of the deposited metal, and that equation (10) provides the distance from the substrate surface to the base of the uppermost microsphere, the two distances can be combined to provide a complete metal layer thickness.

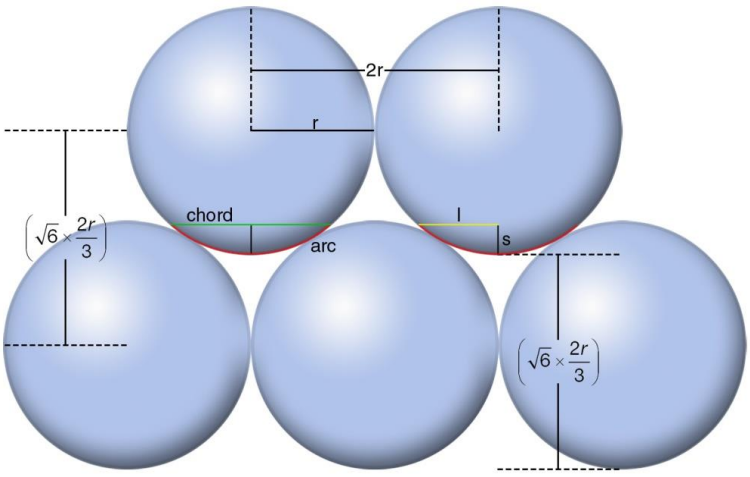

Fig. 66 Horizontal and vertical pitch of hexagonally close packed microspheres

Taking into account the number of lower microsphere layers, n, which have been covered by metal deposition, the following equation for the calculation of the total metal thickness across a multi-layer microsphere template by upper pore diameter measurement is derived:

$$\left(\sqrt{6}\times\frac{2r}{3}\right)_n+\left(r-\sqrt{r^2-l^2}\right) \tag{11}$$

7.S5 Contact Angle Hysteresis

The repeated transition between bands of heavy sphere deposition and very little sphere deposition can be explained by considering the contact angle hysteresis of water droplets during evaporation [152]. In the case of a normal droplet, a stable contact area and angle are formed according to the surface chemistry and topography of the substrate. As evaporation occurs and the volume of liquid decreases and the contact angle drops as shown in Fig. 67 by the transition from state 1 to state 2. This occurs until surface tension causes the liquid front to slip on the substrate surface, receding to a smaller contact area and returning to its original contact angle and stable state, shown in Fig. 67 by the transition from state 2 to state 3.

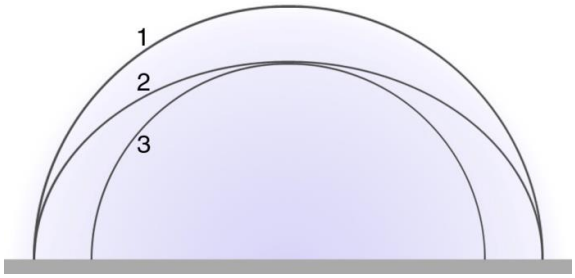

Fig. 67 Water droplet receding through evaporation

With continued evaporation this process repeats in a cycle of static contact area with reducing contact angle and rapidly receding contact area and constant contact angle. The length of each stage is largely determined by the rate of evaporation but also the properties of the substrate. Rougher and more hydrophobic surfaces lead to a greater decrease in contact angle before the drop slips while smoother, more hydrophilic surfaces allow the slip to occur more easily and hence with a less marked step between each stage.

This effect is directly translated into the deposition of particles suspended in the liquid. Particle deposition occurs at the shallowest point, in the case of a water droplet this is outer liquid boundary. As the droplet remains on a constant contact area with decreasing angle this deposition zone remains stationary on the substrate surface and hence an accumulation of particles occurs there. At the point when the liquid slips, the outer boundary moves quickly over the substrate resulting in little or no particle deposition in the area which has been travelled over. The droplet again stabilises and the suspended particles are once more deposited around the outer boundary as the front remains static.

In the microsphere deposition method described above, the liquid is formed into a concave meniscus by the tapered PTFE ring rather than forming a convex dome droplet. Here the shallowest region is not found at the outer edge but rather at the centre with a circular front retreating outwardly towards the PTFE ring as evaporation continues. Despite this difference, the process of the liquid front recession over the substrate surface follows the same principles as described above for water droplets. As the untreated glass is hydrophobic, the liquid cannot retreat smoothly and instead moves in marked steps. As microsphere deposition occurs at the shallowest region of liquid, thick microsphere deposits form at the liquid front during static periods while very few microspheres are deposited as the liquid slips. This leads to the formation of the concentric rings.

CHAPTER 8

THE NANOPOROUS METALLISATION OF POLYMER MEMBRANES THROUGH PHOTOCATALYTICALLY INITIATED ELECTROLESS DEPOSITION

Symposium on Processes at the Semiconductor Solution Interface 5, *ECS Transactions*, 53, 1, (2013)

Michael A. Bromley*, Colin Boxall

Engineering Department, Lancaster University, Lancaster LA1 4YR, UK

"You must remember that he is operating on a completely different level to us now. To him, we are the intellectual equivalent of domestic science teachers."

Kryten 2X4B-523P

8.1 Publication Summary

- ECS Transactions paper to accompany presentation of the nanoporous metallisation of insulating substrates
- Detailed report of the application of previously developed techniques to the nanoporous metallisation of PVDF membranes
- Report of the nucleation and growth patterns occurring during metal deposition around a microsphere template on PVDF membrane
- Account of the difficulties encountered in the nanoporous metallisation of PVDF membranes through PIED
- The formation of two independently conductive electrodes on a single membrane is demonstrated

8.2 Author Contributions

- M.A.B.: designed and performed all experiments, analysis and characterisation; primary author of the manuscript from first draft to final proof
- C.B.: conceived and supervised the study; co-author of manuscript through review of draft

8.3 Abstract

We present the novel use of Photocatalytically Initiated Electroless Deposition (PIED) for the deposition of metal films with highly ordered arrays of sub-μm (hemi) spherical pores directly onto the surface of insulating organic membrane-based substrates. This is achieved by sensitisation of the target substrate with a TiO_2 photocatalyst followed by the self-assembly of a hexagonally close packed polystyrene microsphere template at the substrate surface. Metallisation then occurs through PIED into the template interstices and directly onto the TiO_2 sensitised membrane surface. The dimensions of the resultant pores in the deposited metal are determined by the size of the template microspheres while metal film thickness may be controlled by the deposition period.

The fabrication of nanoporous metal by this novel method adds a conductive and permeable metallic structure of high surface area to an otherwise electrically insulating polymer membrane surface. Such metallised insulating membranes have potentially wide applications in membrane and separation technology, desalination and electrode / solid electrolyte composites for fuel cells.

8.4 Introduction

Fast, controllable and selective separation of metal ions from complex solutions is key to a wide range of activities including pre-analytical separation, environmental monitoring, environmental remediation, metal recycling, desalination and process control. These activities are important in a wide range of industries including pharmaceuticals, mining, foodstuffs, wastewater processing, power generation and nuclear. Using our recently reported insulator metallisation process of Photocatalytically Initiated Electroless Deposition (PIED) [137-139,142], we aim to develop novel, highly ion selective membrane-based separation technologies through a combination of supported ligand membranes and supplemental electrochemical control by overlying nano-engineered metal layers. Layers of porous metal with controllable pore size, distribution and metal thickness deposited on ion selective membranes (ISMs) may act as *in-situ* electrodes offering electrochemical control over the environment at the ISM-solution interface. The result is an ability to manipulate the valence state of target ions at the ISM surface, providing greater selectivity in extraction than achieved with a supported ligand membrane-only system.

The principles of PIED have been described in detail elsewhere [137-139,142] but may be summarised as follows. Metal deposition is initiated through a semiconductor photocatalysis based process whereby, initially, electron-hole pairs are generated in TiO_2 particles upon the absorption of ultra-band gap light energy (λ = 315 nm). These photogenerated electrons may then reduce metal precursor ions in solution [12], forming metal nuclei on the semiconductor surface, Fig. 68 (i). Once sufficient nucleation sites have been photocatalytically generated, these begin to grow through an auto-catalytic electroless deposition reaction, driven by a reductant present in the electroless plating bath, Fig. 68 (ii); the growing nuclei eventually coalesce to form a coherent metal layer. This second step can occur both in the presence and absence of light, the latter being particularly advantageous for producing thick, non-transparent metal layers.

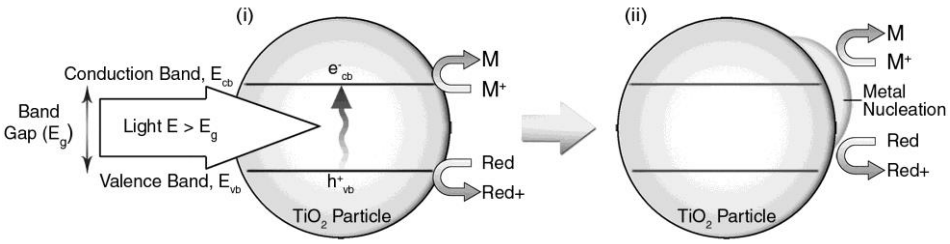

Fig. 68 Two stages of PIED: (i) photoreductive metal nucleation on irradiated photocatalyst; (ii) auto-catalytic electroless deposition process

In this basic form, the resulting metal film has no artificially induced structure. In order to produce a metal film with a nanostructure / nanoporosity, the metal deposition must take place around some form of template. We have deposited metal via PIED into the interstitial spaces of hexagonally close packed polystyrene (PS) microsphere arrays in a similar manner to that reported by Bartlett *et al* [54] wherein porous metal films are prepared by electrodeposition into the interstitial spaces between PS spheres assembled on metal electrode surfaces. In each case, the microsphere template is removed post-deposition, by dissolving in toluene, to leave a metal film with a regular nanostructure. Furthermore, polystyrene spheres are commercially available in sizes ranging from 50 nm to 3 μm, allowing for the production of metal films with a wide range of pore sizes using the same deposition technique as demonstrated in parallel work from this laboratory [153].

Having previously developed PIED for the deposition of non-porous and porous metals onto glass [137,142], the same fabrication techniques can be utilised for the metallisation of other insulating substrate materials. As the TiO_2 sensitisation of the substrate material is of prime significance to the deposition process, theoretically, any sensitised substrate should be receptive to subsequent photocatalytically initiated electroless deposition. However, this sensitisation process on glass usually involves annealing of the TiO_2 coating at 773 K to produce a robust layer of the anatase crystal phase [137], known to display the highest photocatalytic activity [133]. As the anatase phase is formed at temperatures from 623 - 823 K, it is likely that any such thermal treatment will cause damage to many potential organic polymer membrane-based substrate materials.

Hence, this paper concerns the development of PIED for membrane metallisation using a porous polyvinylidene fluoride (PVDF) substrate as an exemplar ISM material.

8.5 Experimental

8.5.1 Materials and Reagents

All reagents used are AnalaR grade or higher, and purchased from Sigma Aldrich (Gillingham, Dorset, UK) or Alfa Aesar (Heysham, Lancashire, UK) with the exception of nanoparticulate TiO_2 sol (TiPE® O502, TitanPE Technologies Inc., Shanghai, China). All water used is Ultrapure doubly deionised water from a Direct-Q 3 UV Millipore water purification system (Millipore (U.K.) Limited, Watford, UK) to a resistivity of 18.2 MΩ / cm. Nitrogen Whitespot grade is provided by BOC Ltd., Guildford, Surrey, UK.

8.5.2 TiO_2 Sensitisation of Substrates Using Nanoparticulate Colloids

PVDF membranes, 0.22 μm pore size (Millipore), were sensitised by coating with a nanoparticulate TiO_2 sol (TiPE® O502, TitanPE Technologies Inc., Shanghai, China) deposited via spin-coating for 5 seconds at 2900 rpm using an inverted model 636 rotating disk electrode system (Princeton Applied Research, Tennessee, USA) for single side sensitisation and by manual dip-coating for two sided sensitisation. The sol contains nanoparticulate anatase TiO_2 with average primary particle size of < 8 nm in water based solution. Coated PVDF membranes were oven dried at 373 K to remove solvent and so produce a coating of anatase nanoparticles. Sensitised substrates were stored in darkness at room temperature prior to use.

8.5.3 Polystyrene Microsphere Array Formation

Polystyrene Microspheres of 1 μm diameter were purchased from Alfa Aesar as a 2.5 wt% solution in water. For template preparation purposes this was further diluted to 1.0 wt% with doubly deionised water. TiO_2 coated surfaces exhibit super-hydrophilicity upon irradiation with UV light [59], a phenomenon that we have explored for optimising the self-assembly of

ordered microsphere arrays. In this, TiO_2 sensitised substrates were irradiated with UV light for 60 min prior to the application of the microsphere solution, the photo-induced substrate hydrophilicity facilitating an even spreading of that solution (see below). 12.35 µl of the microsphere solution was applied to the substrate via micro-pipette inside an 11 mm diameter PTFE ring with tapered inner edge, Fig. 69. This ring was sealed to the substrate surface with silicone grease to ensure there is no solution leakage while the tapered edge creates a permanent concave meniscus on the liquid surface, essential for the ordered template self-assembly process, again shown in Fig. 69. Upon application of the sphere solution, substrates were left undisturbed for 12 hours on a level surface (to prevent gravitational bias) and in an enclosed environment (to ensure no uneven evaporation is caused by local air currents). Ordered template self-assembly then occurs through the capillary action of the surface tension force of the evenly evaporating liquid meniscus on the component microspheres.

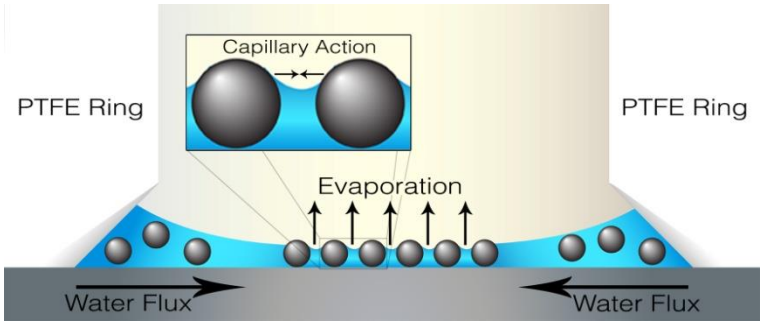

Fig. 69 Self-assembly of polystyrene microsphere template

8.5.4 Preparation of Ag Electroless Plating Baths

Electroless Ag plating solutions were prepared to the composition given in Table 15. All components are added to a small quantity of distilled water in the order listed, ensuring full dissolution with each addition. The completed solution was made up to volume with doubly deionised water and purged with N_2 for 20 min to deoxygenate. The pH of the solution was 11.5 and PIED was carried out at 298 K. Electroless plating solutions are freshly made immediately before use for optimum performance. As $AgNO_3$ is light sensitive, Ag solutions are prepared and stored in amber flasks in darkness.

Role	Component	Concentration
Metal precursor	Silver Nitrate	1.496 g / dm^3 (8.8 mmol / dm^3)
Complexant	Ethylenediamine	3.245 g / dm^3 (54 mmol / dm^3)
Stabiliser	3,5-diiodotyrosine	0.017 g / dm^3 (39.2 µmol / dm^3)
Reducing agent / scavenger	Potassium Sodium Tartrate	0.7356 g / dm^3 (26 mmol / dm^3)
pH	-	11-12
Temp	-	298 K

Table 15 Composition of Ag electroless plating solution

8.5.5 Photocatalytically Initiated Electroless Deposition

TiO_2 sensitised, microsphere template coated substrates were placed directly into freshly prepared electroless plating solutions in a quartz reaction vessel for optimal UV transmittance. Plating solutions were bubbled with N_2 during deposition in order to purge the solution of oxygen which can compete with the metal precursor ions for reduction at the photocatalytic surface. The N_2 stream also provides a source of agitation to prevent local depletion of the metal ion concentration at the substrate surface. The reaction vessel is then placed inside a photoreactor (Lidam Scientific, Dartford, UK) comprised of two hemi-cylinders, each containing 6 x 8W UVA lamps. A thermostatically controlled water supply, passed through the incorporated jacket of the quartz vessel by means of a peristaltic pump, allowed the plating solution to be maintained at a constant temperature. The immersed substrates were exposed to UV light for varying irradiation periods during which PIED occurs.

8.5.6 Polystyrene Microsphere Array Removal

Post-PIED, removal of the microsphere template was achieved by immersing the substrate in a toluene bath to dissolve the polystyrene spheres. Dissolution is rapid, with typical immersion times being in the order of 30 seconds leaving a structure of ordered (hemi) spherical voids within the deposited metal; no adverse effects are observed on the deposited metal or PVDF membrane substrate.

8.5.7 Metal Deposit Characterisation

Morphology and dimensions of the deposited metal layers were determined by scanning electron microscopy (FEI Phenom, Lambda Photometrics Ltd, UK).

8.6 Results and Discussion

8.6.1 Metallisation of PVDF Membrane through PIED

With a melting point of ~443 K, PVDF is not able to withstand the high annealing temperatures (773 K) applied during the TiO_2 sensitisation of more robust substrates such as glass using sol-gel derived titanias [137,142]. Due to this necessity to lower the firing temperature, these sol-gel derived coatings would have to be used in a photocatalytically less active, non-crystalline state [154]. Thus, an alternate means of providing a TiO_2 coating was explored by using a commercially available / proprietary nanoparticulate TiO_2 suspension sourced from TitanPE Technologies Inc. in Shanghai, China. This suspension contains primarily anatase particles in its stock form. The use of TiPE TiO_2 allows the sensitisation of substrates with predominantly anatase TiO_2 without the need for high temperature annealing.

The surface of an unmodified PVDF membrane is shown in Fig. 70 (i), material porosity and irregularity being clearly visible. When sensitised by spin-coating, the majority of the applied TiO_2 suspension is rapidly removed by centrifugal force leaving only a thin film which closely follows the surface structure of the PVDF surface, Fig. 70 (ii). While the deposited TiO_2 occludes some smaller features of the porous membrane, the structure remains largely recognisable and the porosity remains unobstructed on a larger scale. Sensitisation by dip-coating increases the TiO_2 loading, so enhancing the photocatalytic effect, but the photocatalyst is much more obstructive to the porosity of the PVDF membrane as a consequence, Fig. 70 (iii). This occurs because, unlike with spin-coating, TiO_2 particles are not discarded with the excess solvent by centrifugal force; oven drying at 373 K removes only the volatile solvent while the TiO_2 particles remain on the substrate as an evaporation residue. Only part of the membrane porosity is lost, a factor of significance for the ion separation membranes under consideration here, and, importantly for PIED the concentration

of TiO_2 at the membrane surface is much greater than that at a similar substrate sensitised by spin-coating.

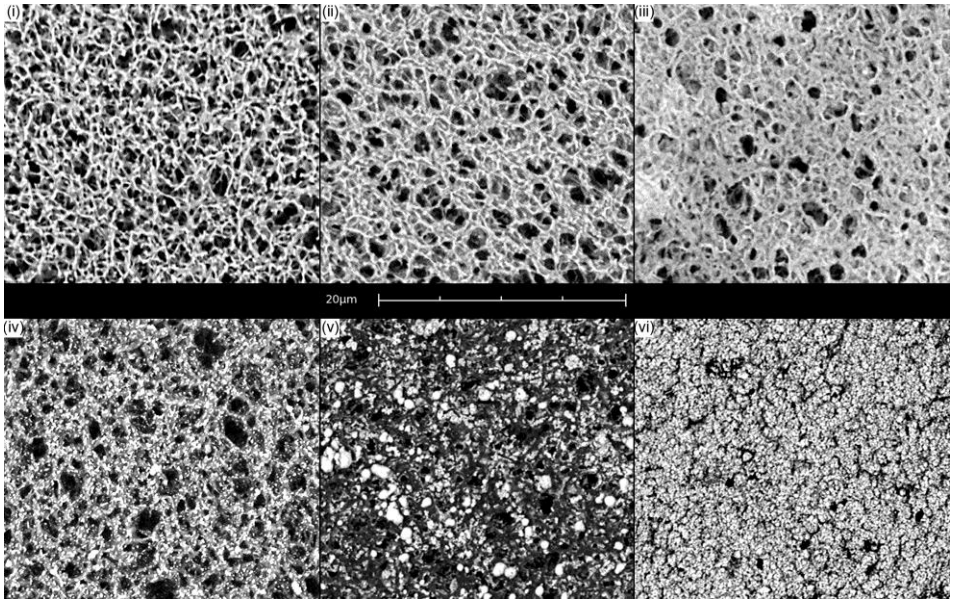

Fig. 70 SEM images of (i) un-modified PVDF membrane, (ii) TiO_2 loading on PVDF after spin-coating, (iii) TiO_2 loading on PVDF after dip-coating; TiO_2 sensitised PVDF membrane with (iv) Ag nucleation, t = 15 min, (v) continued Ag growth, t = 30 min and (vi) non-porous, conducting Ag film, t = 60 min

Once suitably sensitised with TiO_2, the PVDF membrane can be metallised through PIED. Metal deposition occurs via a number of distinct growth stages, as previously observed with PIED on glass substrates [139]. Photocatalytic reduction of metal ions from the electroless plating solution results in metal nucleation directly onto the TiO_2 particles. Fig. 70 (iv) shows Ag nucleation, visible as bright white particles across all areas, on TiO_2 sensitised PVDF after a deposition time of 15 min; at this stage the Ag deposit takes shape around the structure of the PVDF membrane, the porosity of which remains largely un-obscured with the formation of a coherent metal film yet to occur. As the deposition period continues, auto-catalytic electroless deposition, driven by the reductant in the electroless plating bath, begins to occur at each photogenerated nucleation site resulting in the growth of larger Ag granules. For the system of Fig. 70, this occurs after approximately 15 – 30 min, Fig. 70 (v).

After a total deposition period of 60 min, these isolated metal granules are seen to coalesce and form a coherent and electrically conductive metal film, Fig. 70 (vi). SEM analysis reveals that this metallic Ag layer is highly granular, more so than similar layers formed on glass

substrates, attributed to the irregularity of the substrate surface and potentially a reduced efficiency of the non-annealed photocatalyst. While a slower electroless deposition is typically expected to produce a deposit of finer granularity, here we see a photocatalytic initiation stage producing fewer nucleation sites than previously observed on m-TiO_2 sensitised glass substrates within the same deposition time [139,142,153]. This, combined with a translation of substrate morphology into the deposited metal, results in a rougher and more granular film. Despite this, the metal film displays good electrical conductivity with a sheet resistivity, R_s, of 0.5 Ω / sq, a value comparable to the R_s of 0.2 Ω / sq observed on fully conductive Ag layers on glass [142,153].

As the dip-coating sensitisation method results in TiO_2 deposition onto all membrane surfaces, including the membrane edges, metal deposition also occurs in the same areas resulting in conductivity between opposite sides of the metallised membrane. However, by simply trimming the metallised edges from the membrane, the electrical connection between these opposing membrane sides is eliminated. This trimming procedure then results in the production of two individually conductive metal layers / electrodes on a single porous PVDF membrane with zero through membrane conductivity. Each deposited metal electrode could therefore be separately controlled, thus offering independent electrochemical control of the solution environment on either side of the membrane. Such a phenomenon could be exploited in enhanced separation processes on ISMs if the deposited electrodes themselves were to be rendered porous. This can be achieved via PIED through the interstices of a hexagonally close packed microsphere array that is subsequently removed. This method forms the subject for the remainder of this paper.

8.6.2 Microsphere Array Formation

As previously described in our studies of the metallisation of glass substrates with nanoporous metal films [142,153], hexagonally close packed arrays of 1 μm microspheres provide the template material around which PIED generated nanoporous metal film may be formed. We have found that such microsphere array templates may also be deposited onto

the PVDF membrane substrates in the same manner as on glass, although the spheres exhibit less regular packing on membranes than on similarly prepared glass substrates [142,155]. This may be attributable to two factors; firstly, the rough surface morphology of the PVDF membrane, Fig. 70, disrupting the self-assembly process of the microspheres, leading to an increased number of dislocations within the array; and secondly, the potentially reduced efficiency of the non-annealed photocatalyst resulting in the super-hydrophilicity of the irradiated TiO_2 surface [59,141] being less readily generated and the microsphere suspension spreading less freely over the substrate surface. While the latter may be true for TiO_2 sensitised membranes in comparison to TiO_2 sensitised – and fully annealed – glass substrates, the photocatalytically induced hydrophilic effect achieved on an irradiated, TiO_2 sensitised membrane remains advantageous over a non-irradiated, TiO_2 sensitised membrane over which the microsphere suspension spreads much less readily due to the lack of hydrophilic assistance.

Due to the aforementioned factors, microsphere templates deposited onto PVDF membranes lack substantial areas of hexagonal close packing as the self-assembly mechanism required for the formation of highly ordered close packed microsphere arrays is disrupted, Fig. 71. Despite this, the microspheres are generally deposited within close proximity and the templates are still appropriate for the induction of widespread nano-scale porosity in subsequently deposited metals – though the porosity of the resultant metals will be expected to exhibit a lower degree of regularity on membranes than on glass substrates. This is discussed in more detail below.

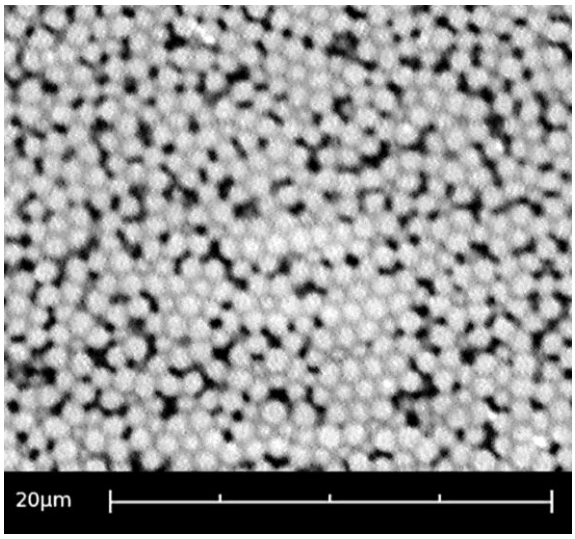

Fig. 71 1 µm polystyrene microsphere array on TiPE O502 sensitised PVDF membrane

8.6.3 Templated Ag PIED on PVDF

Microsphere template coated PVDF substrates are metallised through PIED using the same method as described above. After a short 30 min period of irradiated immersion in the Ag electroless plating bath, isolated Ag deposits are observed, Fig. 72, and can be seen to form via the same initial growth stages as observed for both templated Ag and Pd PIED on glass substrates [142,153]. Initial nucleation occurs around the base of the microspheres with larger islands of Ag forming through lateral growth of the metal deposit. Interestingly, the pores formed in the metal deposit at the point of contact between the microspheres and the substrate can display an irregular size and shape, some being elongated and not wholly comparable to the highly circular pores observed on glass [142,153]. This is attributable to the morphology of the PVDF membrane, resulting in less uniform areas of contact between individual microspheres and the substrate. It is noticeable that fewer photocatalytically generated nucleation sites occur on membranes with a microsphere template in place, Fig. 72, than without, Fig. 70 (v) within a comparable time period; this is due to the microspheres reducing the intensity of UV light reaching the photocatalyst. Despite this, enough nucleation sites are still generated to allow auto-catalytic electroless deposition to occur and Ag islands to develop.

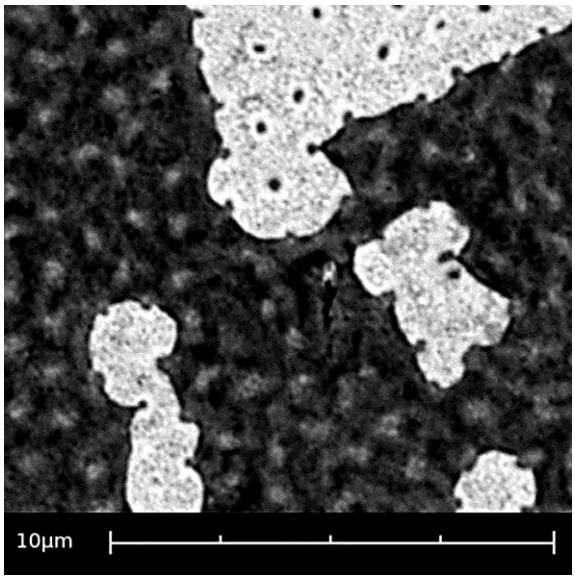

Fig. 72 Ag nucleation and island growth around 1 µm microsphere template on PVDF, t = 30 min

Lengthening the deposition period to 60 min enables further metallisation and the formation of a conductive Ag deposit, with a sheet resistivity of 0.5 Ω / sq over the entire templated area, Fig. 73. All deposited Ag remains adhered to the substrate upon removal of the microsphere template by toluene dissolution, with no delamination occurring during dissolution or drying stages. The underlying membrane also appears impervious to any detrimental effects from the microsphere removal process, with no shrinkage, melting or other deformation evident. Assessment of the adhesion strength between the deposited metal and substrate poses difficulties on flexible polymer membranes such as PVDF; the British Standard metal adhesion test BS EN ISO 2819:1995, the so-called “tape test”, is unsuitable as the method causes tearing of the membrane without properly examining the adhesion of the metal layer. However, the fact that both the sensitising TiO_2 film and the deposited metal are able to penetrate the porous structure of the PVDF membrane and provide a complex, inter-locking interface between the deposits and the substrate suggests that a strong adhesion should be formed.

The SEM analysis of Fig. 73 confirms that nanoporosity is successfully induced into Ag on a PVDF membrane support. The film is seen to be comprised of a monolayer of hemispherical voids in the metal matrix. While less ordered than previously observed in analogous samples on glass [142,153], regular porosity is present across the sample. The diameter of the

mouths to the hemispherical pores / voids is found to be 690 nm. From this, a metal layer depth of 138 nm can be calculated through geometric determination of the sagitta of the hemispherical void; as these measurements are found to be consistent across the sample area, it can be concluded that metal deposition has occurred in a homogenous manner with uniform thickness. Less consistent is the diameter of the sub-pores at the base of each hemispherical void which vary both in regularity of shape and size, ranging from <50 nm to 250 nm across the sample due to the aforementioned irregular contact area between microspheres and the PVDF surface, Fig. 73.

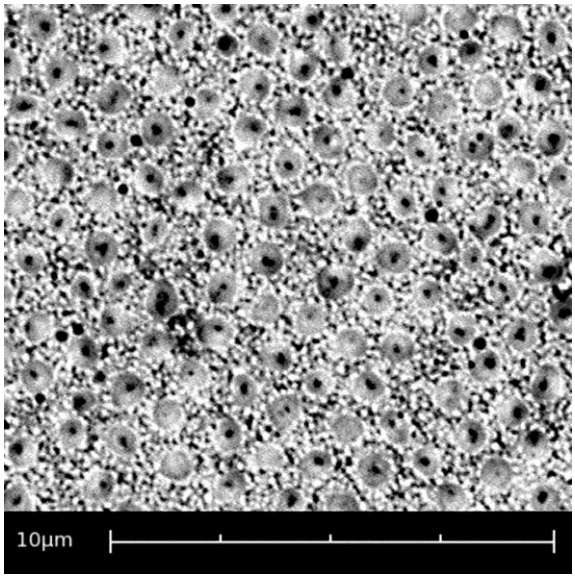

Fig. 73 Nanoporous Ag deposit on TiPE O502 dip-coated PVDF, t = 60 min

When the deposition time is further extended to 120 min, a thicker Ag layer is produced through continued autocatalytic deposition, as would be expected. An average hemispherical void mouth diameter of 950 nm can be measured, Fig. 74, equating to a metal layer thickness of approximately 344 nm. As metal growth continues upwards, the flat, essentially non-templated, regions of metal between pores decrease in size and the overall metal surface area is increased, providing potential advantages for a range of intended applications such as supercapacitors [46,47], fuel cells [45] and surface enhanced resonance Raman techniques [48]. For a monolayer of pores / voids, a deposition period capable of producing a metal layer of thickness equal to one half of the microsphere diameter is desirable for optimal surface area. As the Ag deposit produced in this instance is

less than the 500 nm radius of the microspheres used in the template, it is clear that deposition times greater than 120 min are required to produce a metal layer with optimal surface area.

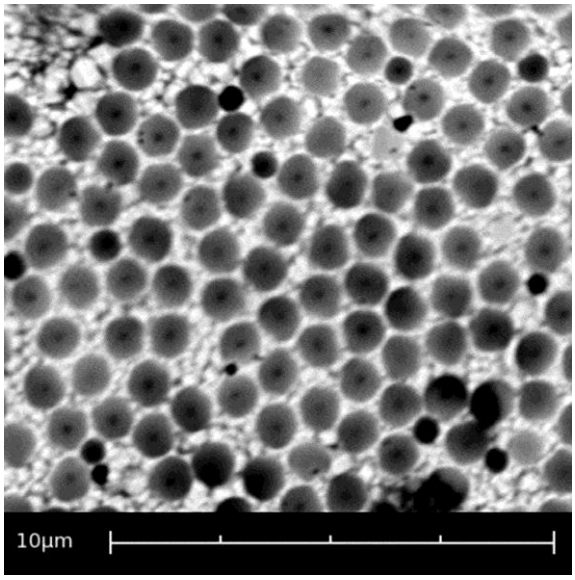

Fig. 74 Nanoporous Ag deposit on TiPE O502 dip-coated PVDF, t = 120 min

8.7 Conclusions

We have reported the photocatalytically initiated electroless deposition of metals with highly ordered nanometre scale porosity onto TiO_2 sensitised PVDF membranes. The use of a PVDF substrate presents a number of process problems such as the lack of facility to anneal the TiO_2 coating, disruption of the microsphere self-assembly process and reduced photocatalytic nucleation. Despite these difficulties, we demonstrate the formation of porous Ag metal films on membrane substrates, with thickness determined by the total deposition period. The initial nucleation and growth patterns of the produced metal films are seen to be similar to those previously described for the same, templated PIED process on glass substrates [142,153].

Potential applications of these membranes, such as analytical and process separations and electrode / solid electrolyte composites for fuel cells, require that the porosity induced in the deposited metal must penetrate through to the PVDF membrane. This is achieved as no metallisation occurs at the points of contact between microspheres and the membrane

surface. Metallised separation membranes may have potentially wide applications in analytical separation technology with work in our laboratories focusing on their application in electrochemically controllable and enhanced actinide separations in new nuclear reprocessing platforms. This will be the subject of the next paper in this series.

8.8 Acknowledgements

We thank the Royal Society of Chemistry UK, EPSRC (Award No EP/I002928/1) and The Lloyds Register Educational Trust (LRET) for financial support. The LRET is an independent charity working to achieve advances in transportation, science, engineering and technology education, training and research worldwide for the benefit of all.

CHAPTER 9

CONCLUSIONS

In this work, a novel photocatalytically initiated electroless deposition (PIED) process that allows for the photogeneration of coherent and conducting metal layers onto electrically insulating surfaces has been reported. PIED can be applied to many different material types, conducting and non-conducting, organic and inorganic, through their sensitisation with chemically stable semiconductor materials. TiO_2 has proven to be particularly applicable with a broad band gap in the near UV (so avoiding adventitious process initiation by ambient light) and a conduction band edge that is more negative than the redox potential of a range of metal ions. The deposition of metal directly onto the semiconductor obviates the need for other, more extensive sensitisation and surface preparation methods, such as the use of Sn–Pd activation catalysts, to provide reduced operational costs and an environmentally cleaner alternative to the traditional techniques of dielectric plating.

Through the use of PIED, conducting Ag, Pd and Ni layers have been generated on m-TiO_2 coated glass, quartz and PVDF substrates. Initial metal reduction is achieved photocatalytically to generate metal nuclei on the sensitised substrate. With an appropriate reductant present, these nuclei then provide sites on which subsequent or simultaneous auto-catalytic metal deposition can occur, resulting in the growth of a coherent metal layer. Metal layers formed through this combined process are smooth and reflective with conductivity achieved after a period of immersion in the electroless bath of as little as 15 min. Deposition occurs only onto the substrate areas which are both sensitised with TiO_2 and irradiated with ultra-band gap light making the process highly controllable and spatially selective.

Timed deposition studies demonstrate that PIED produces thicker, more coherent metal layers as immersion time increases via a combination of photo and auto-catalytic deposition processes. Metal layers of varying thickness can therefore be produced by simple control

over the immersion period. It is also shown that, after a period of photocatalytic initiation, PIED is able to continue through auto-catalytic deposition without the need for further irradiation. A conducting metal deposit can be formed following an initiating irradiation period of as little as 30 s. However, SEM studies indicate that the morphology and appearance of the deposited metal layer is strongly dependent upon the nucleation density arising during the primary photocatalytic stage of PIED as well as the rate of further growth by auto-catalytic deposition. High nucleation density and a slow auto-catalytic growth rate result in a smooth, reflective layer with small grain sizes. Conversely, a lower nucleation density combined with fast auto-catalytic growth results in a more coarsely granular metal deposit with a less reflective surface. Therefore, a photocatalytic initiation period of at least 5 min yields significant improvements in the deposited metal layer quality.

With the addition of a microparticle template, the deposited metal can also be induced with nanoporosity with a highly regular and predictable nanostructure. Accordingly, the PIED of metals with highly ordered nanometre scale porosity onto TiO_2 sensitised insulating substrates has been presented, an achievement which represents the first reported use of electroless deposition with a controllable onset in the creation of ordered nanoporous metals on any kind of support, be it insulator, semiconductor or metal.

The pore diameter of the induced nanoporosity is conveniently controlled via the component particle diameter of the microsphere template while coverage is determined by the spatial application of the template array. Resultant metal deposits can be induced with 2-dimensional monolayer nanoporosity (in thin metal layers) or 3-dimensional multi-layer nanoporosity (in thicker metal layers), each with highly regular and predictable order. The application of PIED with induced porosity to non-temperature resistant materials such as PVDF presents a number of process problems such as the lack of facility to anneal the TiO_2 coating, disruption of the microsphere self-assembly process and reduced photocatalytic nucleation. Despite these difficulties, the formation of porous metal films on membrane substrates, with thickness determined by the total deposition period has been achieved.

PIED therefore represents a flexible yet controllable method for the fabrication of nano-structured metal films with predictable dimensions on the surface of otherwise electrically insulating substrate materials. The fabrication of nanoporous metal by this novel method adds a conductive and permeable metallic structure of high surface area to an otherwise electrically insulating surface. Furthermore, opposing sides of a substrate can be metallised independent conductivity, *i.e.* without electrical connection between each deposited metal layer. Such metallised insulating materials have potentially wide applications in membrane and analytical separation technology, desalination, electrode/solid electrolyte composites for fuel cells, energy storage and sensors – especially surface enhanced resonance Raman spectroscopy (SERRS).

As the primary interest of this project, the use of metallised ion-selective membranes in analytical separation technology is the subject of ongoing work in these laboratories. As part of MBASE: The Molecular Basis of Advanced Nuclear Fuel Separations (EPSRC Award No EP/I002928/1), the focus of this work is on the application of metallised membranes in electrochemically controllable and enhanced actinide separations in new nuclear reprocessing platforms and will form the subject of future publications in this series.

FURTHER WORK

The work presented in this thesis has focussed on the development of a new fabrication technique for the production of nanoporous metallised polymer membranes; something which has been achieved through the novel process of Photocatalytically Initiated Electroless Deposition (PIED) throughout a PS microsphere template on TiO_2 sensitised substrates. As this represents a new process development, scope for further work can be found in the refinement and expansion of the involved production techniques. Specifically, further investigation could be made into the optimal composition of electroless plating baths in order to maximise bath stability and metal yield, particularly in the case of Pd, while PIED may also be applied to the deposition of further metals, such as Pt [156,157]. Different template materials, such as silica microspheres [158], may be investigated to potentially eliminate the difficulties caused by the surface-bound charge of PS microspheres as described in section 7.7.3 while alternative microsphere array formation methods could be investigated for the purpose of arranging microsphere templates over larger surface areas and hence allowing the production of larger area nanoporous metal films. Potentially suitable methods for this may include Langmuir-Blodgett deposition, in which microspheres are arranged in a close packed monolayer on a liquid surface and subsequently transferred onto a solid substrate, as demonstrated in the formation of highly ordered hexagonal arrays of latex spheres on highly ordered pyrolytic graphite (HOPG) [57] and the fabrication of large area polystyrene colloidal crystal monolayers [58]; or vertical deposition processes, in which spheres are transferred to a solid substrate from colloidal solution via vertical extraction of the substrate [159] or lowering of the solution surface [160,161]. Furthermore, variation of the microsphere template structure holds the potential to generate more complex nanostructures within the deposited metal. While the work in this thesis demonstrates the use of microspheres of various diameters to control pore dimensions across individual metal films, it is also possible to combine multiple microsphere sizes within a single template, the structure of which would be directly translated into the porosity of the a metal film deposited around it. Such a template may consist of several microsphere monolayers, each comprising of spheres of a

different diameter, to produce complex multi-layer porosity [44]; or may be in the form of a binary colloidal crystal in which significantly smaller spheres are arranged within the interstitial spaces of a hexagonally packed array of larger spheres [162,163]. In each case, the resultant metal film would have a greater complexity to its porosity and further increase accessible surface area.

In addition to enhancements to the production process, further work may also be carried out to investigate various properties of the nanoporous metal films generated using PIED and how the deposition of such films may affect the properties of various substrate materials. The mechanical strengths of metal films of varied thicknesses and pore dimensions could be assessed through compressive and tensile stress measurements [164,165] and compared to the analogous strengths of non-metallised substrate materials. Additionally, the accessible surface area of the deposited metal films could be determined through simple electrochemical methods or through Brunauer-Emmett-Teller (BET) Theory [166] while porosimetry may be used to quantify the total pore volume.

A number of further work studies could be performed with a view to various potential applications of the developed nanoporous metal films, in particular the use of nanoporous metal films as *in-situ* electrodes on separation membranes. Work in this area is currently underway as part of MBASE: The Molecular Basis of Advanced Nuclear Fuel Separations (EPSRC Award No EP/I002928/1) on the use of nanoporous, metallised ion separation membranes (ISMs) for electrochemically controllable and enhanced actinide separations in new nuclear reprocessing platforms.

Nanoporous metallised ISMs are to be combined with candidate ligands, such as $CyMe_4$-BTBP as developed by MBase collaborators at Reading University [167-170], which show high selectivity towards the complexation of trivalent actinides though suffer from subsequently slow metal ion extraction rates [171]. Ligands may be loaded onto metallised membranes in an appropriate solvent to form a supported liquid membrane (SLM), or through direct chemical attachment to the membrane surface before being mounted

between opposing extraction and stripping process flows in a flow-through dialyser. The nanoporous metal films on the ISM may then act as electrodes, allowing electrochemical manipulation of the valence states of both target ions at the feed-side membrane / solution interface, enhancing uptake by the ligand, and of on-membrane complexed ions at the strip-side to drive de-complexation from the ligand and expulsion from the membrane, potentially offering enhanced extraction selectivity over a ligand only [172] or non-electrochemically controlled SLM systems [173].

Further electrochemical applications of metal films generated through PIED can be found in the miniaturisation of reference electrodes. While the miniaturisation of electrochemical sensors has advance greatly in recent decades, the comparable down-sizing of reliable reference electrodes is often hindered by the need for bulky electrolyte reservoirs and liquid junctions. However, the fabrication of miniature Ag / AgCl-based reference electrodes has been previously reported with some success [174-178]. Given that conducting Ag films can be readily deposited onto electrically insulating substrates using PIED and that the deposited metal may be easily chlorinated by immersion in a saturated KCl solution, the fabrication of Ag / AgCl reference electrodes as a component part of small-scale modular electrochemical sensors is a potentially useful area for further study. As such, work on the integration of a concentric ring Ag / AgCl reference electrode into a novel Graphene Ring Micro Electrode (GRiME) has already been undertaken within the Lancaster research group [179]. In addition, nanoporous metal films generated through PIED may be useful for electrochemical sensing applications given their high surface area, as an example, nanoporous Pt or Au electrodes can be used for H_2O_2 detection offering enhanced sensitivity and selectivity over existing methods [180,181].

Nanoporous electrode materials are also critical components within various electrochemical energy solutions such as fuel cells and energy storage devices. PIED generated, nanoporous metal films can be deposited onto polymers and may be suitable for use in polymer electrolyte membrane fuel cells [45], while porous Pd / Pd alloy films could be investigated for use in H_2 separation, an area where similar films are already of

significance [182]. Similarly, nanoporous metal is highly applicable to capacitors and batteries; in particular, high surface area 3-dimensional structures similar to those generated using PIED have already been shown to offer the potential to produce lithium ion batteries of considerably higher capacity that those currently available [183,184]. Given the ever increasing demand for improved battery technology for powerful mobile devices, this seems to be an area of considerable potential and interest.

Beyond electrochemical applications, porous metal films are regularly associated with surface-enhanced Raman techniques, an area to which Ag and Au films of ordered nanoporosity are particularly suited [49,185-189], and also display interactions with incident light. As a result, PIED may be applicable to the fabrication of plasmonic nanostructures [190], photonic crystals [191] and even holography given sufficient manipulation of the arrangement of pores and hence the iridescent pattern observed within nanoporous metal deposits.

Finally, nanoporous Ag films may be investigated for use in biocidal applications. The antimicrobial properties of Ag are well known [192] and this effect may be enhanced by a material with high surface area, such as that of nanoporous Ag films produced by PIED. However, given that as part of the PIED process, a TiO_2 film remains present beneath the deposited metal film, photocatalysis may also be used to further contribute to disinfection [193]. Furthermore, an additional layer of mesoporous TiO_2 can be deposited on top of the Ag film to create a triple-layered and porous m-TiO_2 – Ag – m-TiO_2 film for photocatalytically enhanced antimicrobial treatments.

"Yes, that sequence of words I said made perfect sense."

Prof. Hubert J. Farnsworth

PRESENTATION SUMMARY

ORAL PRESENTATIONS

"Photocatalytic Initiation of Electroless Deposition", S.Galea, F.Andrieux, M.A.Bromley, C.Boxall, P.S.Goodall, S.Woodbury, 2nd Meeting of the UK / EPSRC Photocatalysis Network, University of Strathclyde, Glasgow, 9th Jan, 2008

"The Development of Metallised Membranes for Analytical Separation Purposes", M.A.Bromely, S.Galea, C.Boxall, P.S.Goodall, S.Woodbury, Analytical Research Forum (ARF08), University of Hull, 21st – 23rd July 2008

"The Development of Metallised Membranes for Radioanalytical Separation Processes", M.A.Bromely, S.Galea, C.Boxall, P.S.Goodall, S.Woodbury, Universities' Nuclear Technology Forum, University of Cambridge, 18th – 20th March 2009

"The Development of Metallised Membranes for Analytical Separations", M.A.Bromely, S.Galea, C.Boxall, P.S.Goodall, S.Woodbury, Emerging Analytical Professionals 2009, Carnegie Conference Centre, Dunfermline, 8th – 10th May 2009

"The Development of Metallised Membranes for Analytical Separations", M.A.Bromely, S.Galea, C.Boxall, P.S.Goodall, S.Woodbury, 3rd International Conference on Semiconductor Photochemistry (SP3), University of Strathclyde, 12th – 16th April 2010

"MBase WP2: Innovative Approaches to Separation", M.A.Bromley, C.Boxall, MBase Consortium Meetings, University of Manchester, 7th April 2011; Reading University, 4th October 2011; Lancaster University, 25th May 2012; Imperial College London, 6th November 2012

"The Nanoporous Metallisation of Insulating Substrates through Semiconductor Photocatalysis", M.A.Bromley, C.Boxall, 223rd ECS Meeting, Toronto, ON, Canada, 12th – 17th May 2013

POSTER PRESENTATIONS

"Photocatalytic Initiation of Electroless Deposition", M.A.Bromley, S.Galea C.Boxall, UCLan Faculty Science & Technology Annual Research day, 18th June 2008

"The Development of Metallised Membranes for Analytical Separations Purposes", M.A.Bromely, S.Galea, C.Boxall, Analytical Winter Workshop, Warwick University, 1st – 5th December 2008

"The Metallisation of Insulating Substrates through Photocatalytically Initiated Electroless Deposition", M.A.Bromley, S.Galea, C.Boxall, UCLan Faculty Science & Technology Annual Research day, 17th June 2009

"The Development of Metallised Membranes for Radioanalytical Separation Processes", M.A.Bromely, S.Galea, C.Boxall, Actinides 2009, San Francisco, California, USA, 12th – 17th July 2009

"The Nanoporous Metallisation of Insulating Substrates through Photocatalytically Initiated Electroless Deposition", M.A.Bromley, S.Galea, C.Boxall, Analytical Research Forum (ARF09), University of Kent, 13th – 15th July 2009

"The Development of Metallised Membranes for Analytical Separation Purposes", M.A.Bromely, C.Boxall, Sci-Tech Christmas Conference 2009, Lancaster University, 15th December 2009

"The Development of Metallised Membranes for Analytical Separations", M.A.Bromely, C.Boxall, Analytical Research Forum (ARF10), Loughborough University, 26th – 28th July 2010

"The Development of Nanoporous Metallised Membranes for Analytical Separations", M.A.Bromely, C.Boxall, Sci-Tech Christmas Conference 2010, Lancaster University, 14th December 2010

"The Development of Metallised Membranes for Radioanalytical Separation Processes", M.A.Bromely, C.Boxall, Energy Lancaster Launch Event, Lancaster University, 10th March 2010

"The Development of Nanoporous Metallised Membranes for Analytical Separations", M.A.Bromely, C.Boxall, Analytical Research Forum (ARF11), University of Manchester, 25th – 27th July 2011

"The Nanoporous Metallisation of Insulating Substrates through Semiconductor Photocatalysis", M.A.Bromley, C.Boxall, MRS Fall Meeting, Hynes Convention Centre, Boston, 28th November – 2nd December 2011

"The Development of Metallised Membranes for Radioanalytical Separation Processes", M.A.Bromely, C.Boxall, IChemE Nuclear Fuel Cycle Conference, Manchester Conference Centre, 23rd – 25th April 2012

BIBLIOGRAPHY

[1] E.P. Horwitz, M.L. Dietz, R. Chiarizia, H. Diamond, S.L. Maxwell, M.R. Nelson, Separation and preconcentration of actinides by extraction chromatography using a supported liquid anion exchanger: application to the characterization of high-level nuclear waste solutions, *Analytica Chimica Acta*, 310, 1, (1995), 63-78

[2] E.P. Horwitz, M.L. Dietz, R. Chiarizia, H. Diamond, A.M. Essling, D. Graczyk, Separation and preconcentration of uranium from acidic media by extraction chromatography, *Analytica Chimica Acta*, 266, 1, (1992), 25-37

[3] A.G. Adriaens, J.D. Fassett, W.R. Kelly, D.S. Simons, F.C. Adams, Determination of uranium and thorium concentrations in soils: a comparison of isotope dilution-secondary ion mass spectrometry and isotope dilution-thermal ionization mass spectrometry, *Analytical Chemistry*, 64, 23, (1992), 2945-2950

[4] J.R. Cadieux, S.H. Reboul, *Radioactivity and Radiochemistry*, 7, (1996), 30

[5] J.H. Kaye, R.S. Strebin, R.D. Orr, Rapid, quantitative analysis of americium, curium and plutonium isotopes in Hanford samples using extraction chromatography and precipitation plating, *Journal of Radioanalytical and Nuclear Chemistry*, 194, 1, (1995), 191-196

[6] M. Pourbaix, Atlas of Electrochemical Equilibria in Aqueous Solutions, Pergamon Press, Oxford, (1966)

[7] G.O. Mallory, Chemical deposition of metallic films from aqueous solution, in, Electroless Plating - Fundamentals and Applications, (1990), 511-517

[8] B. Abner, G.E. Riddell, Nickel plating by chemical reduction, United States Patent 2,532,283, (1950)

[9] M. Paunovic, M. Schlesinger, Electroless Deposition, in, Fundamentals of Electrochemical Deposition, Second Edition, (2006), 139-167

[10] G.O. Mallory, Plating on plastics, in, Electroless Plating - Fundamentals and Applications, (1990), 377-399

[11] C.R. Shipley, Method of electroless deposition on a substrate and catalyst solution therefor, United States Patent 3,011,920, (1961)

[12] A. Mills, S. Le Hunte, An overview of semiconductor photocatalysis, *Journal of Photochemistry and Photobiology A: Chemistry*, 108, 1, (1997), 1-35

[13] H. Chun, J. Kim, S.m. Yoon, C. Kim, Physical properties and photocatalytic performance of TiO_2 coated stainless steel plate, *Korean Journal of Chemical Engineering*, 18, 6, (2001), 908-913

[14] J.W.M. Jacobs, Photochemical nucleation and growth of palladium on titanium dioxide films studied with electron microscopy and quantitative analytical techniques, *The Journal of Physical Chemistry*, 90, 24, (1986), 6507-6517

[15] V. Vamathevan, R. Amal, D. Beydoun, G. Low, S. McEvoy, Photocatalytic oxidation of organics in water using pure and silver-modified titanium dioxide particles, *Journal of Photochemistry and Photobiology A: Chemistry*, 148, 1-3, (2002), 233-245

[16] M.I. Litter, Heterogeneous photocatalysis: Transition metal ions in photocatalytic systems, *Applied Catalysis B: Environmental*, 23, 2-3, (1999), 89-114

[17] H. Jonker, C.J.G. Janssen, C.J. Dippel, Thijssen.Tp, L. Postma, Physical development recording systems .4. Pd photoplating, *Photographic Science and Engineering*, 13, 2, (1969), 45

[18] E. Berman, Reduction reactions with irradiated photoconductors, *Photographic Science and Engineering*, 13, 2, (1969), 50

[19] K. Tanaka, K. Harada, S. Murata, Photocatalytic deposition of metal ions onto TiO_2 powder, *Solar Energy*, 36, 2, (1986), 159-161

[20] J.-M. Herrmann, J. Disdier, P. Pichat, Photocatalytic deposition of silver on powder titania: Consequences for the recovery of silver, *Journal of Catalysis*, 113, 1, (1988), 72-81

[21] T. Kanki, H. Yoneda, N. Sano, A. Toyoda, C. Nagai, Photocatalytic reduction and deposition of metallic ions in aqueous phase, *Chemical Engineering Journal*, 97, 1, (2004), 77-81

[22] J.Y. Jimmy C. Yu, Wingkei Ho, Zitao Jiang, Lizhi Zhang, Effects of F-doping on the photocatalytic activity and microstructures of nanocrystalline TiO_2 powders, *Chemistry of Materials*, 14, 9, (2002), 3808-3816

[23] Y. Yang, X.-j. Li, J.-t. Chen, L.-y. Wang, Effect of doping mode on the photocatalytic activities of Mo/TiO_2, *Journal of Photochemistry and Photobiology A: Chemistry*, 163, 3, (2004), 517-522

[24] T. Sakata, T. Kawai, K. Hashimoto, Photochemical diode model of Pt-TiO_2 particle and its photocatalytic activity, *Chemical Physics Letters*, 88, 1, (1982), 50-54

[25] S. Sakthivel, M.V. Shankar, M. Palanichamy, B. Arabindoo, D.W. Bahnemann, V. Murugesan, Enhancement of photocatalytic activity by metal deposition: characterisation and photonic efficiency of Pt, Au and Pd deposited on TiO_2 catalyst, *Water Research*, 38, 13, (2004), 3001-3008

[26] C.-C. Chan, C.-C. Chang, W.-C. Hsu, S.-K. Wang, J. Lin, Photocatalytic activities of Pd-loaded mesoporous TiO_2 thin films, *Chemical Engineering Journal*, 152, 2-3, (2009), 492-497

[27] C.H. Noh, J.Y. Kim, O.C. Hwang, S.H. Cho, K.Y. Song, T.V. Byk, V.G. Sokolov, T.V. Gaevskaya, J.B. Kim, Photochemical patterning of Pd with amorphous TiO_2 layer and selective electroless deposition of Ni, *Electrochemical and Solid State Letters*, 8, 2, (2005), C36-C38

[28] C.H. Noh, H.J. Son, J.Y. Kim, O.C. Hwang, K.Y. Song, T.V. Byk, V.G. Sokolov, J.B. Kim, A novel patterning method of low-resistivity metals, *Chemistry Letters*, 34, 1, (2005), 82-83

[29] T.V. Byk, V.G. Sokolov, T.V. Gaevskaya, E.V. Skorb, D.V. Sviridov, C.H. Noh, K.Y. Song, Y.N. Kwon, S.H. Cho, Photochemical selective deposition of nickel using a TiO_2-Pd^{2+} layer, *Journal of Photochemistry and Photobiology A: Chemistry*, 193, 1, (2008), 56-64

[30] E. Stathatos, P. Lianos, P. Falaras, A. Siokou, Photocatalytically deposited silver nanoparticles on mesoporous TiO_2 films, *Langmuir*, 16, 5, (2000), 2398-2400

[31] L.Q. Wu, N. Xu, J. Shi, Novel method for preparing palladium membranes by photocatalytic deposition, *AIChE Journal*, 46, (2000), 1075-1083

[32] L.Q. Wu, N. Xu, J. Shi, Preparation of a palladium composite membrane by an improved electroless plating technique, *Industrial & Engineering Chemistry Research*, 39, 2, (2000), 342-348

[33] X. Li, Y. Fan, W. Jin, Y. Huang, N. Xu, J. Shi, Effect of EDTA on preparation of Pd membranes by photocatalytic deposition, *Desalination*, 192, (2006), 117-124

[34] X. Li, Y. Fan, W. Jin, Y. Huang, N. Xu, Improved photocatalytic deposition of palladium membranes, *Journal of Membrane Science*, 282, (2006), 1-6

[35] X. Li, T.M. Liu, Y.Q. Fan, N.P. Xu, Preparation of composite palladium-silver alloy membranes by photocatalytic deposition, *Thin Solid Films*, 516, 21, (2008), 7282-7285

[36] R. Zhao, R. Ding, S. Yuan, W. Jiang, B. Liang, Palladium membrane on TiO_2 nanotube arrays-covered titanium surface by combination of photocatalytic deposition and modified electroless plating processes and its hydrogen permeability, *International Journal of Hydrogen Energy*, 36, 1, (2011), 1066-1073

[37] S.-E. Nam, K.-H. Lee, Hydrogen separation by Pd alloy composite membranes: Introduction of diffusion barrier, *Journal of Membrane Science*, 192, 1-2, (2001), 177-185

[38] F. Roa, J.D. Way, R.L. McCormick, S.N. Paglieri, Preparation and characterization of Pd-Cu composite membranes for hydrogen separation, *Chemical Engineering Journal*, 93, 1, (2003), 11-22

[39] S.N. Paglieri, J.D. Way, Innovations in palladium membrane research, *Separation and Purification Methods*, 31, 1, (2002), 1-169

[40] T. Sumida, Y. Wada, T. Kitamura, S. Yanagida, Construction of Stacked Opaline Films and Electrochemical Deposition of Ordered Macroporous Nickel, *Langmuir*, 18, 10, (2002), 3886-3894

[41] M.E. Abdelsalam, P.N. Bartlett, J.J. Baumberg, S. Coyle, Preparation of Arrays of Isolated Spherical Cavities by Self-Assembly of Polystyrene Spheres on Self-

Assembled Pre-patterned Macroporous Films, *Advanced Materials*, 16, 1, (2004), 90-93

[42] M.A. Ghanem, P.N. Bartlett, P. de Groot, A. Zhukov, A double templated electrodeposition method for the fabrication of arrays of metal nanodots, *Electrochemistry Communications*, 6, 5, (2004), 447-453

[43] J. Hu, M. Abdelsalam, P. Bartlett, R. Cole, Y. Sugawara, J. Baumberg, S. Mahajan, G. Denuault, Electrodeposition of highly ordered macroporous iridium oxide through self-assembled colloidal templates, *Journal of Materials Chemistry*, 19, 23, (2009), 3855-3858

[44] M. Heim, S. Reculusa, S. Ravaine, A. Kuhn, Engineering of Complex Macroporous Materials Through Controlled Electrodeposition in Colloidal Superstructures, *Advanced Functional Materials*, 22, 3, (2012), 538-545

[45] W. Yuan, Y. Tang, X. Yang, Z. Wan, Porous metal materials for polymer electrolyte membrane fuel cells – A review, *Applied Energy*, 94, 0, (2012), 309-329

[46] G.S. Attard, J.M. Elliott, P.N. Bartlett, A. Whitehead, J.R. Owen, Nanostructured materials for batteries, *Macromolecular Symposia*, 156, 1, (2000), 179-186

[47] V.D. Patake, S.S. Joshi, C.D. Lokhande, O.-S. Joo, Electrodeposited porous and amorphous copper oxide film for application in supercapacitor, *Materials Chemistry and Physics*, 114, 1, (2009), 6-9

[48] W.E. Smith, C. Rodger, Surface-Enhanced Raman Scattering (SERS), Applications, in: J. Lindon (Ed.), Encyclopedia of Spectroscopy and Spectrometry (Second Edition), Academic Press, Oxford, (1999), 2822-2827

[49] S. Mahajan, J.J. Baumberg, A.E. Russell, P.N. Bartlett, Reproducible SERRS from structured gold surfaces, *Physical Chemistry Chemical Physics*, 9, 45, (2007), 6016-6020

[50] S.-K. Ryi, J.-S. Park, S.-H. Choi, S.-H. Cho, S.-H. Kim, Fabrication and characterization of metal porous membrane made of Ni powder for hydrogen separation, *Separation and Purification Technology*, 47, 3, (2006), 148-155

[51] G.S. Attard, P.N. Bartlett, Mesoporous platinum films from lyotropic liquid crystalline phases, *Science*, 278, 5339, (1997), 838

[52] P.N. Bartlett, J.R. Owen, G.S. Attard, J.M. Elliott, Porous film and method of preparation thereof, United Kingdom Patent Application WO/1999/000536, (1999)

[53] G.S. Attard, C. Goeltner, Porous metal and method of preparation thereof, United States Patent 6,203,925, (2001)

[54] P.N. Bartlett, P.R. Birkin, M.A. Ghanem, Electrochemical deposition of macroporous platinum, palladium and cobalt films using polystyrene latex sphere templates, *Chemical Communications*, (2000), 1671-1672

[55] N.D. Denkov, O.D. Velev, P.A. Kralchevsky, I.B. Ivanov, Mechanism of formation of two-dimentional crystals from latex particles on substrates, *Langmuir*, 8, (1992), 3183-3190

[56] N.D. Denkov, P.A. Kralchevsky, I.B. Ivanov, Lateral capillary forces and two-dimensional arrays of colloid particles and protein molecules, *Journal of Dispersion Science and Technology*, 18, (1997), 577-591

[57] M. Marquez, B.P. Grady, The use of surface tension to predict the formation of 2D arrays of latex spheres formed via the Langmuir-Blodgett-like technique, *Langmuir*, 20 (2004), 10998-11004

[58] W.D. Ruan, Z.C. Lu, N. Ji, C.X. Wang, B. Zhao, J.H. Zhang, Facile fabrication of large area polystyrene colloidal crystal monolayer via surfactant-free Langmuir-Blodgett technique, *Chem.Res.Chinese U.*, 23, 6, (2007), 712-714

[59] J.C. Yu, J. Yu, W. Ho, J. Zhao, Light-induced super-hydrophilicity and photocatalytic activity of mesoporous TiO_2 thin films, *Journal of Photochemistry and Photobiology A: Chemistry*, 148, (2002), 331-339

[60] S. Sato, J.M. White, Photodecomposition of water over Pt/TiO_2 catalysts, *Chemical Physics Letters*, 72, 1, (1980), 83-86

[61] Y.A. Yang, Y.B. Wei, B.H. Loo, J.N. Yao, Electroless copper plating on a glass substrate coated with ZnO film under UV illumination, *Journal of Electroanalytical Chemistry*, 462, 2, (1999), 259-263

[62] K. Akamatsu, A. Kimura, H. Matsubara, S. Ikeda, H. Nawafune, Site-selective direct photochemical deposition of copper on glass substrates using TiO_2 nanocrystals, *Langmuir*, 21, 18, (2005), 8099-8102

[63] S. Bruckenstein, M. Shay, An *in situ* weighing study of the mechanism for the formation of the adsorbed oxygen monolayer at a gold electrode, *Journal of Electroanalytical Chemistry*, 189, 1, (1985), 131-136

[64] Z.X. Shu, S. Bruckenstein, Iodine adsorption studies at platinum, *Journal of Electroanalytical Chemistry*, 317, 1-2, (1991), 263-277

[65] A.J. Bard, L.R. Faulkner, Electrochemical Methods: Fundamentals and Applications, Wiley, (2001)

[66] R. Beranek, H. Tsuchiya, T. Sugishima, J.M. Macak, L. Taveira, S. Fujimoto, H. Kisch, P. Schmuki, Enhancement and limits of the photoelectrochemical response from anodic TiO_2 nanotubes, *Applied Physics Letters*, 87, 24, (2005), 243114-243113

[67] A. Kubota, N. Koura, *Journal of the Metal Finishing Society of Japan*, 37, (1986), 131

[68] H.C. Choi, Y.M. Jung, S.B. Kim, Characterization of raman spectra of size-selected TiO_2 nanoparticles by two-dimensional correlation spectroscopy, *Bulletin of the Korean Chemical Society*, 25, 3, (2004), 426

[69] T. Ohsaka, Temperature dependence of the raman spectrum in anatase TiO_2, *Journal of the Physical Society of Japan*, 48, 5, (1980), 1661-1668

[70] S.P.S. Porto, P.A. Fleury, T.C. Damen, Raman spectra of TiO_2, MgF_2, ZnF_2, FeF_2, and MnF_2, *Physical Review*, 154, 2, (1967), 522

[71] H.I. Kazuhito Hashimoto, Akira Fujishima, TiO_2 photocatalysis: A historical overview and future prospects, *AAPPS Bulletin*, 17, 6, (2007), 12-28

[72] T. Shibata, H. Irie, K. Hashimoto, Enhancement of photoinduced highly hydrophilic conversion on TiO_2 thin films by introducing tensile stress, *Journal of Physical Chemistry B*, 107, 39, (2003), 10696-10698

[73] M. Miyauchi, A. Nakajima, K. Hashimoto, T. Watanabe, A highly hydrophilic thin film under 1 μW/cm^2 UV illumination, *Advanced Materials*, 12, 24, (2000), 1923

[74] I. Nakamura, N. Negishi, S. Kutsuna, T. Ihara, S. Sugihara, E. Takeuchi, Role of oxygen vacancy in the plasma-treated TiO_2 photocatalyst with visible light activity for NO removal, *Journal of Molecular Catalysis a-Chemical*, 161, 1-2, (2000), 205-212

[75] R. Asahi, T. Morikawa, T. Ohwaki, K. Aoki, Y. Taga, Visible-light photocatalysis in nitrogen-doped titanium oxides, *Science*, 293, 5528, (2001), 269-271

[76] H. Irie, Y. Watanabe, K. Hashimoto, Nitrogen-concentration dependence on photocatalytic activity of TiO_2-xNx powders, *Journal of Physical Chemistry B*, 107, 23, (2003), 5483-5486

[77] H. Irie, S. Washizuka, N. Yoshino, K. Hashimoto, Visible-light induced hydrophilicity on nitrogen-substituted titanium dioxide films, *Chemical Communications*, 11, (2003), 1298-1299

[78] S. Sakthivel, H. Kisch, Photocatalytic and photoelectrochemical properties of nitrogen-doped titanium dioxide, *Chemphyschem*, 4, 5, (2003), 487-490

[79] S. Sakthivel, H. Kisch, Daylight photocatalysis by carbon-modified titanium dioxide, *Angewandte Chemie-International Edition*, 42, 40, (2003), 4908-4911

[80] M.R. Hoffmann, S.T. Martin, W. Choi, D.W. Bahnemann, Environmental applications of semiconductor ohotocatalysis, *Chemical Reviews*, 95, 1, (1995), 69-96

[81] A. Mills, R.H. Davies, D. Worsley, Water purification by semiconductor photocatalysis, *Chemical Society Reviews*, 22, 6, (1993), 417-425

[82] B. Barni, A. Cavicchioli, E. Riva, L. Zanoni, F. Bignoli, I.R. Bellobono, F. Gianturco, A. De Giorgi, H. Muntau, L. Montanarella, S. Facchetti, L. Castellano, Pilot-plant-scale photodegradation of phenol in aqueous solution by photocatalytic membranes

immobilizing titanium dioxide (PHOTOPERM® process), *Chemosphere*, 30, 10, (1995), 1861-1874

[83] C. Minero, E. Pelizzetti, S. Malato, J. Blanco, Large solar plant photocatalytic water decontamination: Degradation of atrazine, *Solar Energy*, 56, 5, (1996), 411-419

[84] D.F. Ollis, E. Pelizzetti, N. Serpone, Photocatalysed destruction of water contaminants, *Environmental Science & Technology*, 25, 9, (1991), 1522-1529

[85] D. Bahnemann, Photocatalytic water treatment: solar energy applications, *Solar Energy*, 77, 5, (2004), 445-459

[86] J. Blanco-Galvez, P. Fernandez-Ibanez, S. Malato-Rodriguez, Solar photocatalytic detoxification and disinfection of water: Recent overview, *Journal of Solar Energy Engineering-Transactions of the Asme*, 129, 1, (2007), 4-15

[87] A. Mills, A. Belghazi, D. Rodman, Bromate removal from drinking water by semiconductor photocatalysis, *Water Research*, 30, 9, (1996), 1973-1978

[88] M. Kositzi, A. Antoniadis, I. Poulios, I. Kiridis, S. Malato, Solar photocatalytic treatment of simulated dyestuff effluents, *Solar Energy*, 77, 5, (2004), 591-600

[89] I. Oller, W. Gernjak, M.I. Maldonado, L.A. Perez-Estrada, J.A. Sanchez-Perez, S. Malato, Solar photocatalytic degradation of some hazardous water-soluble pesticides at pilot-plant scale, *Journal of Hazardous Materials*, 138, 3, (2006), 507-517

[90] M.H. Perez, G. Penuela, M.I. Maldonado, O. Malato, P. Fernandez-Ibanez, I. Oller, W. Gernjak, S. Malato, Degradation of pesticides in water using solar advanced oxidation processes, *Applied Catalysis B-Environmental*, 64, 3-4, (2006), 272-281

[91] M. Kositzi, I. Poulios, S. Malato, J. Caceres, A. Campos, Solar photocatalytic treatment of synthetic municipal wastewater, *Water Research*, 38, 5, (2004), 1147-1154

[92] A. Fujishima, K. Hashimoto, T. Watanabe, TiO_2 Photocatalysis: Fundamentals and Applications, BKC Inc., Tokyo, (1999)

[93] A. Fujishima, X.T. Zhang, Titanium dioxide photocatalysis: present situation and future approaches, *Comptes Rendus Chimie*, 9, 5-6, (2006), 750-760

[94] W.-K. Jo, K.-H. Park, Heterogeneous photocatalysis of aromatic and chlorinated volatile organic compounds (VOCs) for non-occupational indoor air application, *Chemosphere*, 57, 7, (2004), 555-565

[95] P. Pichat, J. Disdier, C. Hoang-Van, D. Mas, G. Goutailler, C. Gaysse, Purification/deodorization of indoor air and gaseous effluents by TiO_2 photocatalysis, *Catalysis Today*, 63, 2-4, (2000), 363-369

[96] C.H. Ao, S.C. Lee, Enhancement effect of TiO_2 immobilized on activated carbon filter for the photodegradation of pollutants at typical indoor air level, *Applied Catalysis B-Environmental*, 44, 3, (2003), 191-205

[97] C.H. Ao, S.C. Lee, Photocatalyst TiO_2 loaded on an activated carbon installed in air cleaner for air purification, China Environmental Science Press, Beijing, (2004)

[98] I.R. Bellobono, A. Carrara, B. Barni, A. Gazzotti, Laboratory- and pilot-plant-scale photodegradation of chloroaliphatics in aqueous solution by photocatalytic membranes immobilizing titanium dioxide, *Journal of Photochemistry and Photobiology A: Chemistry*, 84, 1, (1994), 83-90

[99] O. Legrini, E. Oliveros, A.M. Braun, Photochemical processes for water treatment, *Chemical Reviews*, 93, 2, (1993), 671-698

[100] C.A. MartÍn, M.A. Baltanás, A.E. Cassano, Photocatalytic Reactors .3. Kinetics of the decomposition of chloroform including absorbed radiation effects, *Environmental Science & Technology*, 30, 7, (1996), 2355-2364

[101] J. Blanco, P. Avila, A. Bahamonde, E. Alvarez, B. Sánchez, M. Romero, Photocatalytic destruction of toluene and xylene at gas phase on a titania based monolithic catalyst, *Catalysis Today*, 29, 1-4, (1996), 437-442

[102] Y. Mao, A. Bakac, Photocatalytic oxidation of aromatic hydrocarbons, *Inorganic Chemistry*, 35, 13, (1996), 3925-3930

[103] N.N. Rao, S. Dube, Photocatalytic degradation of mixed surfactants and some commercial soap/detergent products using suspended TiO_2 catalysts, *Journal of Molecular Catalysis A: Chemical*, 104, 3, (1996), L197-L199

[104] D.C. Schmelling, K.A. Gray, P.V. Kamat, Role of reduction in the photocatalytic degradation of TNT, *Environmental Science & Technology*, 30, 8, (1996), 2547-2555

[105] K.T. Ranjit, T.K. Varadarajan, B. Viswanathan, Photocatalytic reduction of dinitrogen to ammonia over noble-metal-loaded TiO_2, *Journal of Photochemistry and Photobiology A: Chemistry*, 96, 1-3, (1996), 181-185

[106] B.V. Mihaylov, J.L. Hendrix, J.H. Nelson, Comparative catalytic activity of selected metal-oxides and sulfides for the photooxidation of cyanide, *Journal of Photochemistry and Photobiology a-Chemistry*, 72, 2, (1993), 173-177

[107] R.B. Draper, M.A. Fox, Titanium dioxide photooxidation of thiocyanate - $(SCN)_2$ - studied by diffuse reflectance flash-photolysis, *Journal of Physical Chemistry*, 94, 11, (1990), 4628-4634

[108] M.A. Fox, M.T. Dulay, Heterogenous photocatalysis, *Chemical Reviews*, 93, 1, (1993), 341-357

[109] J. Schwitzgebel, J.G. Ekerdt, H. Gerischer, A. Heller, Role of the oxygen molecule and of the photogenerated electron in TiO_2-photocatalysed air oxidation reactions, *Journal of Physical Chemistry*, 99, 15, (1995), 5633-5638

[110] A. Hagfeldt, M. Graetzel, Light-Induced Redox Reactions in Nanocrystalline Systems, *Chemical Reviews*, 95, 1, (1995), 49-68

[111] M.K. Nazeeruddin, A. Kay, I. Rodicio, R. Humphrybaker, E. Muller, P. Liska, N. Vlachopoulos, M. Gratzel, Conversion of light to electricity by cis-x2bis(2,2'-bipyridyl-4,4'-dicarboxylate)ruthenium(II) charge-tranfer sensitisers (X = Cl^-, Br^-, I^-, Cn^- and SCn^-) on nanocrystalline TiO_2 electrodes, *Journal of the American Chemical Society*, 115, 14, (1993), 6382-6390

[112] Y.V. Pleskov, M.D. Krotova, Photosplitting of water in a photoelectrolyser with solid polymer electrolyte, *Electrochimica Acta*, 38, 1, (1993), 107-109

[113] M. Gratzel, Artificial photosynthesis - water cleavage into hydrogen and oxygen by visible-light, *Accounts of Chemical Research*, 14, 12, (1981), 376-384

[114] A. Fujishima, K. Honda, Electrochemical photolysis of water at a semiconductor electrode, *Nature*, 238, 5358, (1972), 37

[115] M.S. Wrighton, Photoelectrochemical conversion of optical-energy to electricity and fuels, *Accounts of Chemical Research*, 12, 9, (1979), 303-310

[116] A.J. Bard, Photoelectrochemistry, *Science*, 207, 4427, (1980), 139-144

[117] S. Licht, Electrolyte modified photoelectrochemical solar-cells, *Solar Energy Materials and Solar Cells*, 38, 1-4, (1995), 305-319

[118] K. Kalyanasundaram, M. Gratzel, Photochemical conversion and storage of solar-energy, *Photochemistry and Photobiology*, 40, 6, (1984), 807-821

[119] T. Matsunaga, M. Okochi, TiO_2-mediated photochemical disinfection of *Escherichia-coli* using optical fibres, *Environmental Science & Technology*, 29, 2, (1995), 501-505

[120] P.C. Zhang, R.J. Scrudato, G. Germano, Solar-catalytic inactivation of Escherichia-coli in aqueous solutions using TiO_2 as a catalyst, *Chemosphere*, 28, 3, (1994), 607-611

[121] S. Lee, K. Nishida, M. Otaki, S. Ohgaki, Photocatalytic inactivation of phage Q beta by immobilized titanium dioxide mediated photocatalyst, *Water Science and Technology*, 35, 11-12, (1997), 101-106

[122] Y. Kubota, T. Shuin, C. Kawasaki, M. Hosaka, H. Kitamura, R. Cai, H. Sakai, K. Hashimoto, A. Fujishima, Photokilling of T-24 humn bladder-cancer cells with titanium dioxide, *British Journal of Cancer*, 70, 6, (1994), 1107-1111

[123] A. Fujishima, D.A. Tryk, T. Watanabe, K. Hashimoto, *International Glass Review*, (1998), 114-116

[124] M. Grätzel, Heterogeneous photochemical electron transfer, CRC Press, (1989)

[125] J.M. Bolts, M.S. Wrighton, Correlation of photocurrent-voltage curves with flat-band potential for stable photoelectrodes for the photoelectrolysis of water, *The Journal of Physical Chemistry*, 80, 24, (1976), 2641-2645

[126] B.I. Lemon, F. Liu, J.T. Hupp, Electrochemical, spectral, and quartz crystal microgravimetric assessment of conduction band edge energies for nanocrystalline

zirconium dioxide/solution interfaces, *Coordination Chemistry Reviews*, 248, 13-14, (2004), 1225-1230

[127] I. Ohno, M. Schlesinger, M. Paunovic, Electroless Deposition of Palladium and Platinum, in, Modern Electroplating, Fourth Edition, (2000), 699-704

[128] G.O. Mallory, Electroless plating of platinum group metals, in, Electroless Plating - Fundamentals and Applications, (1990), 421-440

[129] G.O. Mallory, The fundamental aspects of nickel plating, in, Electroless Plating - Fundamentals and Applications, (1990), 1-56

[130] K.R. Wy, J.J. Wang, W.C. Liu, Z.S. Chen, J.K. Wu, Deposition of graded TiO_2 films featured both hydrophobic and photo-induced hydrophilic properties, *Applied Surface Science*, 252, (2006), 5829-5838

[131] L. Kavan, B. O'Regan, A. Kay, M. Grätzel, Preparation of TiO_2 (anatase) films on electrodes by anodic oxidative hydrolysis of $TiCl_3$, *Journal of Electroanalytical Chemistry*, 346, 1-2, (1993), 291-307

[132] R. Flood, B. Enright, M. Allen, S. Barry, A. Dalton, H. Doyle, D. Tynan, D. Fitzmaurice, Determination of band edge energies for transparent nanocrystalline TiO_2-CdS sandwich electrodes prepared by electrodeposition, *Solar Energy Materials and Solar Cells*, 39, 1, (1995), 83-98

[133] G.-J. Yang, C.-J. Li, F. Han, X.-C. Huang, Effects of annealing treatment on microstructure and photocatalytic performance of nanostructured TiO_2 coatings through flame spraying with liquid feedstocks, *Journal of Vacuum Science & Technology B*, 22, 5, (2004)

[134] J.Y. Kim, C.H. Noh, E.C. Hwang, Method for forming pattern of one-dimensional nanostructure, United States Patent 7,067,237, (2006)

[135] J.Y. Kim, S.H. Cho, K.Y. Song, C.H. Noh, E.C. Hwang, Method for forming highly conductive metal pattern on flexible substrate and EMI filter using metal pattern formed by the method, United States Patent Application 2006/0019076 A, (2006)

[136] C. Liu, L. Fu, J. Economy, A simple, template-free route for the synthesis of mesoporous titanium dioxide materials, *Journal of Materials Chemistry*, 14, 7, (2004), 1187-1189

[137] M.A. Bromley, C. Boxall, S. Galea, P.S. Goodall, S. Woodbury, Photocatalytic initiation of electroless deposition, *Journal of Photochemistry and Photobiology A: Chemistry*, 216, 2-3, (2010), 228-237

[138] M.A. Bromley, C. Boxall, Method for formation of porous metal coatings, United Kingdom Patent Application WO/2012/042203, (2012)

[139] M.A. Bromley, C. Boxall, Semiconductor photocatalysis and metal deposition, in: J.C. Taylor (Ed.), Advances in Chemistry Research, vol 13, Nova Publishers, (2011)

[140] J. Yu, X. Zhaoa, Q. Zhaoa, G. Wang, Preparation and characterization of super-hydrophilic porous TiO_2 coating films, *Materials Chemistry and Physics*, 68, (2001), 253-259

[141] K.R. Denison, C. Boxall, Photoinduced "Stick–Slip" on Superhydrophilic Semiconductor Surfaces, *Langmuir*, 23, 8, (2007), 4358-4366

[142] M.A. Bromley, C. Boxall, Photocatalytically Initiated Electroless Deposition of Macroporous Metal Films onto Insulating Substrates, *Electrochemistry Communications*, 23, (2012), 87-89

[143] Y.H. Ogata, K. Kobayashi, M. Motoyama, Electrochemical metal deposition on silicon, *Current Opinion in Solid State and Materials Science*, 10, 3–4, (2006), 163-172

[144] C. Haginoya, M. Ishibashi, K. Koike, Nanostructure array fabrication with a size-controllable natural lithography, *Applied Physics Letters*, 71, 20, (1997), 2934-2936

[145] N. Takeyasu, T. Tanaka, S. Kawata, Metal Deposition Deep into Microstructure by Electroless Plating, *Japanese Journal of Applied Physics*, 44, Copyright (C) 2005 The Japan Society of Applied Physics, (2005), L1134

[146] N.D. Denkov, O.D. Velev, P.A. Kralchevsky, I.B. Ivanov, H. Yoshimura, K. Nagayama, Two-dimensional crystallisation, *Nature*, 361, (1993), 26

[147] P.N. Bartlett, P.R. Birkin, M.A. Ghanem, C. Toh, Electrochemical synthesis of highly ordered macroporous conducting polymers grown around self-assembled coloidal templates, *Journal of Materials Chemistry*, 11, (2001), 849-853

[148] J.M. Lee, J.H. Kim, C.C. Ho, I.W. Cheong, Dense and square lattice-free colloid crystals of highly charged monodisperse latex particles on 3-aminopropyl trimethoxysilane-modified glass subrstrate, *Polymer*, 48, 16, (2007), 4804-4813

[149] E.J. Tull, P.N. Bartlett, K.R. Ryan, Controlled Assembly of Micrometer-Sized Spheres: Theory and Application, *Langmuir*, 23, (2007), 7859-7873

[150] Y. Takata, S. Hidaka, M. Masuda, T. Ito, Pool boiling on a superhydrophilic surface, *International Journal of Energy Research*, 27, 2, (2003), 111-119

[151] W.C. Conner, J.L. Falconer, Spillover in Heterogeneous Catalysis, *Chemical Reviews*, 95, 3, (1995), 759-788

[152] L. Gao, T.J. McCarthy, Contact angle hysteresis explained, *Langmuir*, 22, 14, (2006), 6234-6237

[153] M.A. Bromley, C. Boxall, The metallisation of insulating substrates with nano-structured metal films of controllable pore dimension, *Journal of Materials Chemistry A*, 1, 20, (2013), 6152-6161

[154] Z. Wang, U. Helmersson, P.-O. Käll, Optical properties of anatase TiO_2 thin films prepared by aqueous sol-gel process at low temperature, *Thin Solid Films*, 405, 1-2, (2002), 50-54

[155] M.A. Bromley, C. Boxall, The nanoporous metallisation of insulating substrates through Photocatalytically Initiated Electroless Deposition (PIED), *MRS Proceedings*, 1409, (2012)

[156] C.R.K. Rao, M. Pushpavanam, Electroless deposition of platinum on titanium substrates, *Materials Chemistry and Physics*, 68, 1–3, (2001), 62-65

[157] R.K. Paul, H.-D. Jang, B.-T. Lee, Fabrication of platinum coating on continuous porous SiC–Si3N4 composites by the electroless deposition process, *Journal of Materials Processing Technology*, 209, 6, (2009), 2958-2962

[158] Y.G. Lee, J.H. Park, C. Oh, S.G. Oh, Y.C. Kim, Preparation of highly monodispersed hybrid silica spheres using a one-step sol-gel reaction in aqueous solution, *Langmuir*, 23, 22, (2007)

[159] A.S. Dimitrov, K. Nagayama, Continuous Convective Assembling of Fine Particles into Two-Dimensional Arrays on Solid Surfaces, *Langmuir*, 12, (1996), 1303-1311

[160] Z. Zhou, X.S. Zhao, Flow-Controlled Vertical Deposition Method for the Fabrication of Photonic Crystals, *Langmuir*, 20, (2004), 1524-1526

[161] R.G. Shimmin, A.J. DiMauro, P.V. Braun, Slow Vertical Deposition of Colloidal Crystals: A Langmuir-Blodgett Process?, *Langmuir*, 22, 15, (2006), 6507-6513

[162] J. Wang, Q. Li, W. Knoll, U. Jonas, Preparation of Multilayered Trimodal Colloid Crystals and Binary Inverse Opals, *Journal of the American Chemical Society*, 128, 49, (2006), 15606-15607

[163] Y. Wan, Z. Cai, L. Xia, L. Wang, Y. Li, Q. Li, X.S. Zhao, Simulation and fabrication of binary colloidal photonic crystals and their inverse structures, *Materials Letters*, 63, 24–25, (2009), 2078-2081

[164] S.K. Hyun, K. Murakami, H. Nakajima, Anisotropic mechanical properties of porous copper fabricated by unidirectional solidification, *Materials Science and Engineering: A*, 299, 1–2, (2001), 241-248

[165] H.S.T. Ahmed, A.F. Jankowski, The mechanical strength of submicron porous silver foils, *Surface and Coatings Technology*, 204, 6–7, (2009), 1026-1029

[166] S. Brunauer, P.H. Emmett, E. Teller, Adsorption of Gases in Multimolecular Layers, *Journal of the American Chemical Society*, 60, 2, (1938), 309-319

[167] M.G.B. Drew, M.R.S.J. Foreman, C. Hill, M.J. Hudson, C. Madic, 6,6′-bis-(5,6-diethyl-[1,2,4]triazin-3-yl)-2,2′-bipyridyl the first example of a new class of quadridentate heterocyclic extraction reagents for the separation of americium(III) and europium(III), *Inorganic Chemistry Communications*, 8, 3, (2005), 239-241

[168] M.J. Hudson, C.E. Boucher, D. Braekers, J.F. Desreux, M.G.B. Drew, M.R.S.J. Foreman, L.M. Harwood, C. Hill, C. Madic, F. Marken, T.G.A. Youngs, New

bis(triazinyl) pyridines for selective extraction of americium(iii), *New Journal of Chemistry*, 30, 8, (2006), 1171-1183

[169] M.R.S. Foreman, M.J. Hudson, M.G.B. Drew, C. Hill, C. Madic, Complexes formed between the quadridentate, heterocyclic molecules 6,6[prime or minute]-bis-(5,6-dialkyl-1,2,4-triazin-3-yl)-2,2[prime or minute]-bipyridine (BTBP) and lanthanides(iii): implications for the partitioning of actinides(iii) and lanthanides(iii), *Dalton Transactions*, 13, (2006), 1645-1653

[170] C. Madic, B. Boullis, P. Baron, F. Testard, M.J. Hudson, J.O. Liljenzin, B. Christiansen, M. Ferrando, A. Facchini, A. Geist, G. Modolo, A.G. Espartero, J. De Mendoza, Futuristic back-end of the nuclear fuel cycle with the partitioning of minor actinides, *Journal of Alloys and Compounds*, 444–445, 0, (2007), 23-27

[171] D. Magnusson, B. Christiansen, M.R.S. Foreman, A. Geist, J.P. Glatz, R. Malmbeck, G. Modolo, D. Serrano-Purroy, C. Sorel, Demonstration of a SANEX Process in Centrifugal Contactors using the CyMe4-BTBP Molecule on a Genuine Fuel Solution, *Solvent Extraction and Ion Exchange*, 27, 2, (2009), 97-106

[172] T. Nagaoka, N. Nakao, K. Tabusa, J. Yano, K. Ogura, Dynamic elution control in electrochemical ion chromatography using pulse perturbation of stationary phase potential, *Journal of Electroanalytical Chemistry*, 371, 1–2, (1994), 283-286

[173] A. Bhattacharyya, P.K. Mohapatra, S.A. Ansari, D.R. Raut, V.K. Manchanda, Separation of trivalent actinides from lanthanides using hollow fiber supported liquid membrane containing Cyanex-301 as the carrier, *Journal of Membrane Science*, 312, 1–2, (2008), 1-5

[174] D. Desmond, B. Lane, J. Alderman, J.D. Glennon, D. Dermot, D.W.M. Arrigan, Evaluation of miniaturised solid state reference electrodes on a silicon based component, *Sensors and Actuators B: Chemical*, 44, 1–3, (1997), 389-396

[175] A.W. Hassel, K. Fushimi, M. Seo, An agar-based silver|silver chloride reference electrode for use in micro-electrochemistry, *Electrochemistry Communications*, 1, 5, (1999), 180-183

[176] H. Suzuki, H. Shiroishi, S. Sasaki, I. Karube, Microfabricated Liquid Junction Ag/AgCl Reference Electrode and Its Application to a One-Chip Potentiometric Sensor, *Analytical Chemistry*, 71, 22, (1999), 5069-5075

[177] I.Y. Huang, R.-S. Huang, Fabrication and characterization of a new planar solid-state reference electrode for ISFET sensors, *Thin Solid Films*, 406, 1–2, (2002), 255-261

[178] J. Zhou, K. Ren, Y. Zheng, J. Su, Y. Zhao, D. Ryan, H. Wu, Fabrication of a microfluidic Ag/AgCl reference electrode and its application for portable and disposable electrochemical microchips, *ELECTROPHORESIS*, 31, 18, (2010), 3083-3089

[179] J. Dickinson, M. Bromley, F. Andrieux, C. Boxall, Fabrication and Characterisation of the Graphene Ring Micro Electrode (GRiME) with an Integrated, Concentric Ag/AgCl Reference Electrode, *Sensors*, 13, 3, (2013), 3635-3651

[180] J.T. Zhang, C.M. Li, Nanoporous metals: fabrication strategies and advanced electrochemical applications in catalysis, sensing and energy systems, *Chemical Society Reviews*, 41, 21, (2012), 7016-7031

[181] A.V. Mokrushina, M. Heim, E.E. Karyakina, A. Kuhn, A.A. Karyakin, Enhanced hydrogen peroxide sensing based on Prussian Blue modified macroporous microelectrodes, *Electrochemistry Communications*, 29, (2013), 78-80

[182] Ø. Hatlevik, S.K. Gade, M.K. Keeling, P.M. Thoen, A.P. Davidson, J.D. Way, Palladium and palladium alloy membranes for hydrogen separation and production: History, fabrication strategies, and current performance, *Separation and Purification Technology*, 73, 1, (2010), 59-64

[183] A. Eftekhari, 3D deposition of LiMn2O4: enhancement of lithium battery performance, *Solid State Ionics*, 161, 1-2, (2003), 41-47

[184] J.H. Pikul, H. Gang Zhang, J. Cho, P.V. Braun, W.P. King, High-power lithium ion microbatteries from interdigitated three-dimensional bicontinuous nanoporous electrodes, *Nat Commun*, 4, (2013), 1732

[185] A. Mills, G. Hill, M. Stewart, D. Graham, W.E. Smith, S. Hodgen, P.J. Halfpenny, K. Faulds, P. Robertson, Characterization of Novel Ag on TiO2 Films for Surface-Enhanced Raman Scattering, *Applied Spectroscopy*, 58, 8, (2004), 922-928

[186] Y.S. Li, H.M. Su, K.S. Wong, X.Y. Li, Surface-Enhanced Raman Spectroscopy on Two-Dimensional Networks of Gold Nanoparticle-Nanocavity Dual Structures Supported on Dielectric Nanosieves, *Journal of Physical Chemistry C*, 114, 23, (2010), 10463-10477

[187] W.F. Hu, S.L. Zou, Proposed Substrates for Reproducible Surface-Enhanced Raman Scattering Detection, *Journal of Physical Chemistry C*, 115, 11, (2011), 4523-4532

[188] M.K. Fan, G.F.S. Andrade, A.G. Brolo, A review on the fabrication of substrates for surface enhanced Raman spectroscopy and their applications in analytical chemistry, *Analytica Chimica Acta*, 693, 1-2, (2011), 7-25

[189] Q.H. Hong, X.F. Liu, Y. Fang, Templated Fabrication of Periodic Array of Nanovoids and Its SERS Performance, *Acta Chimica Sinica*, 71, 2, (2013), 255-259

[190] M.R. Jones, K.D. Osberg, R.J. Macfarlane, M.R. Langille, C.A. Mirkin, Templated Techniques for the Synthesis and Assembly of Plasmonic Nanostructures, *Chemical Reviews*, 111, 6, (2011), 3736-3827

[191] S.O. Klimonsky, V.V. Abramova, A.S. Sinitskii, Y.D. Tretyakov, Photonic crystals based on opals and inverse opals: synthesis and structural features, *Russian Chemical Reviews*, 80, 12, (2011), 1191-1207

[192] D.R. Monteiro, L.F. Gorup, A.S. Takamiya, A.C. Ruvollo-Filho, E.R.d. Camargo, D.B. Barbosa, The growing importance of materials that prevent microbial adhesion: antimicrobial effect of medical devices containing silver, *International Journal of Antimicrobial Agents*, 34, 2, (2009), 103-110

[193] J.A. Byrne, Fernandez-Iba, #241, P.A. ez, P.S.M. Dunlop, D.M.A. Alrousan, J.W.J. Hamilton, Photocatalytic Enhancement for Solar Disinfection of Water: A Review, *International Journal of Photoenergy*, 2011, (2011)

"I'm gonna drink 'til I reboot!"

Bender Bending Rodríguez